Analysis of Transformer Insulation under High-frequency Transients

by

Anurag Anand Devadiga

A thesis

presented to the University of Waterloo

in fulfillment of the

thesis requirement for the degree of

Doctor of Philosophy

in

Electrical and Computer Engineering

Waterloo, Ontario, Canada, 2022

Examining Committee Membership

The following served on the Examining Committee for this thesis. The decision of the Examining Committee is by majority vote.

External Examiner	Hans Edin Dr
Supervisor(s)	Shesha Jayaram Dr
Internal Member	Hany Aziz Dr
Internal Member	Ayman A. El-Hag Dr
Internal-external Member	Alexander Penlidis Dr

Author’s Declaration

I hereby declare that I am the sole author of this thesis. This is a true copy of the thesis, including any required final revisions, as accepted by my examiners.

I understand that my thesis may be made electronically available to the public.

Abstract

In recent times, there have been an increase in installation of wind turbines for generation of electricity through renewable energy sources. The wind energy is a clean and cost effective source of generating power, but integrating the wind farm to the grid has brought additional concerns for the insulation of the installed step-up transformers. The wind-turbine step-up transformers are subjected to high-frequency high dV/dt transient voltage due to the operation of power electronic converters and vacuum circuit breakers. These high-frequency transients are responsible for the premature failure of the transformer's turn-to-turn and layer-to-layer paper-oil insulation. Thus, the current research work addresses the effect of the transient voltage parameters on the degradation of the transformers paper-oil insulation.

The distribution of the transient voltage along the transformer winding as a function of transient voltage parameters including rise time (290 ns and 1000 ns), duty cycle (10% and 50%) and amplitude (100 V and 1000 V) are analysed to obtain the transient voltage that can cause the highest tap-to-tap voltage amplification. The switching frequency of the transient voltage (square wave) is fixed at 1 kHz. The investigation of the transient voltage parameters that lead to the highest tap-to-tap voltage level will help the industry to design the insulation level for the windings of the step-up transformers based on the transient stresses generated in a wind farm chain. The installation of RC snubbers and surge arresters at the transformer terminal will help reduce the transient voltage amplitude, rise time, and switching frequency, but it is very difficult to design an arrestor or an RC snubber for a complicated wind turbine topology, and the installation cost of these RC filters are high. Thus, the transformer winding behaviour as a function of the transient voltage parameters are obtained. The transient voltage with an amplitude of 100 V, rise time of 290 ns, and duty cycle of 50 % had the highest tap-to-tap transient voltage level along the transformer winding. The mitigation technique used to minimize the transient voltage level are designed to reduce the transients at the transformer terminal but the internal voltage of the transformer under the transient voltage stresses can be high due to inter-winding resonance.

In order to analyse the importance of inter-winding resonance, the thesis presented three types of transfer function frequency response for two transformers, T1 and T2. Transformer T1 had been aged under the application of the sinusoidal voltage, and transformer T2 had been aged under the application of the repetitive transient voltage. The transfer function frequency responses obtained were magnitude of voltage difference response in dB, impedance difference response, and voltage ratio difference

response. The tap-to-tap difference response for each of the transfer functions were obtained to analyse the inter-winding voltage distribution and respective resonance frequency. All three transfer functions were compared to obtain the sensitivity of these transfer function to distinguish between the two aged transformers. The transformer windings can be modelled as a network of resistance (R), inductance (L), and capacitance (C). The RLC network is due to the transformers inductance (self and mutual), capacitance and resistance of the winding structure, and the dielectric resistance and capacitance of the paper-oil insulation. Various transfer function frequency responses can emphasize on certain elements of these RLC network and ignore certain other elements of the RLC network. These lead to differences in sensitivity for the above mentioned transfer function frequency responses.

Furthermore, the influence of the transient voltage parameters on the ageing of transformer paper-oil insulation is analysed to obtain the degradation level of the insulation under repetitive transient voltages. The dissipation factor, polarisation current, and depolarisation current are the ageing responses used to obtain the degradation level under transient voltage ageing of the transformer paper-oil insulation. The paper-oil insulation was aged under repetitive transient voltage for a long duration of 130 hours with Voltesso 35 as the insulating oil. Two-level, two-factor design of experiments were used to obtain the effect of transient voltage parameters on the ageing of the paper-oil insulation. Rise time and duty cycle were the two factors (parameters) of the transient voltage selected for the ageing experiments. The two levels of rise time were 220 ns and 650 ns, and two levels of the switching frequency were 1 kHz and 3 kHz. The amplitude and the duty cycle of the transient voltage (square wave) are fixed at 6 kV and 50 % respectively. The study of transient voltage parameters that lead to the highest degradation of the transformer paper-oil insulation will help the transformer manufacturer decide the quality of the insulation that needs to be used on the step-up transformer based on the measured transient voltage signature in the wind farm. Additionally, the installation cost of the RC filters are high, thus the above analysis can be used to evaluate the requirement of such expensive filters to be installed at the transformer terminals. The research work obtained that a faster rise time (220 ns) and higher switching frequency (3 kHz) of the transient voltage led to a higher ageing degradation level for the paper-oil insulation.

The transient voltage ageing of paper-oil insulation are carried out and compared for two mineral oils, they are, Luminol^{TM} TRi oil and Voltesso 35 oil. The two oils have difference in their electrical and chemical properties, thus their ageing responses under repetitive transient voltage are studied. The ageing of the two mineral oils under transient voltage are studied to obtain their ability to withstand the

transient voltage, and to select the best oil that does not degrade/age the paper-oil insulation under the repeated voltage stress. For the transient voltage ageing studies conducted in the current research work, the paper-oil insulation with Luminol TRi as insulating oil performed better compared to the paper-oil insulation with Voltesso 35 as insulating oil.

The transient voltage ageing of transformer paper-oil insulation at room temperature is compared with the transient voltage ageing at elevated temperature of 50° C with Voltesso 35 A as the insulating oil. The Voltesso 35 A oil is used to replicate the transformer that has been in service for long duration. The wind turbine step-up transformers undergo thermal stress due to varying load cycle depending on the wind speed. The thermal stress can also be caused due to harmonics generated during the power electronic converter operation. Thus, the transient voltage ageing with additional thermal stress is studied in the current research work. The ageing degradation level of paper-oil insulation stressed under transient voltage at elevated temperature of 50° C was significantly higher compared to the ageing degradation level of paper-oil insulation stressed under transient voltage at room temperature.

Acknowledgements

Firstly, I would want to thank God, the Almighty, for bestowing me many benefits, knowledge, and opportunities during my Ph.D. program, and for allowing me to finally complete the thesis.

I sincerely thank my supervisor, Dr. Shesha Jayaram for her guidance and support throughout my Ph.D. program. I appreciate her motivation, patience, and desire to communicate her wisdom in the field of high voltage engineering.

I would like to thank Dr. Ayman A. El-Hag, Dr. Hany Aziz, Dr. Alexander Penlidis, and Dr. Hans Edin who honored me by being on the committee of my thesis examination. Their valuable feedback and suggestions are deeply appreciated.

My special thanks go to my colleagues and friends Mohana, Mahdi, Ibrahim, Amin, Alireza, Satish, Khadija, Arathi, Marcelo, Basharat, Jagdish, and Gowri for their technical and moral support.

Amongst all the wonderful people in the ECE department, I am extremely grateful to Susan, Cassandra, Jessica, and Lisa for helping me accomplish the milestones of the doctoral program.

I sincerely thank the Natural Sciences and Engineering Research Council of Canada (NSERC) for funding the research work.

I acknowledge and thank the Northern Transformers and the Communications & Power Industries Canada Inc. for providing transformer oils for the experimental work.

Dedication

To my father, mother, brother, and sister-in-law.

To my grandfather, grandmother, and uncle, who are always in my heart. May the blessing of God be upon them and may they rest in peace.

Table of Contents

List of Figures

List of Tables

Chapter 1
Introduction

1.1 Introduction

Over the past decade, Canada has increased the installation of wind energy sources compared to other forms of renewable energy [1]. Black Spring Ridge in Alberta is Canada's largest wind farm with 166 wind turbine networks. There are a lot of untapped wind energy sources in Canada that can be utilised to generate power to match the increase in energy demand of the country. Moreover, generating electricity through wind turbines does not produce greenhouse gases and other hazardous waste. There is an added economic benefit since it is one of the cheapest electric energy sources, and provides jobs as well as income to landowners and municipalities.

The sequence of wind farm structure consists of a wind turbine generator, back-to-back frequency converter, cable, circuit breaker, and a step-up transformer. For the purpose of energy conversion, the wind turbine generator can be designed with gearboxes, or there are gearless generators connected to power electronic converters. Modern wind turbine generators are made with type IV configuration, as it provides control features over the output voltage, slip, and reactive power [2], [3]. Connecting the generator to the grid via a back-to-back frequency converter provides greater flexibility in terms of operation [2]. The step-up transformers are implemented in the system to convert the turbine generator voltage level to medium level voltage for the collector system.

The wind turbine step-up transformer is one of the critical components in the system, and its design must be carefully analysed and evaluated. In the past, the wind turbine step-up transformer was a conventional distribution transformer, but a large number of recent failures have directed towards the use of a robust design for these transformers. Design of the transformer should consider transformer loading, transformer sizing, voltage variation, harmonics and voltage spikes, and steep fronted transients initiated by vacuum circuit breaker (VCB) [2], [4].

1.2 Wind turbine step-up transformers

Discussion in Doble conference indicates a high level of gassing problem in the pad-mounted wind turbine transformer. It was reported that the turbine transformers designed for about 25-30 years of life were failing in 3-5 years [5]. The gas levels are suspected to be generated due to partial discharge within

the insulation of the transformer. Partial discharge can cause premature failure of the transformer, thus, very high operation and maintenance expenses to the wind energy distributors. A study conducted by Myers Inc. [6] diagnostic group on gassing in wind-farm connected transformers considered often retesting of the transformer due to high hydrogen gas generation. IEEE C57.104 gives required guidelines for retesting frequency of transformers based on condition level and generation rate of key gases [7]. The condition level is classified from condition 1 to condition 4 based on the total combustible gas level present in the transformer oil sample. It was noticed that greater than 23% of the wind farm connected transformers have condition 2 to 4 for hydrogen generation, whereas only 5.3 % have the condition 2 to 4 for hydrogen generation in the case of non-wind applications. The hydrogen gas can be generated by electrolysis due to the presence of excessive moisture or due to partial discharge condition that creates a path within the void/surface of insulation materials. It is necessary to evaluate the reason for premature failure of wind turbine step-up transformers. The probable cause for premature failure [2], [4], [8], [9] are briefly discussed below:

1.2.1 Transformer loading:

Wind generation primarily depends on the local wind and climatic conditions that vary rapidly, and thus, their average load factors are as low as 35 percent. This low load factor introduces the issue of the thermal cycle due to varying loads. Varying load introduces repetitive thermal stress on the winding, clamps, and gaskets, thus, weakens the physical structure of the transformer. Also, thermal cycling causes the generation of nitrogen gas that forms bubbles within the oil due to the heating and cooling of the oil. The bubbles can cause hot spots and partial discharges in the insulation and the winding. The above processes can result in progressive degradation and accelerated ageing of the transformer insulation.

1.2.2 Harmonics and voltage spikes:

The solid-state device (converters) used to control the grid voltage can create harmonics along with generation of high dV/dt, high-frequency transient voltage. The converter operation gives rise to harmonics that are an odd multiple of system frequency, which in-turn produce eddy current and stray losses in the transformer’s winding and core structure. The losses lead to local hot-spots, resulting in problems like partial discharge, dissolved gas, and deterioration of the transformer insulation.

The power electronic converters use pulse with modulation (PWM) to generate the sinusoidal voltage. The generated sinusoidal voltage has high dV/dt, high-frequency transient voltage superimposed on it. These transient voltages impose severe threat on the insulation of the wind turbine step-up transformers. Additionally, these transient voltages travel along the transformer winding, and when the transformer's internal winding frequency response matches the high-frequency content of the transient voltage, it can lead to internal voltage amplification along the transformer winding due to resonance. The internal voltage amplification can deteriorate the winding insulation due to high field conduction and partial discharge (PD).

1.2.3 Transformer sizing:

The transformer is not designed to withstand the voltage fluctuation since higher insulation to withstand the fluctuation can lead to a higher cost for the transformer. The transformer should be designed to handle dielectric loading and overheating of insulation material during voltage fluctuations. Otherwise, it can lead to the failure of transformer insulation. One of the solutions is increasing the power rating of the transformer to withstand various stresses on the transformer.

1.2.4 Withstand fault currents:

The wind turbine generator remains in the system during network disturbance to maintain network stability. So, this feature of staying through the fault without degrading mechanically, electrically, and thermally is called fault ride-through. During this time, the transformer will have very low voltage for a few cycles, and it has to be designed to handle the short circuit current, and mechanical stress on the winding during the withstand fault period.

1.2.5 Vacuum circuit breaker initiated steep fronted transients:

Fast rise time overvoltages are mainly caused by switching action of the vacuum circuit breaker. The wind speed varies significantly over a day, and thus, the wind turbine unit switch multiple times a day. The circuit breakers are used to isolate the wind turbine from the main grid. The switching operation of the circuit breakers leads to high-frequency, and very steep front transients. These transients amplify due to the resonance caused by circuit breaker, long cable, and transformer network in large wind farms.

1.3 Impact of High-frequency transients on the transformer insulation

Currently, wind farms use type IV generator, AC-DC-AC converter, circuit breaker, cable, and the step-up transformer. The transformer has fast circuit breakers on both converters and grid regions. The breakers are on both sides to facilitate connection and disconnection of the wind turbine to the main grid during a fault condition, and varying wind speed [2]. Figure 1.1 shows the schematic of the wind turbine system, which consists of a generator, converter, breaker, and cables.

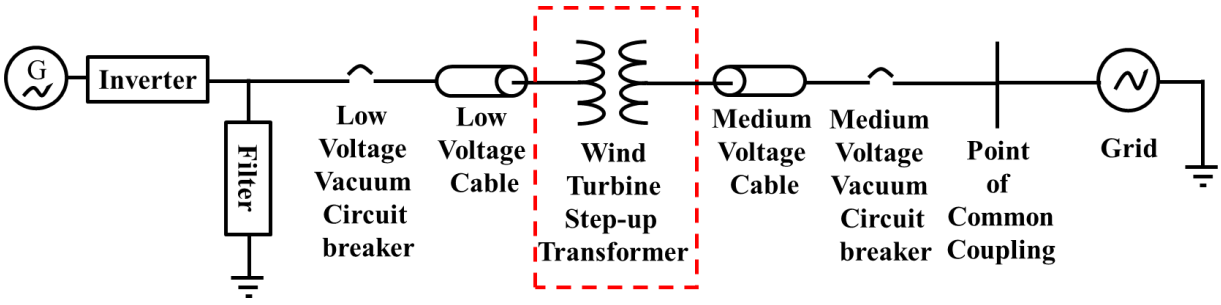

Figure 1.1: Schematic of the wind turbine system [2].

The converter operation, along with the switching operation of the vacuum circuit breakers can introduce very high dV/dt, and di/dt stresses on the transformer insulation that can lead to partial discharge and overheating within the insulation structure. These transients are low in amplitude but can cause progressive degradation of insulation due to repeated high-frequency impression. Also, the transient's amplitude can increase due to resonance caused by transients' interaction with capacitive cable and inductive step-up transformer.

The vacuum circuit breaker is a suitable switching device due to its excellent interruption capability and dielectric recovery characteristics [10]. Also, these breakers are durable, have a low maintenance cost, and suitable for medium voltages [11]. But the transformer's insulation has failed due to the creation of dangerous surges while switching operation of VCBs, even though the transformer design met all the standards and quality [12]. Also, it has been observed that the switching transients generated by such vacuum circuit breakers cause a surge of 4.6 per unit magnitude and very fast rise times with motors [13].

While opening and closing of the breaker, fast transients are generated due to repetitive re-strike and pre-strike operations of the circuit breaker. During opening operation, the vacuum circuit breaker

interrupts high-frequency currents. The interruption of the current leads to fast rise time high-frequency transient overvoltage that can propagate to transformers in the system. Due to the influence of the high-frequency transients on the transformer, it is worth-while to analyse in detail the effect of voltage level, rise time, repetition frequency, and duty cycle of the high-frequency transient voltage on the transformer insulation.

Power electronic converters are used to convert AC-DC-AC in the wind farm system in order to stabilise the electricity generated by intermittent wind energy source. The power electronic switches are controlled to obtain sinusoidal voltage; the voltage is then increased through a step-up transformer to supply to the grid. The waveform generated by the switching of power electronic converter includes a sine wave superimposed with repetitive transients that impose a threat on transformer insulation. Various researchers have worked extensively on the influence of adjustable speed drives (ASD) created transients on motor insulation; however, very few works have dealt with their detrimental effect on transformer insulation [14]. The insulation of transformers is quite different from the motor insulation. These repetitive transients have high rise time, magnitudes, and repetition frequency. Also, the derivative of the repetitive transient overvoltage caused by the fast switching operation of power electronic converters, and the vacuum circuit breaker is increased significantly when the frequency component of the transient voltage matches the frequency response of the transformer winding. Thus, the influence of parameters like voltage magnitude, rise time, repetition frequency, and duty cycle of these repetitive transients on the transformer insulation need to be researched. This knowledge can help the industry to evaluate the condition and remaining life of the transformer.

1.4 Transformer design modification under high-frequency transients:

Modifications are suggested and incorporated in the design of wind-farm transformers to reduce the high-frequency transient effect that reaches the terminal of the transformers. Some of the methods to reduce the effect of transients on the transformer when the transient enters the transformer body are:

- The electrostatic shield that decouples the transfer of harmonics from the secondary winding of the transformer to the primary side or vice versa, but the work reported in [15] does not support this claim.

- Bio-SLIM transformer, are reported to have excellent thermal, electrical, and mechanical stability for paper-oil insulation material under transients [8].

To understand the advantages of the above mentioned design changes on the transformer, and to evaluate the condition and remaining life of the transformer, it is important to analyse the behavior of the transformer under high-frequency transients. The regions of high field and overvoltage points on the transformer under high-frequency transients need to be analysed to design the transformer insulation optimally. Thus, the research focusses on understanding the winding response of the transformer, and analyse paper-oil insulation ageing dynamics under high-frequency transients. The transformer winding frequency response and its high-frequency transient response will help to investigate the voltage amplification in the transformer winding. The paper-oil insulation ageing study will involve a detailed understanding of the insulation degradation by using dielectric frequency response, polarisation current response, depolarisation current response, partial discharge analysis, and hydrogen gas analysis as a technique to evaluate the transformer ageing under repetitive transient voltage.

1.5 Summary

The current energy industry focuses largely on generating power by renewable energy like solar, wind, tidal, etc. The main advantage of renewable energy are: the sources are clean, and the cost of fuel is low depending on the availability of the resources. The availability of these resources, especially wind energy, is intermittent. This requires the circuit breaker operation and the power electronic converter operation to stabilize the voltage on the grid side. The switching operation of the circuit breaker and power electronic components combined with the network impedance can produce very steep front high-frequency transients along the winding of the wind turbine transformer. These transient stresses can lead to progressive degradation of the transformer turn-to-turn or layer-to-layer paper-oil insulation and eventually reducing the lifetime of the transformer. There is very little research focussing on the influence of high-frequency transients on the transformer paper-oil insulation. Thus, the current research focusses on the influence of the transient parameters on its distribution along the transformer winding. Also, the degradation level of the transformer paper-oil insulation for various transient parameters is studied to obtain the extent of transformer ageing under high-frequency transients.

The structure of the thesis is the following:

- Chapter 2 briefly describes various literature about the influence of repetitive voltage transient parameters on the distribution of transient voltage and the influence of repetitive transient voltage parameters on the paper-oil insulation ageing along with the thesis motivation and objective.
- Chapter 3 outlines the methodology and materials used in the research.
- Chapter 4 presents results pertaining to the distribution of transients along the transformer winding and ageing of transformer paper-oil insulation under repetitive transient voltage.
- Chapter 5 discusses the results obtained in the research work and provides recommendations about the endurance of the transformer mineral oils under repetitive transient ageing.
- Chapter 6 provides a summary of the research work and concludes the research work along with potential contributions and recommendations for future work.

Chapter 2
Literature Review

To analyse the influence of very fast transients on the transformer insulation a detailed literature survey has been carried out in steps. The literature review is divided into four sections. Section 2.1 reviews the literature about the distribution of fast transients along the transformer winding to study the overvoltage that arises due to the transients. The study of the influence of converter generated transients on machine insulation was extensively carried out in the past, and thus section 2.2 details a brief review of the influence of fast transient parameters on the machine insulation. The influence of fast transients on machine insulation is described to understand the relation between the transient voltage parameters on the ageing of the machine insulation, and correlate it with the transient voltage ageing study for transformer insulation. Section 2.3 deals with the influence of fast transient parameters on the ageing of transformer paper-oil insulation. Section 2.4 describes various diagnostic techniques available for analysing the ageing behavior of transformer paper-oil insulation under various transients.

2.1 Distribution of fast transients along the transformer winding

High-frequency fast transients are generated during the switching operation of the circuit breakers and natural lightning. When the frequency component of the transients matches the resonant frequency of the wind farm system containing inductive transformer and capacitive cable, extremely high overvoltage stress appears on the transformer winding terminal. In this context, the following section provides literature review on the characteristics of the generated high-frequency transients and distribution of the high-frequency transients along various sections of the winding. For example, the transient distribution along the winding can help to analyse the winding turn-to-turn or layer-to-layer voltage stress so that an adequate insulation system can be designed. Experimental and simulation studies can be carried out to study the characteristics of high-frequency transients generated by switching operation of the breakers. The simulation study involves high-frequency modeling of the breaker, cable, and transformer. The section discusses briefly about various mitigation techniques for reducing the high-frequency transient in-turn reducing the overvoltage stress along the transformer winding.

The operation of vacuum circuit breakers (VCBs) and switching devices produce transient voltages that cause the insulation failure of wind turbine transformers, particularly the first and the last transformers in the wind farm chain that are most vulnerable to these transients [16]. These voltage transients have a high amplitude, high rate of rise, and high-frequency components that can overstress the wind turbine step-up transformer leading to premature ageing and failure of transformer insulation. The voltage transients due to prestrike and reignition of the VCB are amplified based on the cable parameters, circuit breaker type, and transformer type present in the wind farm [2], [17]. Liu et al. simulated switching operation of the vacuum circuit breaker in an offshore wind farm and obtained a transient voltage with rate of rise of 142 kV/μs and an amplitude of 1.3 per-unit [18]. Xin et al. obtained transient voltage with an oscillation frequency of 0.78 kHz and rate of rise of 148 kV/μs at the wind turbine transformer during switching operation of the vacuum circuit breaker [19].

Devgan simulated a vacuum circuit breaker (VCB) initiated switching transient for a type IV wind farm taking into account high-frequency modeling of VCB, cable, and transformer [2]. The VCB modeling was carried out, considering chopping current, rate of rise of dielectric strength, transient recovery voltage, and current quenching capability. The cable was modeled by a frequency-dependent phase model that considered the skin effect, wave reflection, and electromagnetic wave propagation. A high-frequency black box model for the transformer was obtained by the transformer admittance frequency matrix, which is subjected to vector fitting and passivity enforcement algorithm. The opening and closing of VCB on the LV/HV side of the transformer were simulated under no-load and inductive load conditions. The highest transient voltage was obtained for VCB operation under the inductive load on the HV side of the transformer. The transformer terminal peak voltage, peak breaker current, rate of voltage change, frequency of oscillation, and the number of breaker reignitions obtained by Devgan were 3.03 per-unit, 0.73 kA, 28 kV/μs, 0.56 kHz, and 74, respectively. In [20], Zhou et al. showed that the increase in rate of rise and amplitude of the transient voltage are caused due to increase in reignition rate of the circuit breaker. Various mitigation techniques like the use of surge arresters were designed to reduce the overvoltage at the transformer terminals caused by high-frequency transients, but the arresters are unable to reduce the voltage rate of rise [17]. The amplitude of the transients can be reduced by the arresters; whereas, the amplitude and the rate of rise of the high-frequency transients can be reduced by the RC snubber installed in wind turbine transformer terminal but the cost and installation space need to be considered while considering RC snubbers [21]-[24]. The amplitude and frequency of

the switching overvoltages in a wind farm can be suppressed by increasing inter-phase capacitance of the cable, and by reducing the operating capacity of the wind turbine generator [22]. To reduce the rate of rise of the breaker generated transient voltages, Smugala et al. designed a series-connected choke [17]. Xin et al. studied the voltage transient developed in a 690 V/33 kV wind turbine transformer by simulating the switching operation of a vacuum circuit breaker for an offshore wind farm [25]. A voltage rise of 1.6 per-unit at the transformer for switching operation of VCBs was obtained, and it is claimed that the R-L choke helped in reducing the rate of rise of the transient voltages; whereas, the RC filters helped in reducing the transformer terminal voltage amplitude to 1.02 per-unit [25]. Although the surge arrestors and RC snubbers can be used to mitigate the transient amplitude, repetitive occurrence, and rate of rise, it is difficult to design an arrestor or an RC snubber for a complicated wind turbine topology, and also, the cost of RC filters are high. Thus, the transformer behaviour during the high-frequency transient voltage needs to be studied to design the transformer turn-to-turn insulation that can withstand high-frequency transients.

Furthermore, the amplitude of the transient voltage generated by the switching operation of the circuit breaker may be lower but when the frequency of oscillation of the transient matches the frequency characteristics of the transformer, it may lead to large internal voltages within the transformer [26]. These large voltages can cause permanent damage to the insulation of the transformer. The switching device, load, transformer, and cable interact to produce steep internal transients in the transformer. The resistor-capacitor snubber, controlled switching, and nonlinear resistors across the transformer can reduce the internal voltage caused due to transient voltage but it is very difficult to design these mitigation techniques at each natural frequency of the transformer. Zhao et al. showed that a transient impulse voltage with a rise time of less than 2 μs can have frequency components of about 1 MHz in its energy spectrum, hence there are high chances for the resonance frequency of the transformer to match the frequency component of the transient [27]. A standard lightning impulse has most of its energy density in the frequency range below a few kHz; whereas, transients with steep rise time, front/tail chopped, oscillating components have higher energy in the high-frequency region (1 kHz to 10 MHz) [28]. These resonance frequency oscillation is highest for turn-to-turn as compared to layer-to-layer and section-to-section resonances [29]. The maximum turn-to-turn voltage appears in the end turn of the winding [29]. The internal voltage distribution as a function of frequency was studied by Soloot et al. [30], [31] for resonance overvoltages in three transformer designs, namely layer, disc, and

pancake windings. Based on the internal resonance frequency response analysis the authors conclude that the disc winding configuration of wind turbine transformer is more vulnerable to gassing and insulation failures during voltage transients [30]. Also, the authors obtain that the pancake winding is the least vulnerable design for the resonance overvoltage [31].

Khanali et al. studied the effects of the electrostatic shield between LV and HV windings in reducing the transfer of high-frequency transient voltages between the windings [32]. The authors showed that the addition of an electrostatic shield between LV and HV windings reduces the transfer of high-frequency transients at certain frequencies but it also amplifies the transfer of high-frequency transients at other frequencies. The electrostatic shield reduced the internal voltage gradient by a factor of 20 % but it did not impact the resonance frequency of the voltage gradient. Elhaminia et al. studied the influence of disk space, turn insulation thickness, and distance between LV and HV windings on the internal resonance amplification for a wind turbine transformer [33]. The authors suggested that the winding resonance can be shifted by increasing the distance between LV and HV windings while the disk space and turn insulation thickness should be low to reduce the resonance frequency amplification. Sriyono et al. used sweep frequency response analysis and found that above frequencies of 200 kHz, there is an increased potential of internal winding resonance amplifications for a 10-kVA layer type transformer [34]. It was shown that the voltage level at the full winding can be lower than the voltage level at three-quarters of the winding due to internal winding resonance. There has been a lot of research work to study the transfer function frequency response of the transformer, but the literature is unable to demonstrate the difference in various transfer functions to show the resonance frequency amplification.

Considering the transient voltage parameters, Hassan et al. [35] studied the influence of cable length, fall time, and rise time of the impulse on the peak of the transient voltage. The authors found that the increase in rise time leads to decrease in the amplitude of the lightning impulse striking the transformer terminal but the fall time does not affect the amplitude significantly. As the length of the cable increases, the peak voltage of the transient at the transformer terminal decreases. There is a critical length for the cable where the lightning impulse frequency can match the transformer resonance frequency that can lead to very high stresses on transformer insulation. Yang et al. analysed the influence of the pulse width and the tail time of the transient impulse voltage on its distribution along the transformer winding

[36]. The authors found that decrease in transient's pulse width or decrease in transient's tail time can lead to an increase in the uneven (non-linear) distribution of voltage along the transformer winding.

Abdulahovic [37] studied the distribution of the lightning and switching transients along the winding for a single-phase reactor rated at 10 kV and 200 kVA. The impulse voltage applied were the step voltage with rise time ranging from 35 ns to 500 ns, and standard lightning impulse voltage with rise time of 1.2 μs. The turn-to-turn voltage was studied for three consecutive disks to study the influence of rise time on the distribution of voltage along the disks. For lightning impulse for the first disk, the highest turn-to-turn voltage of 0.4 per-unit were obtained at the end of the disk, and the highest voltage derivative of 7.2 per-unit/μs is recorded at the beginning of the disk. The highest turn-to-turn voltage and voltage derivative were obtained for delta connected winding as compared to wye connected winding because the delta winding is stressed at both ends. The turn-to-turn voltage, and voltage derivative are highest for the first disc as compared to second and third discs; this is because the transient wave has to propagate long distances into the disc, and the resistance and stray capacitance reduced the voltage as it travels down the winding. A delta connected winding with applied step voltage of rise time 35 ns had the highest turn-to-turn voltage of 0.49 per-unit recorded at the beginning of the disk 1 and the highest voltage derivative of 35 per-unit/μs recorded at the beginning of the disk 1. But for the same delta winding with applied step voltage of rise time, 500 ns gave the highest turn-to-turn voltage of 0.13 per-unit recorded at the end of the disk 1 and the highest voltage derivative of 3 per-unit/μs recorded at the beginning of the disk 1. The turn-to-turn voltage is 3.7 times higher for a step voltage with the rise time of 35 ns as compared to 500 ns, and also, the turn-to-turn voltage derivative is ten times higher. Shorter rise time can lead to interlayer resonance that can cause very high voltage at the initial turns of the disc. Thus, shorter rise time leads to higher turn-to-turn voltage, and its derivative along the disk. In general, standard lightning impulse are applied to design basic insulation level for a transformer. It can be seen that when the winding terminals are stressed by shorter rise time step voltage, the turn-to-turn voltage can be higher than lightning impulse stress, so care must be taken while designing the insulation considering the high-frequency very fast transients [37].

Ansari et al. used a 12-coil and an 18-coil sections transformer simulation models to evaluate the non-uniform voltage distribution along the transformer for fast rise time impulse voltages [38]. For lightning, switching, and chopped voltage waveforms, the highest voltage stresses were observed at the

initial two coils of the transformer winding. Liu et al. studied the distribution of lightning impulse along each section of a dry-type transformer winding [39]. They found that the maximum of impulse voltage exceeds the input and is located in sections 3, 4, 5 of the transformer rather than in the first section. Florkowski et al. compared the distribution of sinusoidal sweep, rectangular, chirp signal, and sweep ramp waveforms along the transformer winding with the lightning impulse distribution [40]. The above mentioned waveforms were used to replicate the transient voltage generated during the operation of the surge arrester and the circuit breaker. The overvoltage along 1/3 of the transformer turn due to the application of rectangular, sinusoidal sweep, sweep ramp waveforms exceeded the overvoltage caused by the standard lightning impulse voltage. Studying the conventional steel core and amorphous core transformers for distribution of internal and transferred overvoltages under fast rectangular impulse, Florkowski et al. found that transferred overvoltages are higher for the amorphous core as compared to the silicon steel core [41]. Bagheri et al. applied a standard lightning impulse voltage on a continuous, interleaved, inter-shield disk with one shield turn per disk, and an inter-shield disk with six shield turns per disk windings to analyse the impulse voltage distribution along each of the windings [42]. Among all the configurations, the inter-shield with six shield turns per disk winding provided the best linear voltage distribution because the total series capacitance is highest for the configuration which also leads to low oscillation. The transient voltage stresses the transformer insulation due to non-linear initial distribution, resonance, and induced voltage. The non-linear distribution of the transient voltage, resonance, and induced voltage along the transformer depends on the configuration of the transformer based on the transformer capacitances [29]. Although, considerable work was carried out in understanding the distribution of transient voltage along the transformer winding but the experiments were carried out for a single pulse and not for the repetitive transient voltage. The distribution of the repetitive transient voltage along the transformer winding based on transient parameters including the amplitude, duty cycle, and rise time is not considered in the literature in detail even though it is an important aspect to design the transformer inter-turn insulation.

2.2 Influence of fast transient parameters on machine insulation

Ageing of machine insulation under repetitive fast transients has been studied extensively in the literature due to the converter driven machines that are susceptible to these transients [43]-[47]. Switching converter fed induction machine can be subjected to repetitive steep voltage pulses that can

lead to partial discharge in the machine insulation, in turn, causing its failure. Fast transients generated by the IGBT (Insulated Gate Bipolar Transistor) converters have rise time in the range of 50 - 1000 ns and the switching frequency in the range of 1 - 20 kHz. The effect of rise time, voltage amplitude, duty cycle, switching frequency, and polarity of the transients on the machine insulation have been considered in the above studies. Observation made by the researchers points out that the insulation is aged faster with the faster rise time, higher voltage amplitude, and higher switching frequency. Also, the ageing is faster for a unipolar pulse as compared to bipolar pulse. But there are few contradicting results with regards to the influence of the repetitive transient parameters on the ageing factor of the machine insulation. For instance, Yin reported that the bipolar pulses have a shorter time to failure of the insulation due to higher partial discharge as compared to unipolar pulses [44]. Also, Moonesan et al. [47] reports that time to failure of the insulation were independent of the rise time for a 50% duty cycle; whereas, for a 15 % duty cycle faster rise time resulted in faster time to failure, so the influence of the rise time depends on the duty cycle of the transient. The present section describes the influence of the transient parameters on the ageing of machine insulation considering the vast literature on this topic, and the study of machine insulation ageing can be used to understand the basics of transformers paper-oil insulation failure aged under repetitive transient voltage.

2.3 Influence of fast transients on the transformer paper-oil insulation

The high dV/dt and high-frequency repetitive transients generated by the operation of voltage source converters (VSC) and switching of vacuum circuit breakers can impose significant deterioration of transformer paper-oil insulation, and thus, the current section describes in detail different works carried out on the influence of transients on paper-oil insulation.

Khanali et al. examined the influence of distorted voltages on wind turbine step-up transformer considering the effects of internal resonance and high-frequency dielectric behavior [48]-[51]. The authors considered two studies to understand the transient influence on paper-oil insulation. The first study involved a comparison of paper-oil insulation ageing under AC supply and voltage source converter transient with switching frequency of 3 kHz and rise time of 1.4 kV/μs on two identical wind turbine step-up model transformers. The authors measured partial discharge, oil temperature, dissolved gas content, and dielectric frequency response to understand the deterioration level of the insulation. The above measurements were carried out at 100, 200, 500, and 960 hours of ageing. It was shown that

the partial discharge level of transformer stressed under transient reached 9300 pC; whereas, for sinusoidally stressed transformer, the PD level was as low as 21pC. The temperature measured for the transient aged transformer was higher than for the sinusoidally aged transformer, but the difference was not predominant. For gas analysis, the transient fed transformer had higher dissolved gas as compared to AC fed transformer. The percentage dissipation factor versus frequency (dielectric frequency response) for the transient aged transformer was greater than sinusoidally aged transformer by an amount of 50, which indicates that the transformer aged severely under transient conditions. The second study involved the relation of repetitive transient voltage parameters viz., rate of rise, and repetition frequency on the PD inception of the paper-oil insulation. The electromagnetic detection technique to measure partial discharge for paper-oil insulation is difficult due to high interference when the test voltage is a pulse. Thus, the researchers used the hydrogen gas generation rate under a controlled environment to obtain the PD parameter. A linear relation between PD energy level and hydrogen gas generation has been obtained, in which the PD energy is proportional to the repetition frequency because the dead time of the pulse is very large as compared to its decay time. A similar observations have been made with machine insulation by Moonesan et al [52].

For a peak amplitude of 4.4 kV impulse, the slower rise time showed an increase in hydrogen gas content with time; whereas, faster rise time showed no hydrogen gas generation and, no PD inception. Thus, it was concluded that slower rise time leads to lower partial discharge inception voltage (PDIV). Also, the authors showed that the PDIV decreased with an increase in repetition frequency, especially when the dead time is almost comparable to the duration of the impulse. Thus, the higher frequency voltage can lead to faster degradation of the paper-oil insulation. The transient voltage of 6 kV peak (greater than PDIV) with a repetition frequency of 1 kHz and varying rise time of 1 kV/μs, 2 kV/μs, 5 kV/μs and 11 kV/μs were applied on the paper-oil insulation. Faster rise time had a greater rate of generation of hydrogen gas, which indicated higher PD energy levels. The authors conclude that a faster rise time increased PDIV, but once PD begins, it had PD energy higher as compared to the slower rise time [15].

Koltunowicz et al. [53]-[60] demonstrated the degradation of paper-oil insulation under repetitive transients and proposed an ageing model correlating time to breakdown and repetition frequency of the transients. The study used square wave, single pulse, and AC waveform with superimposed repetitive

transient voltage along with temperature effect on the ageing of paper-oil insulation. The diagnostic technique used for obtaining the deterioration level of paper-oil insulation was time to breakdown, breakdown voltage, loss tangent of the insulation, and life curve Weibull distribution parameters. The rise time and repetition frequency of the square pulse were varied to study their effect on breakdown voltage and partial discharge inception voltage of the paper-oil insulation when stressed under square waveform. The repetition frequency was incremented in steps of 1 kHz ranging between 1 kHz and 10 kHz. The 63.2 % failure rate probability voltage of the insulation decreased with an increase in repetitive frequency and a decrease in rise time (faster rise time). Thus, it was concluded that the insulation degrades faster for higher repetition frequency and lower rise time. The research also focussed on the application of a single voltage pulse on the paper-oil insulation to investigate the influence of the rise time and the polarity on the breakdown voltage of the paper-oil insulation. For rise time varying from 0.3 μs to 2.7 μs, the faster rise time leads to lower breakdown voltage. Also, it was shown that the paper-oil insulation has a higher dielectric strength for negative impulse voltages as compared to positive impulse voltage. The paper-oil insulation was stressed with AC voltage superimposed with 1 kV transient having a dV/dt of 1 kV/μs and variable switching frequency from 1 kHz to 10 kHz. The author considered the frequency of the repetitive transients and magnitude of the AC signal as the main parameters for the ageing process of paper-oil insulation. The average time to breakdown for 1 kHz transient voltage were 34 hours ± 13 hours reduced to 21 hours ± 5 hours for 5 kHz and 10 hours ± 3 hours for 10 kHz. The reduction in the magnitude of the AC signal leads to an increase in the time to the breakdown of the insulation. The authors also measured the loss factor for the paper-oil insulation for a varying frequency of the repetitive transient voltage ageing. High electric stress and increased repetition frequency caused the scission of the paper's polymer chain in the paper-oil insulation, which in turn caused the increase in loss factor. Moreover, time to breakdown follows an exponential relationship with repetition frequency; whereas, the time to breakdown follows the inverse power relationship with the magnitude of the carrier sinusoidal waveform.

Vandermaar et al. compared the 50 % breakdown probability voltage of the paper-oil insulation for the steep front (10 ns/2500 μs), switching (120/1400 μs, and 250/2500 μs), and lightning impulse (1.2/50 and 5.7/130 μs). They obtained the breakdown voltage versus time and multiple impulse breakdown data for steep front impulse waveform [61]. The 50 % breakdown strengths were lowest for steep front impulse and highest for switching impulse. It was also reported for paper-oil insulation

under steep front waveform, the 50 % breakdown strength showed values lower than the basic impulse level (BIL). The breakdown voltage versus time curve had a discontinuity at 50 ns due to the difference in the breakdown process at a lower time scale. Also, the multiple impulse breakdown obtained by applying 9 million pulses at the same location had proved that the risk of insulation failure could occur at the field of 100 kV/mm.

Kiiza et al. studied the phase-resolved partial discharge pattern (PRPD) for a cavity in the sheets of paper-oil insulation under three different electric stresses [62]. The first stress applied was HV impulse along with early PD at elevated AC stress for short duration, second stress was HV impulse with the prolonged application of PD at elevated AC stress, and thirdly prolonged PD at elevated AC stress application alone. The first stress of HV impulse and elevated AC stress for short duration did not cause substantial changes in the PRPD pattern and did not degrade the insulation, which was cross-checked by visual inspection. The prolonged AC test caused changes in the PRPD pattern but did not damage the insulation significantly. Prolonged AC, along with the impulse, caused changes in PRPD pattern and significant damage to the insulation. The combined prolonged AC and impulse stress caused a large drop in the total PD charge and repetition rate, thus the authors concluded it as a sign of heavy insulation degradation. The authors attributed the decrease in PD charge and repetition rate to increased dielectric losses due to ageing when the insulation was stressed with combined impulse and prolonged PD at AC stresses.

Wang et al. studied the influence of AC high-frequency voltage signal on the characteristics of partial discharge and dissolved gas for the paper-oil insulation model [63]. The column-plate electrode was used to simulate the surface discharge on paper-oil insulation. The frequency of the applied signal was 50 Hz, 10 kHz, 20 kHz, and 30 kHz. The maximum partial discharge amplitude under 50 Hz frequency was greater than the high-frequency signal. The distribution of partial discharge for high-frequency is more concentrated as compared to widespread discharge patterns for 50 Hz signal. For high-frequency, maximum discharge amplitude increased from 10 to 20 kHz, and above 20 kHz the discharge amplitude started decreasing. The gas production rate for the high-frequency signal was 2-4 times higher than for the 50 Hz frequency applied signal, and thus, the deterioration rate for the high-frequency signal was higher. For high-frequency cases, gas production rate increased till 20 kHz and then decreased similar to partial discharge amplitude pattern. Thus, the increase in frequency increased partial discharge

energy due to the increase of conductance and polarisation losses. But when the frequency reached a particular point (20 kHz), the fast charge absorption, release, and polarisation process reduced the discharge period and thus, reduced the growth of PD number in a single cycle.

The voltage amplitude versus the number of impulses to breakdown (V-N) characteristics of the paper-oil insulation was studied by Li et al. for lightning impulse waveform [64]. The study helped to understand the influence of accumulative effects under repeated application of the impulse. The turn-to-turn insulation model impregnated by oil were used as the test sample. The authors aged the sample at 130 °C for 0 hours (unaged), 278 hours, and 556 hours to simulate the accelerated thermal ageing behavior. For the V-N curve, the number of impulses to breakdown increased with decrease in applied voltage amplitude. For the thermal ageing of the insulation, the breakdown voltage increased with an increase in ageing time. The authors suggest that the thermal ageing weakened the mechanical property of the paper-oil insulation but strengthen the dielectric withstand capacity of the insulation which contradicts general understanding of the influence of thermal ageing time on the dielectric withstand capacity of the paper-oil insulation.

Sima et al. studied the effect of front time (1.2 to 26 µs) and tail time (25 to 300 µs) of the lightning impulse on the 50% breakdown voltage of the paper-oil insulation [65]. They found the relation between the time parameter and displacement current of the insulation subjected under the lightning impulse waveform using COMSOL Multiphysics® simulation studies. The 50% breakdown voltage value decreased with a shorter front time of the lightning impulse. The reason for this phenomenon was the steep front impulse (faster front time) leads to a higher displacement current that contributes primarily to the propagation of arc during the breakdown. From 1.2 to 15.6 µs front time, the 50% breakdown voltage increased drastically, but above 16.7 µs the breakdown voltage saturated. For an increase in tail time, the 50% breakdown voltage does not vary significantly. The simulation study indicated that the front time variation is related to the negative value of displacement current, and tail time is related to the positive value of displacement current. Also, the negative displacement current is very high as compared to the positive displacement current. Thus, the influence of front time is very evident for 50% breakdown voltage variation; whereas, tail time does not affect the breakdown voltage significantly compared to front time.

In [66], Sima et al. studied the influence of various parameters of double exponential impulse wave (DEIW) and bipolar oscillatory attenuated impulse wave (BOAIW) on the 50% breakdown voltage of the paper-oil insulation. The parameters for DEIW were front time (1.2 to 400 μs) and wave tail time (20 – 4500 μs), and for BOAIW, the parameters were oscillation frequency (50 Hz to 100 kHz), and attenuation constant (0.1 to 0.99). For DEIW, the 50% breakdown voltage decreased with an increase in wave tail time and saturated at the end, but this contradicts the results in [65]. Whereas the 50% breakdown voltage increased with an increase in front time and saturated at the end, which matches the result in [65]. For BOAIW, the breakdown voltage increased with an increase in attenuation constant. The breakdown voltage decreased with an increase in oscillation frequency up to 600 Hz. Above 600 Hz, the breakdown voltage started increasing with an increase in oscillation frequency. The authors obtained equivalence mapping between the BOAIW and DEIW data by using amplitude and change in the rate of impulse voltage as the equivalence variable.

Wang et al. studied the influence of front time and the oscillation frequency of the impulse voltage on the 50% breakdown strength of the turn-to-turn transformer paper-oil insulation [67], [68]. The impulse considered were oscillating lightning impulse waveform and very fast transient overvoltage (VFTO) waveforms. They showed that breakdown voltage decreased with an increase in front time (0.25 – 2.5 μs) based on the statistical lag principle. For the case of oscillating lightning impulse (170 - 340 kHz), the breakdown voltage increased with an increase in oscillation frequency. For very fast transient overvoltage (0.84 – 9 MHz), the breakdown voltage increased with an increase in frequency up to 2.4 MHz, above 2.4 MHz the breakdown voltage started decreasing with an increase in frequency. The reason for the “U” shape for breakdown voltage versus oscillation frequency is due to the steep front and high-frequency of the VFTO. The authors also observed that the breakdown voltage increased with an increase in the thickness of insulation for a single impulse voltage.

Balaji et al. studied the influence of repeated impulse front time, tail time, and the time interval between impulse applications on the deterioration of transformer paper-oil insulation [69], [70]. Their study obtained voltage verses number of the impulse to breakdown (V-N) characteristics of the insulation for various front times ranging from 0.064 μs to 1.4 μs, tail times ranging from 6.0 μs to 67 μs, and the time interval between impulse application ranging from 1 to 5 seconds. A decrease in front time leads to a decrease in breakdown voltage because lower front time can lead to higher dV/dt and,

thus, lower breakdown voltage. It was found that the breakdown voltage did not vary significantly with the tail time, but the degradation is quicker for larger rise time due to larger impulse energy. The authors also show that the breakdown voltage of the paper-oil insulation increased with an increase in the time interval between impulse application for a given impulse waveform.

Comparing studies carried out by Khanali [15] and Koltunowicz [71], we can see that the results contradict in terms of the influence of rise time on PDIV. Koltunowicz obtained that the faster rise time decreased PDIV; whereas, Khanali reports faster rise time increased PDIV. Thus, the influence of rise time on the degradation of paper-oil insulation needs to be studied in detail. For the case of the influence of high-frequency on the partial discharge of paper-oil insulation, Koltunowicz [71] considered frequency up to 10 kHz and obtained that partial discharge activity increased with an increase in frequency. Wang et al. [63] also studied the influence of high-frequency on partial discharge and conveyed that partial discharge increased with an increase in frequency up to 20 kHz, and then the discharge amplitude started reducing. Thus, the U curve for the partial discharge versus switching frequency needs to be investigated in detail.

From [66], [69], [71], it is clear that breakdown voltage for a transformer insulation increased with an increase in front time of the impulse voltage; whereas, in [67], it is reported that the breakdown voltage decreased with increase in front time of the impulse voltage. The results obtained for breakdown voltage versus front time are contradicting in the range from 250 ns to 2.5 μs.

In [71], the breakdown voltage decreased with an increase in repetition frequency in the frequency range of 1 kHz to 10 kHz; whereas, in [66], the breakdown voltage increased with an increase in oscillation frequency in the frequency range of 600 Hz – 1 kHz. As the voltage waveforms considered are different, further analysis needs to be carried out to understand the behavior of paper-oil insulation as a function of signal frequency and the rise time of the transients. The analysis of paper-oil insulation ageing under different amplitude, rise time, and switching frequency of the transient voltage are necessary because these transients generated by wind-farm system can lead to deterioration of the insulation. Also, very few researchers have focussed on the influence of rise time, repetition frequency, and amplitude of the transients on the ageing of the transformer paper-oil insulation. Thus, detailed research needs to be carried out for paper-oil insulation ageing under different transient voltage parameters.

2.4 Transformer diagnostic technique

There are various techniques used to diagnose the transformer paper-oil degradation. The techniques include measurement of dielectric frequency response, polarisation and depolarisation currents, sweep frequency response analysis, and partial discharge measurements. The present section discusses in detail each of the measurement technique:

2.4.1 Dielectric frequency response

Dielectric frequency response (DFR) or frequency domain spectroscopy is the measurement of capacitance and loss tangent of transformer insulation for a scan of frequency ranging from 0.2 mHz to 10^7 Hz. The DFR measurement indicates the transformer insulation ageing status; and the literature about the DFR along with the parameters affecting DFR is explained below:

In [72], Anglhuber et al. show the influence of temperature, oil conductivity, insulation geometry, and water content on the dielectric frequency response of the paper-oil insulation. As transformer paper-oil insulation ages, the oil conductivity and water content increase. An increase in oil conductivity or temperature leads to a shift in DFR towards high-frequency. The increase in water content in the insulation increases the DFR at higher frequency (> 10 Hz) and lower frequency (< 0.005 Hz). The water content influence is seen on the loss tangent (DFR) due to an increase in polarisation and conductivity. The frequency range between 0.005 Hz to 10 Hz is not affected significantly due to an increase in moisture content. Generally, higher frequency is not best to detect water content influence since oil conductivity plays a higher role at higher frequency. Thus, increase in water content can be observed more prominently below 0.005 Hz. At certain times tip-up test is also used where the loss tangent is measured at a single frequency but increasing applied voltage. The DFR can measure capacitance and loss tangent for the insulation between transformer high and low voltage windings, between high voltage winding and tank, and between low voltage winding and core. Since the insulation between high voltage and low voltage winding mainly consists of paper, the DFR obtained are predominantly influenced by paper (cellulose) material. The DFR between high voltage winding and tank, and low voltage winding and core are influenced by both oil and paper (cellulose). For measuring the capacitance and the loss tangent between low voltage and high voltage windings, a sinusoidal voltage is applied to the high voltage winding, and the current is measured through low voltage winding. So the change in capacitance indicates a breakdown in the capacitance layer of the insulation; whereas,

an increase in loss tangent can be due to water, ageing, bad connection, and carbonized particle in the insulation. Influence of each parameter viz., oil conductivity, insulation geometry, and water content are visible at each frequency bands of DFR, and the extensive database of DFR can be used to obtain oil conductivity and water content in paper-oil insulation. Figure 2.1 shows the influence of each parameter mentioned above, on the dielectric frequency response of the transformer's paper-oil insulation.

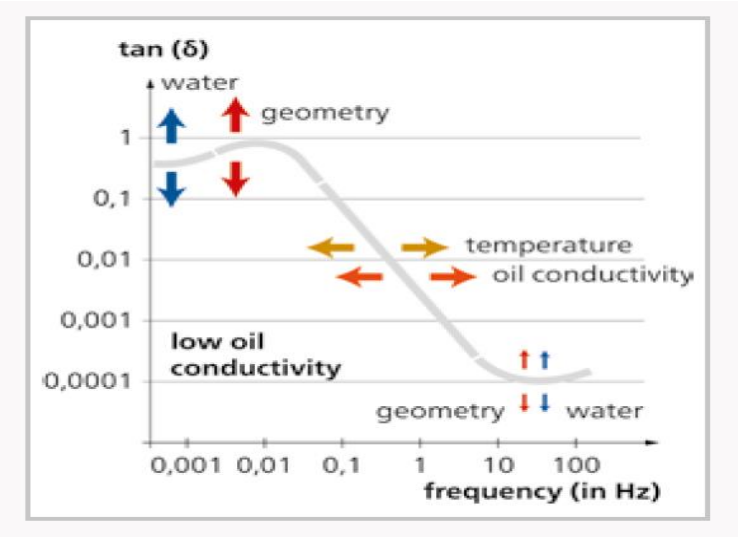

Figure 2.1: Dielectric frequency response of the transformer's paper-oil insulation [72].

Jaya et al. [73] found that for the frequency range between 10 Hz to 1000 Hz, the cellulose insulation (water content) is the prominent factor influencing DFR. The conductivity of the oil causes a steep slope at 0.01 Hz – 1 Hz, the ageing by-product in oil, like acids can increase the conductivity and affect the frequency range between 0.01 Hz and 1 Hz. The peak below 0.01 Hz is due to interface polarisation caused by the ratio of oil to pressboard geometry. The region below 0.0005 Hz is influenced by cellulose paper/pressboard reflecting the water content in the paper as well as ageing by-product like acid in the oil. The authors also conclude that for moisture measurement, lower bound of DFR measurement for new, dry insulation should be very low about 100 µHz; whereas, for the conductive wet hot aged insulation, it can be 10 mHz. Zheng et al. [74] studied the dielectric frequency response in the frequency range from 10 – 10^7 Hz for the insulation of transformer winding, and pressboard barriers of the oil ducts. The authors used four different fitting models viz., Debye, Cole-Cole, Davidson-Cole, and Havriliak-Negami to fit the measured dielectric frequency response. The loss tangent decreased

gradually from 10 Hz to 30 Hz, and then between 40 Hz to 10000 Hz, the values are almost constant. Above 10000 Hz, the loss tangent value starts increasing again till it peaks at 2 MHz. From the various fitting models, it was found that the Havriliak-Negami model provided the best fit. The fitting model also found that the relaxation time of the insulation model is greater for paper-oil insulation as compared to only paper insulation. The reason is the existence of interfacial polarisation in paper-oil insulation that leads to its higher relaxation time.

Jadav et al. [75] studied the DFR for paper-oil insulation for different moisture content aged at 105 °C. They found that the impact of ageing by-product, ageing of pressboard on DFR, is significantly smaller than the influence of moisture content. The increase in moisture content can lead to an increase in polarisation and conduction current and, thus, increase in loss tangent at both low frequency and high-frequency regions of the DFR. The authors also inform that it is very difficult to separate the ageing factor impact from the moisture influence on the DFR measurement. Nikjoo et al. [76] obtained the online DFR by using lightning and switching transients, and studied the influence of moisture content (2.4, 3.0, 5.5 %), and temperature (22, 60, 100 °C) on the DFR response (loss tangent) obtained from the transients. The rise time/fall time of the lightning impulse and switching impulse used were 1.2/50 μs and 250/2500 μs respectively, and the measurement voltage for online DFR was 10 V_{peak}. The increase in moisture content increased loss tangent, and the increase in temperature caused a shift in loss tangent to high-frequency.

Dong et al. [77] explained the DFR based on the polarisation and conduction losses, and also studied the influence of the ageing condition and moisture on DFR. From the DFR, the authors explain that for the frequency range of 0.001 Hz to 0.1 Hz, the conductivity contributes to the DFR; whereas, for the frequency range of 1 Hz to 1 kHz, the polarisation process (paper-oil interfacial polarisation) contributes to the DFR. While the frequency range between 0.1 Hz to 1 Hz is the overlap region where both conduction and polarisation processes contribute to DFR. The increase of moisture content leads to an increase in the DC conductivity at the low-frequency region; thus, the authors obtain an exponential relation between moisture content and DC conductivity. The ageing produces moisture, so it contributes to conduction loss increase at the low frequency, and also, the ageing causes increased polarisation loss at the high-frequency region. Pradhan et al. [78] modeled a non-linear model of paper-oil insulation using a non-sinusoidal excitation for DFR measurements. The approach was followed

since the authors considered that the paper-oil insulation behaves in a non-linear fashion. The non-sinusoidal time-domain signal applied consisted of various combinations of pseudo square waveforms of several frequencies so that it has a constant frequency response from 0 – 1 kHz. The approach mathematically decomposed the measured paper-oil insulation response into nonlinear and linear blocks. The non-linear nature of the paper-oil insulation is removed by the non-linear block, and the analysis is carried out on the remaining linear block of the DFR response. The authors concluded that the non-linear model was able to estimate the moisture content in paper-oil insulation more accurately as compared to the linear sinusoidal DFR model.

2.4.2 Polarisation and depolarisation currents

The polarisation and depolarisation current (PDC) responses are time-domain approach to obtain the dielectric characteristics of the paper-oil insulation. A DC voltage is applied for a long time across the insulator, which charges the insulator, and the polarisation current is measured. The polarisation current activates different polarisation processes with its respective time constants and also has a conductivity component of the insulation. The insulation is shorted for a very long period, and the depolarisation current or discharge current is measured. The depolarisation current does not include the contribution from the conductivity of the insulation material.

Fofana et al. [79], investigated the influence of thermal transients on the PDC measurement of the paper-oil insulation. The temperature variation is expected in the transformer due to the operating condition of the transformer, and moisture migration between paper and oil is affected significantly due to temperature variation. Thus, temperature variation can influence the PDC characteristics of paper-oil insulation. The temperature effect was analysed by the authors by conducting three sets of experiments; (i) constant temperature of 25 °C, 65 °C, 42 °C, (ii) increasing the temperature from 25 °C to 65 °C, and (iii) decreasing the temperature from 65 °C to 31 °C. For first set of experiments, the PDC increased with an increase in temperature due to spontaneous polarisation during an increase in temperature. During the increasing and decreasing of temperature, the PDC measurements are effected because, with increasing temperature, the relative water saturation of oil increases and moisture enters into oil from cellulose. During the decrease in temperature, the water migrates from the oil back to cellulose material. Thus, the authors recommend cooling the transformer for a sufficient interval of time before measuring the PDC.

Jadav et al. [80] used both DFR and PDC measurements to obtain the influence of moisture (0.2 %, 1.8 %, 2.3 %) and temperature (40 °C, 60 °C, 80 °C) on the dielectric response of the paper-oil insulation. The moisture has polar water molecules, thus, an increase in moisture increased polarisation current, and increase in temperature increased the mobility of charge carrier and, thus, the conductivity. The authors obtained the conductivity of the oil and paper from both PDC and DFR measurements. For DFR, the loss tangent shifted towards high-frequency for an increase in moisture and temperature. As expected, the DC conductivity increased with temperature and moisture, and also, the DC conductivity extrapolated from dielectric responses gave similar result. Ma et al. [81] also studied the influence of temperature variation on PDC and DFR measurements and found that an increase in temperature increased the PDC and DFR loss tangent value. Zeng et al. [82] studied the PDC for paper-oil insulation aged at electric field of 10 kV/mm. The ageing time was from 0 (unaged) to 100 hours in steps of 20 hours. With the increase in ageing time, the polarisation and depolarisation current increased, and the authors suggest two reasons to explain this phenomenon. Firstly the ageing of cellulose and oil causes by-products like acid and moisture, increasing the conductivity of the insulation and, thus, the PDC. Secondly, during ageing the cellulose can have an increase in fractal decomposition, and the oil can enter this gap. Thus, there is an increase in the paper-oil interface polarisation, and thus, the PDC increases. From the depolarisation current, the authors also found that with an increase in ageing the trap charge density of the insulation increased, and also, the trap depth deepens. The reason can be attributed to accumulated charges with ageing time due to an increase in paper-oil fractal decomposition and ageing by-products. The authors also show that with an increase in ageing the depolarisation current increased.

2.4.3 Partial discharge measurement

The PD are discharges that bridge a part of insulation between two conducting electrodes. The partial discharge can be used as an indicator to obtain the quality of the insulation. Some of the partial discharge parameters are magnitude, inception voltage, extinction voltage, phase-resolved partial discharge pattern, and the number of PD pulses. The PD signal is measured using a conventional coupling capacitor, UHF antenna, acoustic sensor, and dissolved gas contents. There is a lot of work carried out on measurement and analysis of PD parameters, and few of them addressing the transformer paper-oil insulation considering transient conditions are discussed below.

Nikjoo et al. [83] presented the change of surface and cavity discharge under the influence of the HV impulse on paper-oil insulation. The positive impulse was superimposed at the positive peak of the AC signal to replicate the real transformer situation. The PD pattern before and after impulse for various defects and moisture content in the paper-oil insulation are studied. The partial discharge was measured by a coupling capacitor of 1 nF and a detection impedance of 1 kΩ. The moisture contents were 3 %, and 5.5 %, and different discharges are surface, and cavity discharges. The surface discharge showed an increase in magnitude and number of PD due to the application of impulse. Also, for surface discharge, the PD magnitude decreased at the instant of impulse application, and then it increased. The moisture could create weak spots that can lead to further PD occurrences. For cavity discharge, the increase in moisture leads to an increase in the number and magnitude of the PD pulses. The authors inform that for each of the PD (surface or cavity) along with moisture content had a specific PD pattern that can be used as a signature for future identification of the PD type. Yuan et al. [84] obtained that the degradation of the paper-oil insulation is divided into four stages, starting from partial discharge initiation to the final breakdown. Each stage can be identified by changes in partial discharge parameters like magnitude, repetition rate, power spectrum, phase count, and accumulation of dissolved gas. The PD detection technique used by the authors included the convectional impulse current detection system, and dissolved gas analysis. In the initial period, various partial discharge parameters like magnitude, repetition rate, and dissolved gas were very low. After 200 minutes, the PD parameter started growing, which indicates PD initiation. At about 360 minutes the PD parameter increased rapidly in an irreversible fashion pointing towards intense PD, and finally, it was observed that the PD parameter grew exponentially, marking the breakdown of the insulation.

Yuan et al. [85] studied the partial discharge pattern for power frequency and transient overvoltage for a large step-up transformer using an ultra-high-frequency (UHF) detection technique. The UHF sensor were installed in the maintenance hole of the operating transformer. The authors conclude that the PD discharge patterns are stochastic for transient overvoltage, but the patterns are periodic for power frequency voltage under stable operating conditions. Thus, the PD pattern and signature can be used to identify various discharge patterns and to obtain the reason for discharges. Kiiza et al. [62] discussed the influence of HV impulse with the early stage of elevated AC stress PD activity, HV impulse with prolonged elevated AC stress PD activity, and only prolonged elevated AC stress PD activity on the phase-resolved partial discharge pattern (PRPD). The PD was analysed for a cavity embedded in the

paper-oil insulation. The PD measurements were carried out with a coupling capacitor of 1000 pF and detection impedance of 1 kΩ. The PD parameters were PD charge and average number of PD pulse per 50 Hz cycle. The prolonged AC stresses were 8 kV/mm, and lightning impulse of 1.2/50 µs rise time/fall time, peak stress of 40 kV/mm field were applied. The results showed that high voltage impulse along with prolonged elevated AC stress PD activity provided the highest change in PRPD pattern. The impulse with prolonged elevated AC stress PD activity also caused a decrease in PD parameters like PD charge and average number of pulses. The reason could be due to an increase in dielectric losses and, thus, can lead to damage of paper-oil insulation.

2.4.4 Frequency response analysis

Frequency response analysis (FRA) is the measurement of the transfer function of a transformer over a wide frequency range, typically from 20 Hz to 2 MHz. The transfer function can be voltage ratio, input impedance, or admittance of the transformer. The input voltage is applied on one end of the transformer winding, and the response voltage can be measured either at another end of the same winding or different winding of the transformer. The windings not included in measurement can either be open-circuited or short-circuited. The transformer can be viewed as a network of circuit elements like inductance, capacitance, and resistance, and these elements are responsible for the variation of transformer transfer function with the frequency (FRA). Any changes in the transformer's geometry, and insulation property can vary the transformer's circuit element, and affect the FRA. Each transformer has a unique FRA signature, and any changes in the signature due to transformer defects, and degradation can be identified in the FRA signature. Thus, FRA is used as a diagnostic tool to measure the amount of damage to the transformer by comparing the FRA signature of the transformer with suspected damage to the reference signature measured during healthy state of the same transformer. The FRA measurements are highly sensitive in detecting winding damage (mechanical deformation). FRA can also detect paper-oil degradation since they sense changes in oil temperature, and insulation moisture content.

Khanali et al. [86] studied the influence of internal short circuit fault on the transfer voltage, and input impedance frequency response of the transformer. The authors used three transformer models with different winding, and core designs to understand the trend of frequency response for varying locations of internal short circuits. The transformer model tested was 500 kVA three-phase, 9 kVA

single-phase, and 1 kVA single-phase transformers. The creation of nine artificial shorts was made by pulling various connection leads from different layers of the transformer. The FRA signature for healthy and artificial short circuits was compared by visual inspection and mathematical difference factor. The difference factor is the difference between healthy and short circuit FRA signatures. The study concludes that for transfer voltage measurement the difference factor is higher for short circuit in the inner layer close to the core, and the difference factor reduces as the short circuit move towards the outer layer of the transformer. For input impedance, the difference factor was highest when the short circuit is in the middle region of the winding. And also, the input impedance difference factor decreased as the short circuit was moved from the middle layer towards the inner layer, and middle layer towards the outer layer. Thus both the input impedance FRA and voltage transfer FRA can be used as a complementary technique to obtain the location of the short circuit fault along the layers of the transformer.

Gustavsen et al. [87], [88] used a combination of the transformer terminal admittance matrix, and the voltage transfer frequency response to obtain a high-frequency black box model for the transformer. The admittance matrix was obtained for two winding transformers in the sweep frequency range of 50 Hz to 1 MHz. It was informed that the measurement cable could affect the frequency response results, and the authors successfully removed this effect by deleting the capacitance of the cable from the admittance matrix. The obtained admittance frequency response matrix was subjected to rational approximation, passivity enforcement, and converted into time domain EMTP model. The model was used to simulate the transformer response under step voltage input, and it could be seen that the simulated and measured response of the transformer matches closely. Thus, the model can be used to simulate the terminal response of the transformer for various high-frequency transient studies. Soloot et al. [89] discussed the typical signature of voltage ratio frequency response for a 500 kVA transformer with three different winding designs viz., layer, disc, and pancake winding. The internal and external voltage ratios were obtained for the 11/0.240 kV 500 kVA transformer for the sweep frequency range from 10 kHz to 10 MHz. The internal voltage ratio frequency response was obtained for various taps in the winding, and the voltage difference between the taps was obtained. The authors found that the transformer voltage ratio FRA had a resonance at 800 kHz, and the amplitude of the resonance were 6, 20, and 38 per-unit for the disc, layer, and pancake windings. The layer winding had another resonance frequency at 1.6 MHz, which was the dominant frequency with the amplitude of the voltage ratio equal

to 80 per-unit. For the internal voltage ratio, the voltage ratio difference between the taps indicates the internal stress between the transformer turn-to-turn insulation. For layer and pancake windings the turn-to-turn voltage ratio difference at resonance frequency is highest near HV terminal, and it decreased when the turn-to-turn voltage ratio difference at resonance frequency is taken in the middle and near the ground end of the winding. For disc winding, the turn-to-turn voltage ratio difference at resonance frequency is high all along the winding from HV terminal to ground. Thus, the authors suggest that the turn-to-turn voltage ratio difference FRA signature can be used to indicate turn-to-turn stress during the resonance amplification of the transformer. When the transformer is stressed with high-frequency transients generated by circuit breaker operation in the wind farm system, the transient can have a frequency component that can match the transformer turn-to-turn resonance frequency. Thus, the internal turn-to-turn stress can be very high during resonance frequency matches and can lead to degradation of the transformer insulation.

Yousof [90] discussed different models to represent transformer winding and their accuracy in simulating the frequency response. The models used were a ladder network, multi-conductor transmission line (MTL), and hybrid multi-conductor transmission line (Hybrid MTL) model, and the author compared the simulation results with the measurement results. The ladder network model was extremely time-consuming since the transformer electric circuit needs to be drawn, and also, the model could not differentiate the FRA response between the continuous and interleaved transformer designs. The MTL model took into account each conductor in the winding and was able to distinguish between FRA of various transformer designs, but the modeling takes a lot of computation time. The Hybrid MTL model divided the transformer winding into each disc and modeled its frequency response. Thus, the Hybrid MTL model took less computation time as compared to the MTL model, but the Hydrid MTL model can not differentiate FRA response between the continuous and interleaved transformer design. The MTL model was used by the author to simulate the changes in the geometrical parameters (resistance, inductance, and capacitance) during different transformer fault conditions. Thus, the influence of various fault conditions on the FRA was observed. The author shows that slight changes in transformer winding construction, tap position, and non-tested winding condition can considerably affect the frequency response. The author also informs that similar winding damage with different transformer designs can produce different changes in FRA response. Two main FRA interpretation techniques viz., statistical technique, and Nyquist plot were used to obtain the difference between a

healthy transformer and a faulty transformer. A severity level for various deformation like tilting and bending of the conductor was recognized by the Nyquist plot and statistical technique (correlation coefficient) of the FRA interpretation. The author also confirms that FRA measurement is significantly affected by the changes in moisture content in paper-oil insulation. Since moisture content increased with an increase in the ageing status of the paper-oil insulation, thus, the author shows the applicability of FRA in obtaining the ageing status of the transformer.

The author in [37] shows that when the rise time of applied step voltage was 35 ns the highest turn-to-turn voltage due to the transient occurred in the initial turn of the winding; whereas, when the rise time was 500 ns, the highest turn-to-turn voltage occurred on the end of the winding. The operation of the circuit breaker can lead to very high-frequency steep repetitive voltage transients, and when the frequency of transient matches the natural frequency of turn-to-turn voltage, the voltage escalation can be very high. The voltage amplification can be either in the initial turns or at the end of the winding. The literature focusses on the influence of transient parameters on the distribution of turn-to-turn voltage along only one test transformer winding, and it does not correlate the transient distribution with the transformer's natural oscillation frequency. Studies have been carried out in the past to analyse the transformer internal resonance frequency characteristics [28]-[34] but the correlation between the transient response along the transformer winding and its internal frequency response is not completely understood, hence, it is important to match the transient voltage amplification with the internal frequency response of the transformer. Although, considerable work was carried out in understanding the distribution of transient voltage along the transformer winding [35]-[41] but the experiments were carried out for a single pulse and not for the repetitive transient voltage. Also, the earlier researchers were unable to show the capability of various transfer functions to demonstrate the transformer’s resonance frequency amplification. Thus, the current thesis presents the methodology of frequency response and transient response measurements, and internal frequency response characteristics for two model transformers aged under different voltage waveforms. The capability of three transfer function frequency responses; namely, magnitude of voltage difference response in dB, voltage ratio difference response, and impedance difference response to demonstrate the tap-to-tap voltage difference resonance amplification are presented in the thesis. The transient distribution of the transformer as a function of repetitive transient voltage parameters (rise time, amplitude, and duty cycle) is studied for obtaining the maximum tap-to-tap transient voltage for different cases of transient voltage parameters. The

correlation between transfer function frequency response and the transient response of the transformer is analysed. In addition, simulation of the transformer equivalent circuit is carried out in PSCAD simulation software to study the transient voltage distribution along the transformer winding for different transient voltage parameters.

Comparing studies carried out by Khanali [15] and Koltunowicz [71], we can see contradicting results in terms of the influence of rise time on PDIV. Wang et al. [63] studied the influence of high-frequency transient on partial discharge activity and conveys that partial discharge increases with an increase in frequency up to 20 kHz, and then the discharge amplitude started reducing. Thus, the U curve for partial discharge versus switching frequency needs to be analysed in detail. The results obtained for breakdown voltage of paper-oil insulation versus front/rise time in [66], [69], [71] are contradicting with [67] in the range from 250 ns to 2.5 µs. Also, in spite, the frequency of consideration are repetitive frequency [71] and oscillation frequency [66], it can be seen that the relationship between breakdown voltage and the frequency of the impulse contradict each other. Also, the analysis of responses like dissipation factor, polarisation and depolarisation current are extensively studied for thermal ageing of the paper-oil insulation [72]-[82]. But the influence of the parameters (rise time and switching frequency) of the repetitive transient voltage on the ageing responses including the dissipation factor, polarisation, and depolarisation current for the long-term ageing of paper-oil insulation are not analysed in detail. Thus the current thesis involves the study of the influence of transient parameters including rise time, and switching frequency on the transient voltage ageing of the transformer paper-oil insulation. Additionally, the influence of transient voltage parameters on the dissipation factor response of the aged paper-oil insulation is obtained by following two-factor design of experiments.

2.5 Thesis motivation

In the present power industry, there is considerable amount of pressure in extending the limits of the transformer to their maximum life for economic purposes. This leads to evaluation of life expectancy of the transformer paper-oil insulation for various parameters of the applied voltage. In recent years, the advent of renewable energy resources has introduced new high-frequency stresses on paper-oil insulation. These stresses are developed due to operation of power electronics converters and circuit breakers during integration of renewable power like wind power to the main electric grid. Under such

stresses, various parameters like rise time, switching frequency, voltage magnitude, and duty cycle influence transient voltage distribution along the transformer winding. Also, these transient stress may contribute to the internal voltage resonance within the transformer windings.

Transformers are of different rating and have different behavior under varying transient parameters. So in-depth analysis needs to be carried out to understand the influence of transient voltage distribution along various transformers subjected under different transient parameters. The transformer transient voltage distribution mainly stresses the paper-oil insulation, and the degradation of the insulation leads to decrease in life of the transformer. Very few researchers [15], [37], [63], [66], [67], [69], [71] have studied the influence of transient parameters on paper-oil degradation using indicators like partial discharge, breakdown voltage but the results are contradicting for transient parameters effects and are inconclusive. The influence of repetitive transient voltage parameters on the dissipation factor, polarisation, and depolarisation current responses of the aged paper-oil sample are not investigated thoroughly. The detailed analysis of the influence of transient parameters on the paper-oil insulation is essential to obtain the ageing degree of the transformer under new repetitive transient stresses. This knowledge can help in checking the health of the transformer to prevent any major outage that can occur due to amalgamation of the renewable energy system into the grid.

2.6 Thesis objectives

Based on the mentioned shortcomings in the literature, the present research involves understanding the transformer insulation degradation under repetitive transients. The parameter of repetitive transient voltage considered are rise time, voltage amplitude, switching frequency, and duty cycle. Specific objectives are categorized into the following fields:

1. To obtain the distribution of repetitive transients along the transformer winding for varying rise time, voltage amplitude, and duty cycle, and relate the responses with the frequency response of the transformers in order to quantify the stresses on winding insulation under transient conditions.
2. To assess the abilities of various transfer function frequency responses in demonstrating the tap-to-tap voltage difference resonance amplification using model transformers.

3. To understand the basics of insulation degradation of the paper-oil composites under repetitive transient voltage by analysing the ageing response including dielectric frequency response, polarisation and depolarisation current, and partial discharge measurements.
4. To obtain the effects of the transient voltage parameter including rise time and switching frequency on the ageing response of the transformer paper-oil insulation by following two-level two-factor design of experiments.
5. To compare the transient voltage ageing of paper-oil insulation for two mineral oils, namely Luminol TRi oil and Voltesso 35 oil in order to obtain the oil that is best suited for the transformers facing repetitive transient voltage.

Chapter 3
Methodology

The present chapter describes the methodology and test set-up to carry-out the research objective. The chapter is divided into two sections. Section 3.1 describes the set-up to obtain the distribution of the repetitive transients along the transformer winding. Section 3.2 describes the experiments carried out to obtain the influence of repetitive transient parameters on the ageing of paper-oil insulation.

3.1 Distribution of transient voltage along the winding of the transformer

3.1.1 Transformer model

In the current study, four test transformers namely transformer 1, 2, 3, and 4 were used [15]. The transformers are transformer 1 (T1, 1 kVA aged under application of sinusoidal voltage), transformer 2 (T2, 1 kVA aged under application of repetitive transients), transformer 3 (T3, 9 kVA unaged transformer) and transformer 4 (T4, 9 kVA unaged transformer having an electrostatic shield between the secondary and primary winding) [15]. The specifications for transformers 1 and 2 are provided in Table 3.1, and specifications of transformers 3 and 4 are provided in Table 3.2.

Table 3.1: Transformer T1 and T2 specifications [15].

Output kVA rating	1 kVA
Transformer Type	Single-phase, Oil filled
Low/High Voltage Rating	115 V/6.6 kV
Connection Taps (10)	One in every layer
Nominal Frequency	60 Hz
Number of turns for Low Voltage winding	130
Number of turns for High Voltage winding	7480

Table 3.2: Transformer T3 and T4 specifications [15].

Output kVA rating	9 kVA
Transformer Type	Single-phase, Oil filled
Low/High Voltage Rating	345 V/19.8 kV
Connection Taps (10)	One in every layer
Nominal Frequency	60 Hz
Number of turns for Low Voltage winding	130
Number of turns for High Voltage winding	7462

The transformers (T1 to T4) are layer-type transformer consisting of 10 connection taps taken out from each layer (Figure 3.1) of the high voltage winding [15]. All four transformers were made of paper-oil insulation. Transformers T3 and T4 were scaled-up versions of T1 having turns ratio of wind turbine step-up transformers used in Ontario, Canada. The electrostatic shield between the primary and secondary winding of transformer T4 was connected to the ground using a telfon insulated wire.

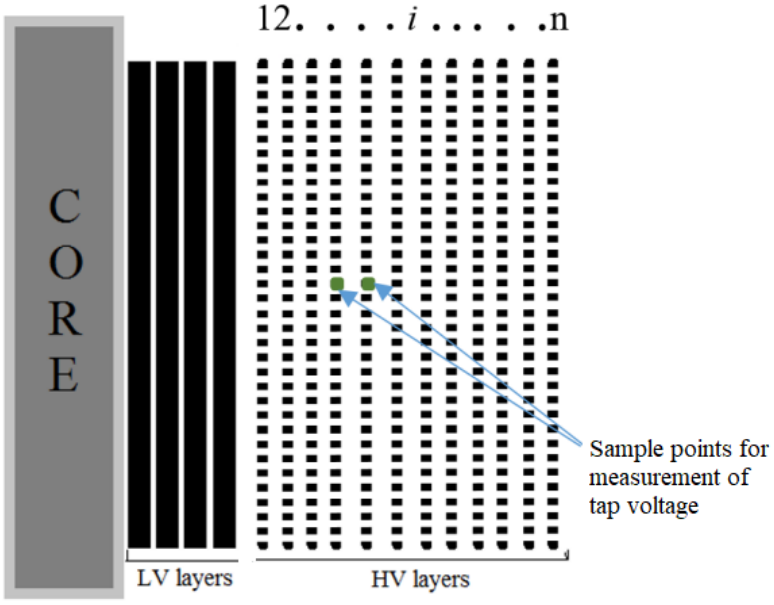

Figure 3.1: Numbering of layers along the transformer winding [15].

Transformer T1 was aged under the application of a sinusoidal voltage (60 Hz) with a magnitude of 138 V at the primary winding. Transformer T2 was aged under repetitive transient voltage with a rate of rise of 1.4 kV/μs and a switching frequency of 3 kHz. The magnitude of repetitive transient voltage were adjusted to a level similar to the sinusoidal voltage. Both the power frequency and transient ageing were carried out for a duration of 960 hours at room temperature.

3.1.2 Frequency response measurement

The present study compares three types of transfer function frequency responses; they are, magnitude of voltage ratio frequency response in dB, impedance frequency response, and voltage ratio frequency response. The magnitude of voltage ratio frequency response in dB of transformers is measured using the experimental set-up shown in Figure 3.2. A sinusoidal voltage with varying frequency from 20 Hz – 2 MHz and amplitude of 10 V peak-to-peak is applied across the line terminal (tap 11) of the transformer (source, S) and the ground. The voltage across tap 11 and ground is the reference voltage, VREF. The voltage measured individually across the taps 1 to 10 with respect to ground is the response voltage, VRES. The magnitude of voltage ratio frequency response in dB as a function of source voltage frequency is calculated by the following formula:

$$Magnitude\ of\ voltage\ ratio\ frequency\ response\ in\ dB = 20\ log\frac{VRES}{VREF} \qquad (3.1)$$

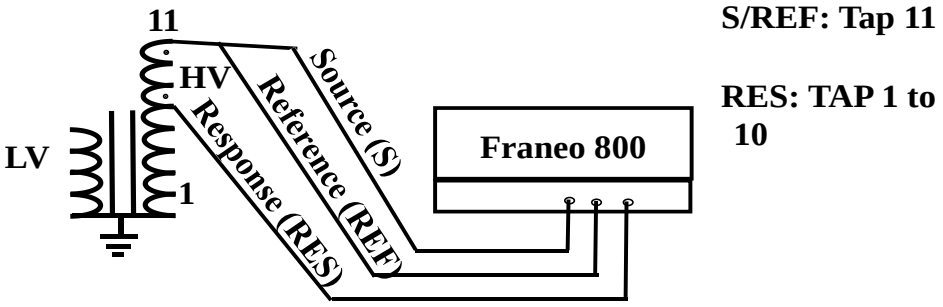

Figure 3.2: A schematic of a frequency response measurement set-up [91].

The frequency response is measured by using the OMICRON Franeo 800 device. The Franeo 800 is a sweep frequency response analyser (SFRA) [91]. For the frequency response measurement, three coaxial cables having an impedance of 50 ohms each were used to obtain the source, reference, and response voltages. All three coaxial cables were of the same length.

The impedance frequency response of transformers is measured using the experimental set-up shown in Figure 3.3. The source voltage is a sinusoidal voltage with varying frequency from 20 Hz – 2 MHz, and amplitude of 10 V peak-to-peak applied across tap 1 to tap 11 independently. The voltage measured across the source is the reference voltage, VREF. The response voltage, VRES is measured at fixed tap position, tap 0. The impedance frequency response as a function of source voltage frequency is obtained by the following formula:

$$Impedance\ frequency\ response = \frac{V}{I} = \frac{(\mathrm{VREF} - \mathrm{VRES})}{(\frac{\mathrm{VRES}}{50\ \Omega})} \qquad (3.2)$$

50 Ω in equation 3.2 is the impedance used to measure the response voltage, VRES. The voltage ratio frequency response of transformers is measured using the experimental set-up shown in Figure 3.2. The source voltage is always applied at tap 11. The voltage measured across the source is the reference voltage, VREF. The response voltage, VRES is measured across tap 1 to tap 10 independently. The voltage ratio frequency response as a function of source voltage frequency is obtained by the following formula:

$$Voltage\ ratio\ frequency\ response = \frac{VRES}{VREF} \qquad (3.3)$$

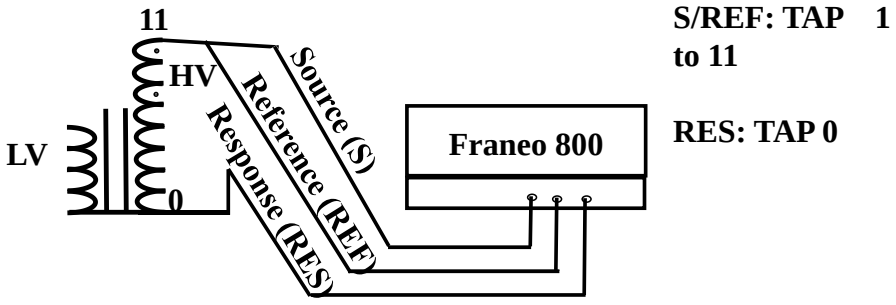

Figure 3.3: An illustration showing the experimental set-up for impedance frequency response measurements.

3.1.3 Transient response measurement

The transient response of transformers is measured using the experimental set-up shown in Figure 3.4. The application of repetitive transient voltage is on tap 11 and the tap 11 voltage is measured by the input probe. The influence of transient's parameter on its distribution along the transformer winding is obtained by measuring the response starting from tap 10 to tap 1 individually using an output probe. Tektronix P6015A probe (silicone dielectric) is used to measure the input voltage and the output response. The rise time and bandwidth of the probe are 4 ns and 75 MHz respectively. Rohde & Schwarz, RTO 1024 oscilloscope with bandwidth of 2 GHz and sampling frequency of 10 Gsa/s is used to record the input transient voltage and transient output response. Table 3.3 shows four cases indicating the values chosen for the parameters of the repetitive transient voltage. The amplitude, rise time, and duty cycle are the parameters of the transient voltage that were varied in the current study. The repetition frequency of the transient voltage is fixed at 1 kHz and the fall time of the transient voltage is 40 μs. Figure 3.5 show the transient voltage applied at tap 11 of the transformer T1, with amplitude = 100 V, duty cycle = 10%, switching frequency = 1 kHz, and rise time = 290 ns (case 1). These high-frequency repetitive transient voltages are representation of the voltages generated by the switching operation of the power electronic converters and the vacuum circuit breakers in a wind farm network.

The selection of transient voltage parameters including voltage amplitude, rise time, and duty cycle are based on the simulation studies carried out by Devgan [2]. By simulating the switching operation of the vacuum circuit breaker, Devgan showed that the switching operation generate repetitive transient voltage of frequency ranging from 450 Hz to 22 kHz, and rate of rise ranging from 1.1 kV/μs to 10 kV/μs respectively. Thus, the rise time (300 ns to 1000 ns), and voltage amplitude (100 V to 1000 V) were chosen based on the rate of rise of the transient voltage obtained in [2]. The influence of the duration of the transient voltage on its distribution along the transformer winding were studied by selecting the duty cycle of 10 % and 50 %.

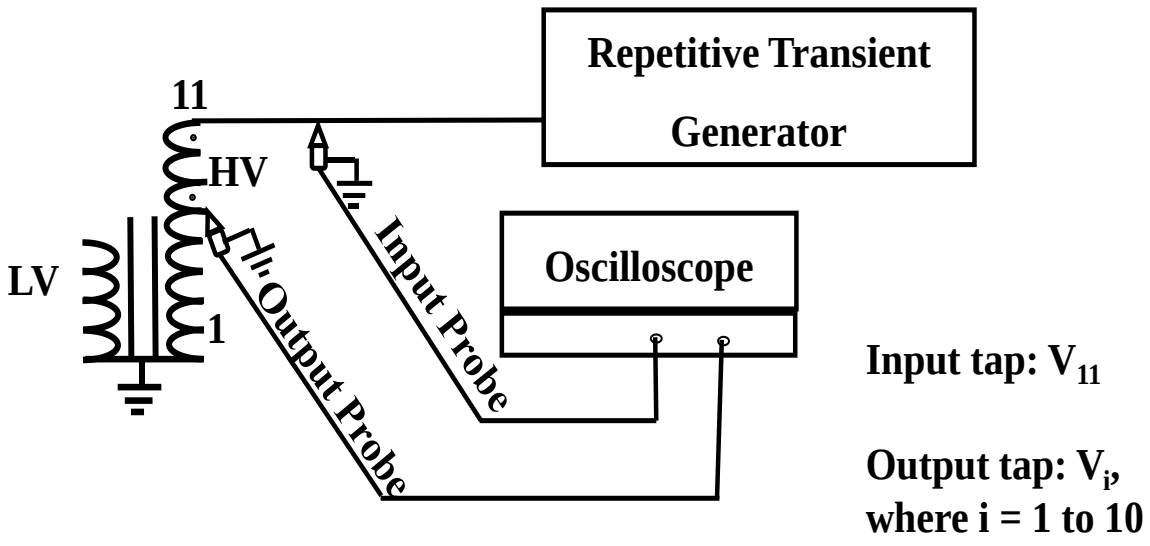

Figure 3.4: An illustration showing the experimental set-up for transient response measurements.

Table 3.3: Chosen values for various parameters of the repetitive transient voltages.

Cases	Voltage (V)	Duty cycle (%)	Rise time (ns)
Case 1	100	10	100 - 300
Case 2	100	50	100 - 300
Case 3	1000	10	100 - 300
Case 4	100	10	900 - 1100

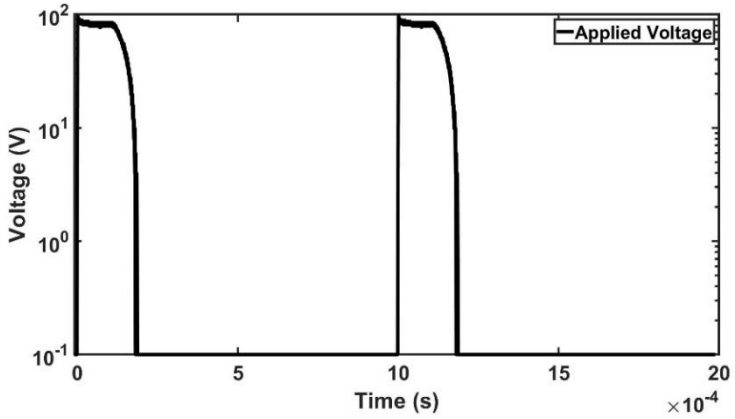

Figure 3.5: Repetitive transient voltage of amplitude = 100 V, duty cycle = 10%, switching frequency = 1 kHz, and rise time = 290 ns applied at tap 11 of the transformer T1 (case 1).

3.2 The influence of repetitive transient parameter on the ageing of paper-oil insulation

3.2.1 Transformer paper and oil details

3.2.1.1 Transformer paper sample

The paper sample is a kraft paper, used in simulating the transformer turn-to-turn insulation, with a breakdown strength of 75 kV/mm [15]. The epoxy coating in diamond shape is applied on the surface of the kraft paper.

3.2.1.2 Transformer oil

Test liquids used are Voltesso 35 oil and Luminol TRi oil. The Voltesso 35 oil is made of mixture of hydrotreated light naphthenic distillate and catalytic dewaxed light paraffinic oil. The Voltesso 35 oil has good heat transfer capability, and known to help in preventing corona discharge and arcing. Two types of Voltesso 35 oil; namely, Voltesso 35 A (was stored in laboratory for long time), and Voltesso 35 B (newly received oil), are used to study the effects of dielectric properties under fast transient conditions. On the other, the Luminol TRi oil is a relatively new oil that is being considered for transformers. It is made of isoparaffinic base oils that is thoroughly hydrotreated in order to minimize power loss. The Luminol oil has high oxidation stability. The electrical and chemical properties of

Voltesso 35 and Luminol TRi oil based on the specification data sheets are shown in Table 3.4. Table 3.5 shows the measured permittivity and electrical conductivity of all three test liquids. As can be seen, the electrical conductivity of Voltesso 35 A is significantly higher than the other two test liquids.

Table 3.4: Electrical and chemical properties of Voltesso 35 [92] and Luminol TRi mineral oil [93], respectively based on their specification data sheets.

Properties	Voltesso 35	Luminol TRi
AC dielectric breakdown voltage, 2.03 mm, ASTM D1816	63 kV *	65 kV
Flash point, ASTM D92	145 °C	170 °C
Tendency for gassing, ASTM D2300	30 µl/min	–10 µl/min
Viscosity @ 40 °C, ASTM D445	7.6 mm^2/s	9.2 mm^2/s
Power factor @ 60 Hz, 25°C, ASTM D924	0.0005	< 0.0001
Oxidation stability, sludge, 164 hours, ASTM D2440	0.2 %	< 0.01 %
Oxidation stability, acid number, 164 hours, ASTM D2440	0.5 mgKOH/g	< 0.01 mgKOH/g

* Measured value

Table 3.5: Relative permittivity and electrical conductivity of the considered oil samples.

Mineral oil	Relative permittivity	Electrical conductivity (pS/m)
Luminol TRi	1.87	1.03
Voltesso 35 A	1.98	24.7
Voltesso 35 B:	2.22	2.42

3.2.1.3 Paper-oil impregnation process

The following section describes the preparation of the paper-oil samples. The paper is first dried at 65 °C in an impregnating chamber at 75 Pa pressure for 24 hours. Separately, the oil is heated at 65 °C at 40 Pa pressure for 24 hours. The paper-oil impregnation is done at 60 °C for 24 hours in atmospheric pressure. The paper-oil sample after impregnation is kept in dry, ventilated, sealed container at room temperature [ASTM D2413-16].

3.2.2 Paper-oil insulation ageing test set-up

The section describes the repetitive transient ageing test for six rod-plane geometry of the paper-oil insulation. Various ageing response measurements including dielectric frequency response, polarisation current, depolarisation current, partial discharge, oil temperature, and hydrogen gas content are explained in the section. The ageing response measurement helps to obtain the ageing degree of the paper-oil insulation.

3.2.2.1 Six rod-plane geometry for paper-oil insulation ageing test

The setup for the ageing of paper-oil insulation using six rod-plane electrodes under a repetitive transient voltage is shown in Figure 3.6. The rise time of the repetitive transient voltage applied to the paper-oil sample is 220 ns and 650 ns, and the switching frequency is 1 kHz and 3 kHz. The amplitude and the duty cycle of the applied voltage transient is fixed at 6 kV and 50% respectively. The study used the above values based on PSCAD simulation of the high-frequency transient voltages on a wind-turbine set-up transformer obtained by Devgan et al [2]. A transient voltage of repetition frequency ranging from 450 Hz up to 22 kHz, and rate of rise ranging from 1.1 kV/µs to 10 kV/µs were obtained by Devgan during simulation of switching operation of the breakers. Thus, an applied voltage amplitude (6 kV), duty cycle (50 %), switching frequency (1 and 3 kHz), and rise time (220 ns and 650 ns) were selected to match the rate of rise obtained in the simulation study. In Figure 3.6, the metallic box has six rod-plane electrodes to age six paper-oil samples at a time. In each of the rod-plane electrodes, the rod electrode is connected to the high voltage (transient voltage supply) and the bottom plane electrode is grounded. The height and diameter of the rod electrode is 15.26 cm and 0.64 cm, respectively. The height and diameter of the bottom plane electrode is 0.79 cm and 4.44 cm, respectively. A circular

paper sample of diameter, 29 mm is chosen with a thickness of 0.127 mm [15]. The metallic box is designed so that a clearance of 5 cm is provided all around.

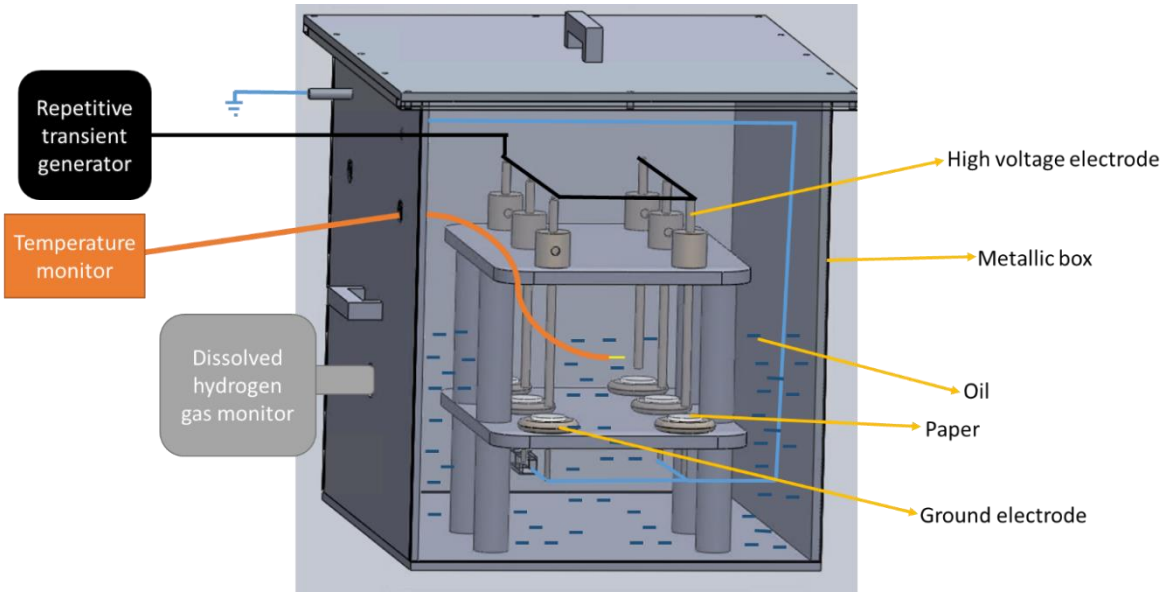

Figure 3.6: Set-up for ageing of paper-oil insulation using six rod-plane electrodes.

3.2.2.2 Dielectric frequency response

The dielectric frequency response measures the dissipation factor (DF/tan delta), capacitances, and power factor (PF) of a dielectric material. In this ageing study, the dissipation factor is measured for a range of frequency between 0.2 mHz to 10 kHz by applying a sinusoidal voltage of 140 Vrms across the paper-oil insulation and measuring the current through the insulation using Megger IDAX-300. The DFR of the paper-oil insulation depends significantly on the moisture level, temperature, and ageing by-products of the paper-oil insulation, and thus, it acts as an indicator for insulation degradation. The DFR measurement setup for an un-grounded specimen test (UST) is shown in Figure 3.7. In the figure, CR (red) represents the ageing chamber shown in Figure 3.6. The DFR measurement is conducted at room temperature [94].

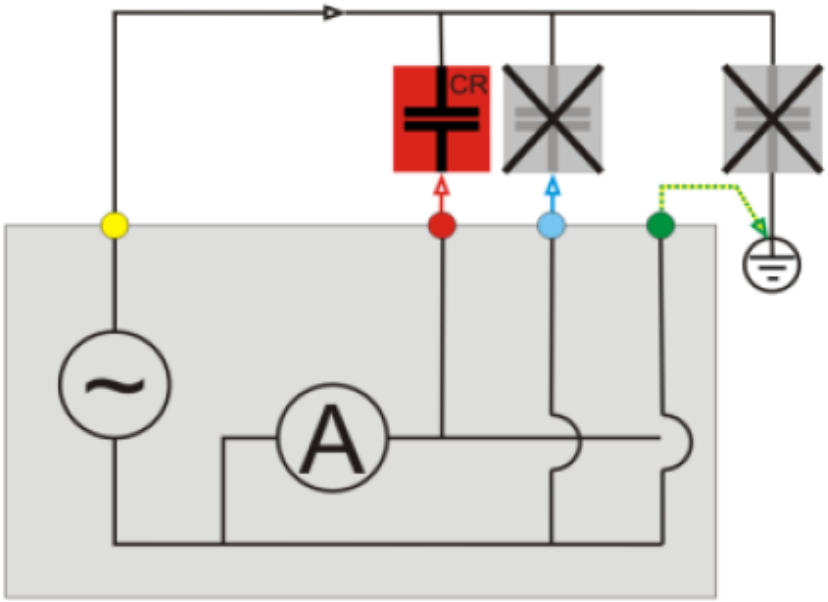

Figure 3.7: Dielectric frequency response measurement set-up for un-grounded specimen test (UST) [94].

3.2.2.3 Polarisation and depolarisation current measurements

A step voltage of 200 V is applied across the paper-oil insulation sample for a period of 2000 seconds, and the current through the insulation sample is the polarisation current. The polarisation current consists of both the conductive and displacement currents of the paper-oil insulation sample. After 2000 seconds the step voltage is removed and the paper-oil insulation sample is short-circuited, this leads to depolarisation current passing through the insulation sample. The depolarisation current is caused due to the relaxation of polarisation mechanisms that were present in the paper-oil insulation sample when the step voltage was applied. The polarisation and depolarisation current values of the paper-oil insulation depend significantly on the moisture level, and ageing by-product of the insulation [95].

3.2.2.4 Partial discharge measurement

Partial discharge is an indicator of ageing level of the paper-oil insulation. The partial discharge inception voltage (PDIV) and the partial discharge extension voltage (PDEV) are measured by using

the OMICRON MPD 600 test set-up. The MPD 600 unit measures the partial discharge level using a coupling capacitor in compliance with the IEC 60270 standard. The AC voltage source used for PD measurement has noise level less than 2 pC, and the PD test is carried out for unaged and aged paper-oil insulation [96].

3.2.2.5 Temperature measurement

The temperature of the paper-oil insulation during ageing is monitored by a Neoptix Reflex fiber-optical thermal sensor and the Neoptix temperature probe is shown in Figure 3.8. The Neoptix temperature probe is placed near the paper-oil insulation sample during the repetitive transient ageing, and the probe meets the electromagnetic compatibility requirement [97].

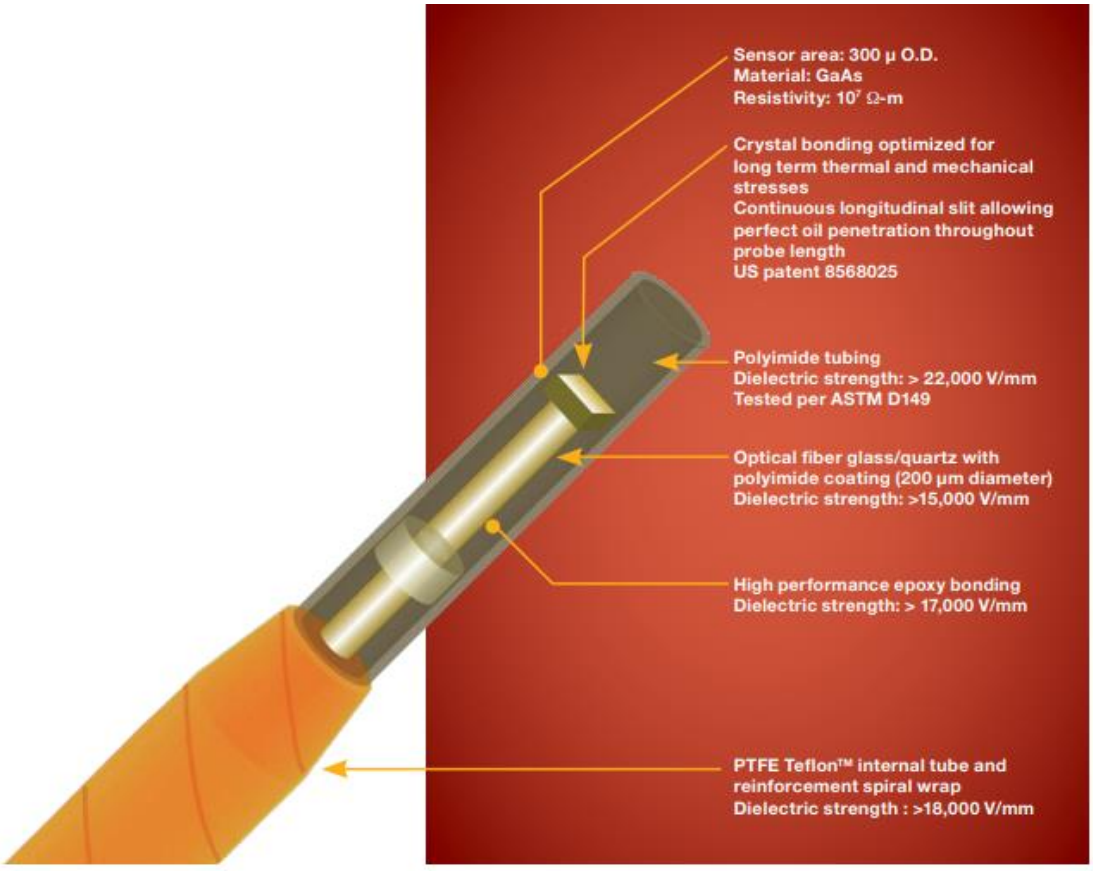

Figure 3.8: Neoptix temperature probe [97].

3.2.2.6 Hydrogen gas monitoring

The ageing of paper-oil insulation under a high electric field can lead to the generation of various gases like ethane, methane, ethylene, acetylene, and hydrogen, indicating the degradation of paper-oil insulation due to overheating, partial discharge and arcing. In the present study, hydrogen gas, which indicates the partial discharge occurrence, is monitored during the ageing of the paper-oil sample under repetitive transients. InsuLogix® H hydrogen monitor used in the current research work measure dissolved hydrogen gas level in oil with an accuracy of 25 ppm and measurement range between 25 ppm and 5000 ppm [98].

3.2.3 Design of experiments

The section describes the design of experiment technique to obtain the influence of transient voltage parameters (factors) on the transient ageing of transformer paper-oil insulation. The ageing responses are obtained for transformer paper-oil insulation aged under two levels of various factors of the transient voltage. The factors and their levels are mentioned in Table 3.6. The total number of treatments for the two-level, two-factor experiment is 4. The ageing response is the dissipation factor obtained for the paper sample sandwiched between standard parallel-plane electrodes of diameter 2.54 cm. For the dissipation factor measurement, the parallel-plane electrode geometry is placed in the position of CR (red) in Figure 3.7.

Table 3.6: Factors affecting ageing of paper-oil insulation with a fixed voltage applied.

Ageing factors	Level	
	Low level for the factor (-)	High for the factor (+)
Rise time of the transient	220 ns	650 ns
Switching frequency of the transient	1 kHz	3 kHz

Chapter 4
Experimental Results

The present chapter describes the results of the research work. The chapter is divided into two sections. Section 4.1 discusses the result pertaining to the voltage distribution of the repetitive transients along the transformer winding. Section 4.2 discusses the result pertaining to the experiments carried out to obtain the influence of repetitive transient voltage on the ageing of paper-oil insulation.

4.1 Distribution of transient voltage along the winding of the transformer

The section shows the frequency response and the distribution of the transient voltage along ten taps of the test transformers. In section 4.1.1, the sweep frequency response along the transformer winding is obtained to understand the behavior of the transformer transfer function as a function of sinusoidal voltage frequency. Section 4.1.2 discusses the influence of different parameters of the transient voltage on the distribution of the transient along the transformer winding. The equivalent circuit of the transformer is simulated by using PSCAD simulation software. The simulation results showing the distribution of transient voltage along the transformer winding as a function of transient voltage parameters, is presented in Appendix A.

4.1.1 Frequency response measurement

The magnitude of voltage ratio frequency response in dB is presented for the four model transformers (T1, T2, T3 and T4). Figure 4.1 and Figure 4.2 show the magnitude of voltage ratio frequency response in dB along the taps of transformers, T1 and T2, respectively. Along the winding, moving from the innermost core-end tap to the outermost high-voltage terminal tap of the transformer, the winding locations are identified with tap numbers. The figures indicate that the magnitude of voltage ratio frequency response in dB increases with an increase tap number in the low-frequency region (<100 Hz). The self-inductance of the winding increases with increase in tap number leading to increase in the magnitude of frequency response in the low-frequency region. In the high-frequency region (10 kHz - 20 kHz), the magnitude of voltage ratio frequency response in dB initially decreases from tap 1 to tap 3, and then the response magnitude increases up to tap 9. The transformer design is the reason for the above mentioned behaviour in the resonance region (10 kHz - 20 kHz). The highest magnitude

(dB) at the resonance frequency of 20 kHz for transformer T1 and T2 are -94 dB and -80 dB, respectively.

The magnitude of voltage difference response in dB as a function of applied voltage frequency for transformers T1 and T2 are shown in Figure 4.3, and Figure 4.4, respectively. By subtracting the magnitude of voltage ratio frequency response in dB for adjacent taps, the magnitude of voltage difference response in dB is obtained. The magnitude of voltage difference at the resonance frequency of 20 kHz for transformer T1 is highest across taps 3-4 with an absolute value of 23 dB (Figure 4.3). Whereas, the magnitude of voltage difference at the resonance frequency of 20 kHz for transformer T2 is highest across taps 1-2 with an absolute value of 16 dB (Figure 4.4). The magnitude of voltage ratio frequency response in dB (Figure 4.1, and Figure 4.2) for transformers T1 and T2 show considerable increase in value from tap 3 to tap 5.

Figure 4.5 and Figure 4.6 show the magnitude of voltage ratio frequency response in dB along the taps of transformers, T3 and T4, respectively. In low frequency region (<100 Hz), the magnitude of voltage ratio frequency response in dB increases with an increasing tap number (similar to transformers T1 and T2). In the high-frequency region (7 kHz), the magnitude of voltage ratio frequency response in dB initially decreases from tap 1 to tap 3, and then the response magnitude increases from tap 3 to tap 9. Compared to the aged transformers T1 and T2, the increase in the magnitude of voltage ratio frequency response in dB from tap 3 to tap 5 is lower for transformers T3 and T4 in the resonance region. The magnitude of voltage difference response in dB as a function of applied voltage frequency for transformers T3 and T4 are shown in Figure 4.7, and Figure 4.8 respectively. Both the transformers T3 and T4 show similar voltage difference magnitude (dB). For the considered frequency range, the highest magnitude of voltage difference is seen for Taps 9 and 10. The transformer, T4 has a metallic shield between the low voltage and high voltage winding; whereas, transformer T3 does not have a metallic shield between the windings. The metallic shield between the primary and the secondary winding of transformer T4 is connected to the ground. The magnitude of voltage difference response (dB) is not influenced by the metallic shield, which was also shown in [32].

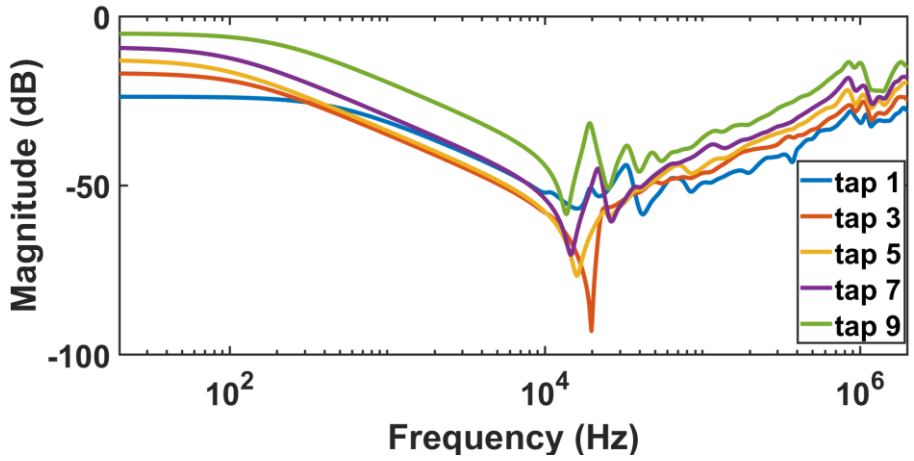

Figure 4.1: Magnitude of voltage ratio frequency response in dB for Transformer T1

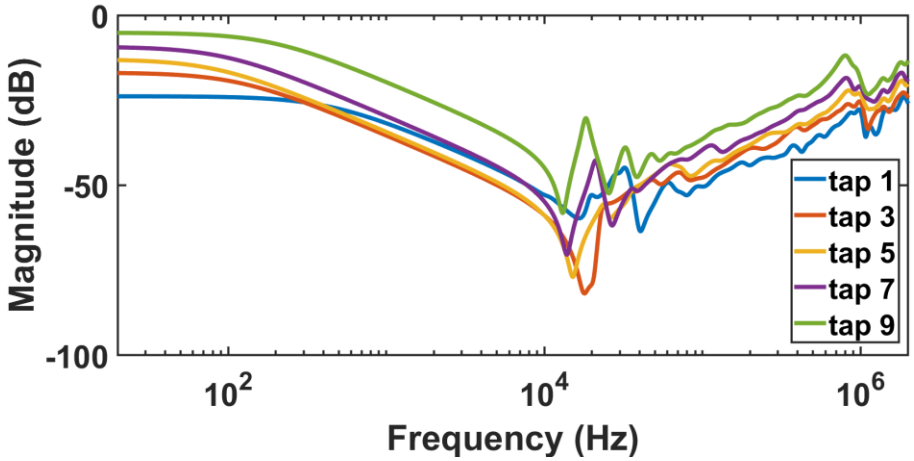

Figure 4.2: Magnitude of voltage ratio frequency response in dB for Transformer T2

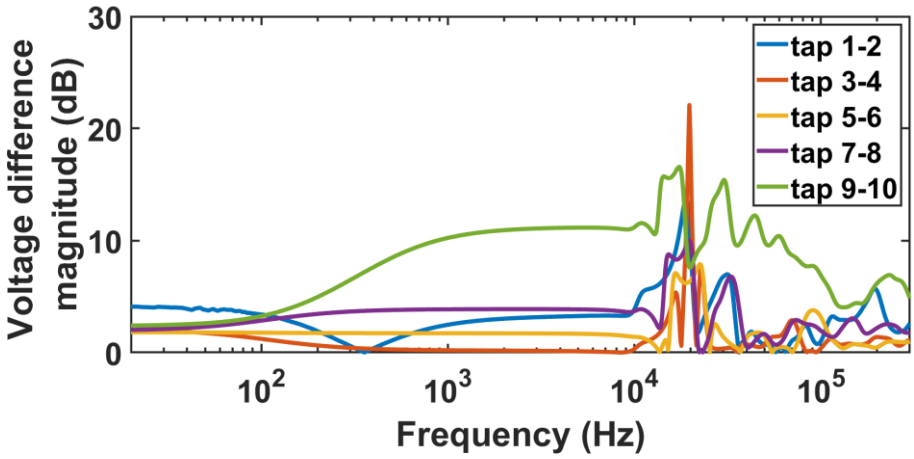

Figure 4.3: Magnitude of voltage difference response in dB as a function of applied voltage frequency for Transformer T1

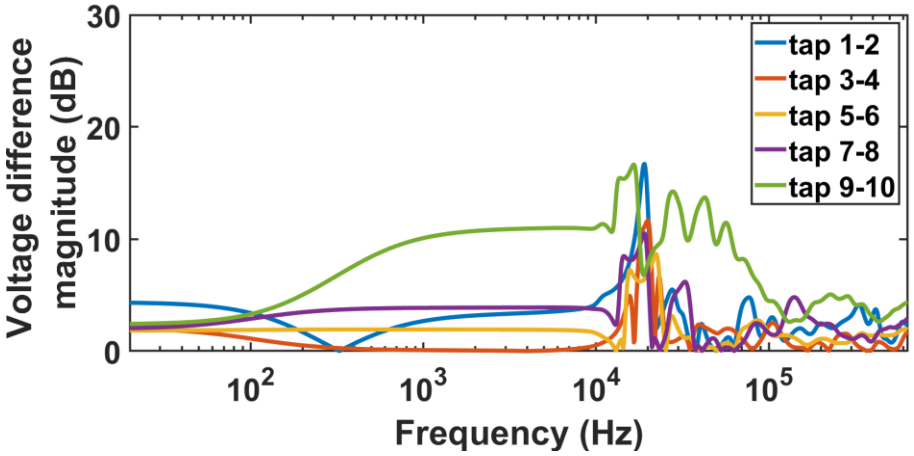

Figure 4.4: Magnitude of voltage difference response in dB as a function of applied voltage frequency for Transformer T2

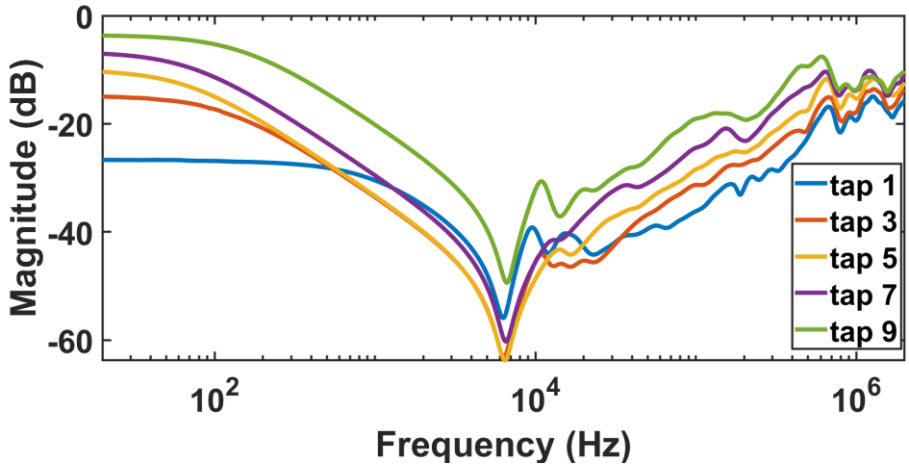

Figure 4.5: Magnitude of voltage ratio frequency response in dB for Transformer T3

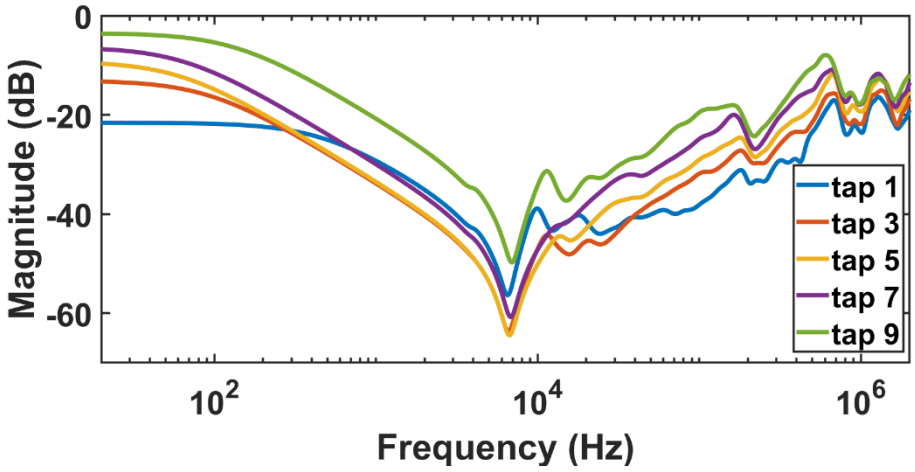

Figure 4.6: Magnitude of voltage ratio frequency response in dB for Transformer T4

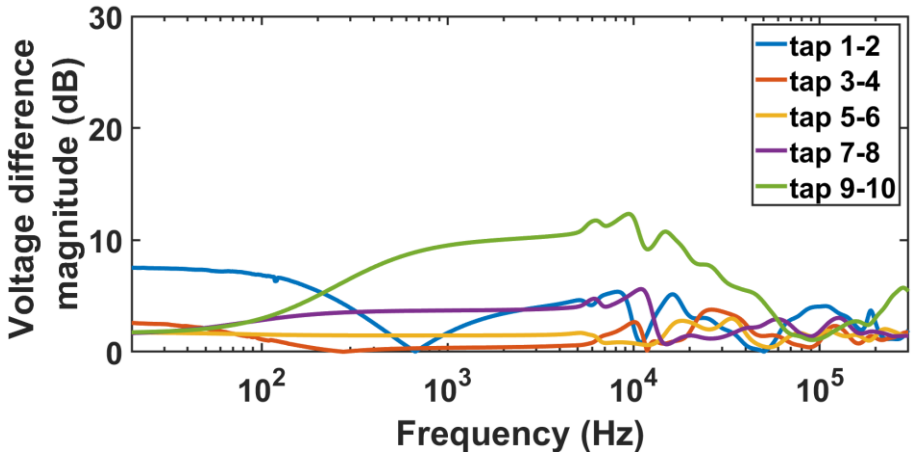

Figure 4.7: Magnitude of voltage difference response in dB as a function of applied voltage frequency for Transformer T3

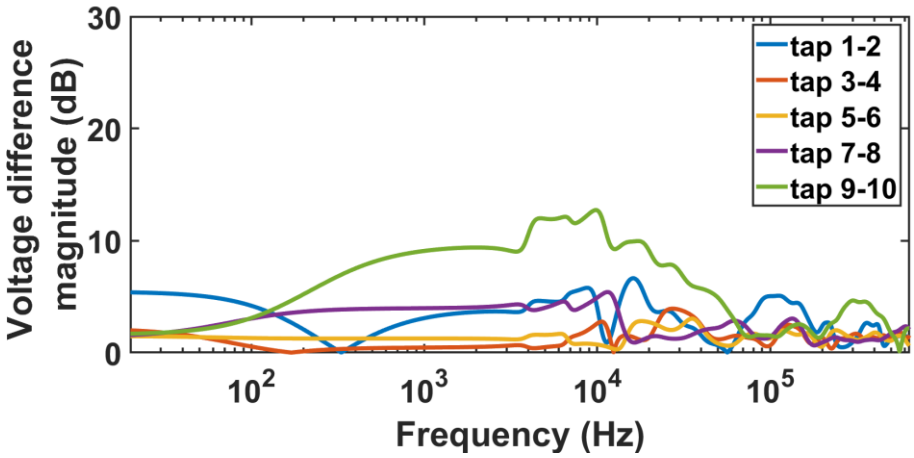

Figure 4.8: Magnitude of voltage difference response in dB as a function of applied voltage frequency for Transformer T4.

Three types of transfer function frequency responses are compared; namely, the magnitude of voltage ratio frequency response in dB, voltage ratio frequency response, and impedance frequency response for transformers T1 and T2. The results for the magnitude of voltage ratio frequency response in dB along the taps of Transformers T1 and T2 were present in Figure 4.1 and Figure 4.2. The impedance response along the taps of Transformers T1 and T2 as a function of applied voltage frequency is shown in Figure 4.9 and Figure 4.10, respectively. The impedance frequency response for transformers T1 and T2 are similar. In the frequency region below 200 Hz, the impedance frequency response curve increases with the increase in tap number. The total inductance of the transformer governs the response in the frequency region below 200 Hz. At low frequencies, the impedance frequency response is inductive in nature, but at high frequencies, the impedance frequency response is capacitive in nature. The resonance frequency caused due to cancelation of series capacitance by inductive reactance, increases with an increase in tap number. There are two resonance frequencies in the impedance response, one around 10000 Hz and another between 100 Hz and 1000 Hz. The resonance frequency is critical when it matches with the frequency characteristics of the transient voltage. Tap-to-tap impedance difference response as a function of applied voltage frequency for Transformers T1 and T2 are shown in Figure 4.11 and Figure 4.12, respectively. By subtracting the impedance frequency response for adjacent taps, the tap-to-tap impedance difference response is obtained. The tap-to-tap impedance difference response is similar for both Transformers T1 and T2. There are two resonance frequencies in the impedance difference response, one around 10000 Hz and another between 100 Hz and 1000 Hz (similar to impedance frequency response). The resonance frequency for the impedance difference response increases with an increase in tap number for the frequency region between 100 Hz and 1000 Hz. It is seen that the resonance frequency and amplitude for impedance difference response are highest for tap 1-2 and tap 3-4, around a frequency of 10000 Hz. If the transient signal has a dominant frequency component around 10 kHz, then based on the impedance difference frequency response, there are chances of tap-to-tap resonance at the initial taps of the transformer winding. Thus, the analysis of transformer impedance response is crucial while designing the insulation for the transformer.

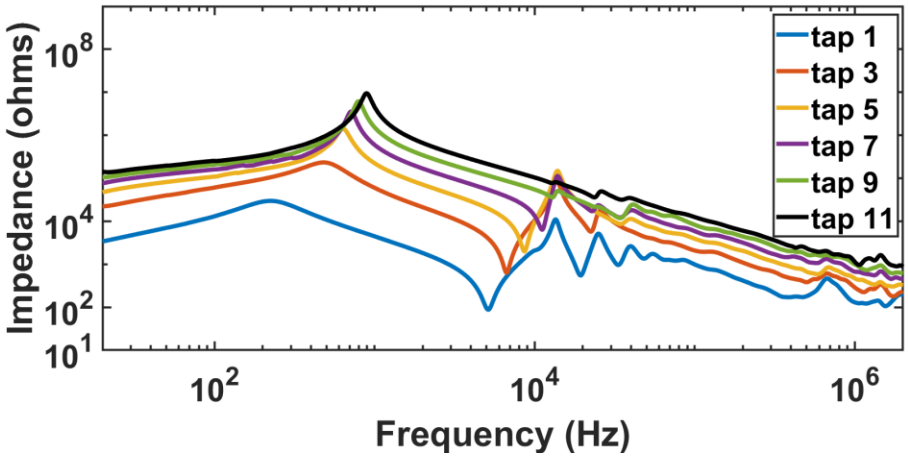

Figure 4.9: Impedance response as a function of applied voltage frequency for Transformer T1.

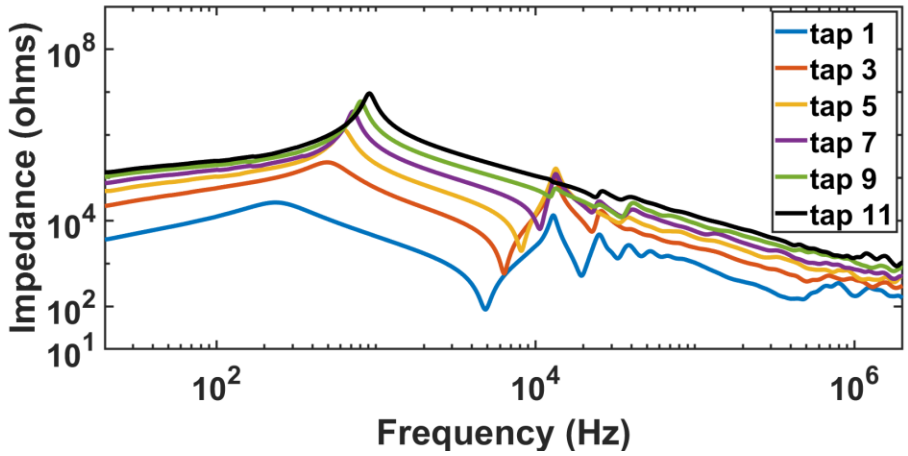

Figure 4.10: Impedance response as a function of applied voltage frequency for Transformer T2.

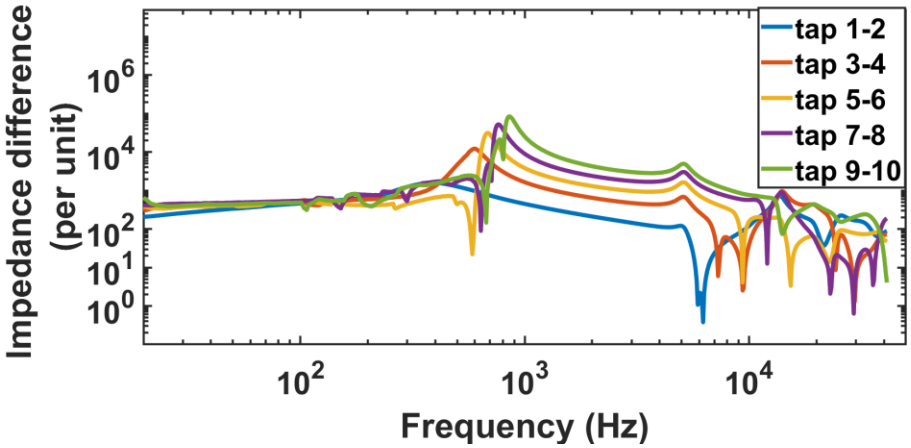

Figure 4.11: Tap-to-tap impedance difference response as a function of applied voltage frequency for Transformer T1.

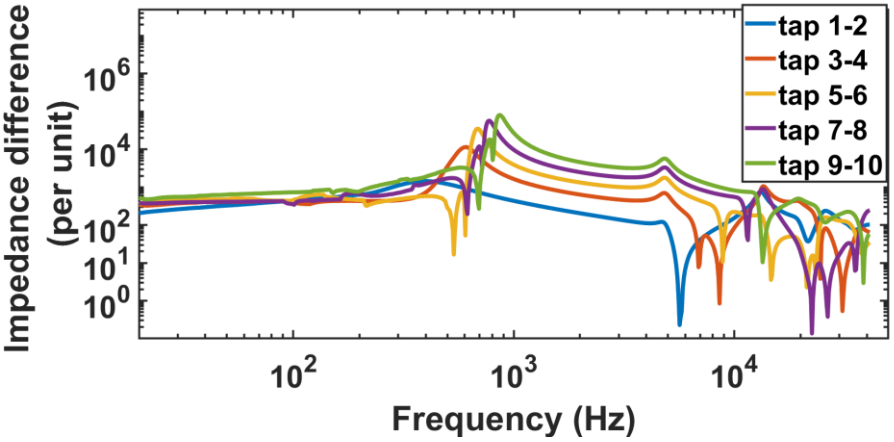

Figure 4.12: Tap-to-tap impedance difference response as a function of applied voltage frequency for Transformer T2.

The voltage ratio frequency response along the taps of Transformers T1 and T2 as a function of applied voltage frequency is shown in Figure 4.13 and Figure 4.14, respectively. The voltage ratio frequency response increases with an increase in tap number in the frequency region below 10 kHz. The voltage ratio frequency response is governed by series capacitance and self-inductance of the transformer in the frequency region below 10 kHz. There are no resonance points for the overall response between 10 kHz and 300 kHz. Tap-to-tap voltage ratio difference response as a function of

applied voltage frequency for Transformers T1 and T2 are shown in Figure 4.15 and Figure 4.16, respectively. In contrary to the impedance frequency difference response, the highest amplitude for voltage ratio difference response is obtained at tap 9-10 (line end taps), and the voltage ratio difference decreases with decrease in tap number.

The highest difference between tap 1-2 is not depicted in the voltage ratio difference frequency response. Both the impedance difference frequency response and the magnitude of voltage difference response in dB (Figure 4.3 and Figure 4.4) show the highest difference between tap 1-2 around the frequency of 10 kHz for both transformers (T1 and T2). But the magnitude of voltage difference response (dB) shown in Figure 4.3 and Figure 4.4 also shows the distinction in response between Transformers T1 and T2; whereas, the impedance difference frequency response is unable to show the distinction between both the transformers. Due to the difference in tap-to-tap winding resistance as we move from tap 1-2 (20 Ω) to tap 9-10 (30 Ω), the tap-to-tap voltage ratios are not the same at 20 Hz. Note that the tap-to-tap impedance difference response is calculated in per-unit because the other two transfer function difference response including voltage ratio difference response and the magnitude of voltage difference response in dB has no units.

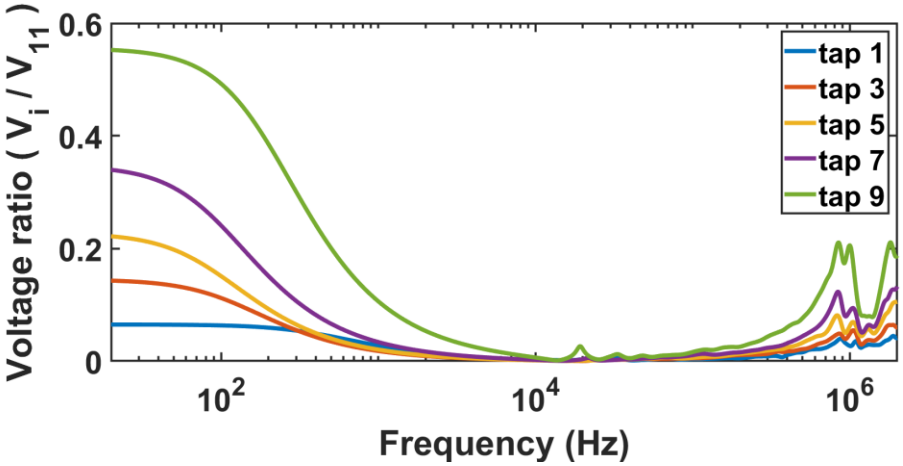

Figure 4.13: Voltage ratio frequency response as a function of applied voltage frequency for Transformer T1.

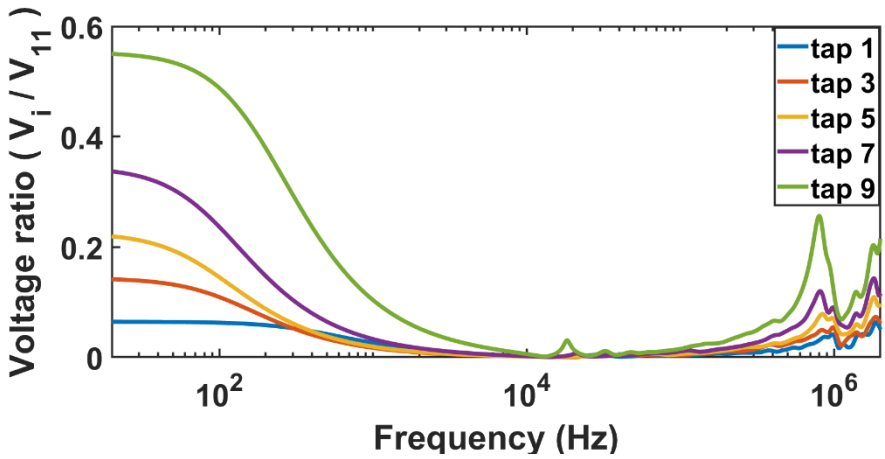

Figure 4.14: Voltage ratio frequency response as a function of applied voltage frequency for Transformer T2.

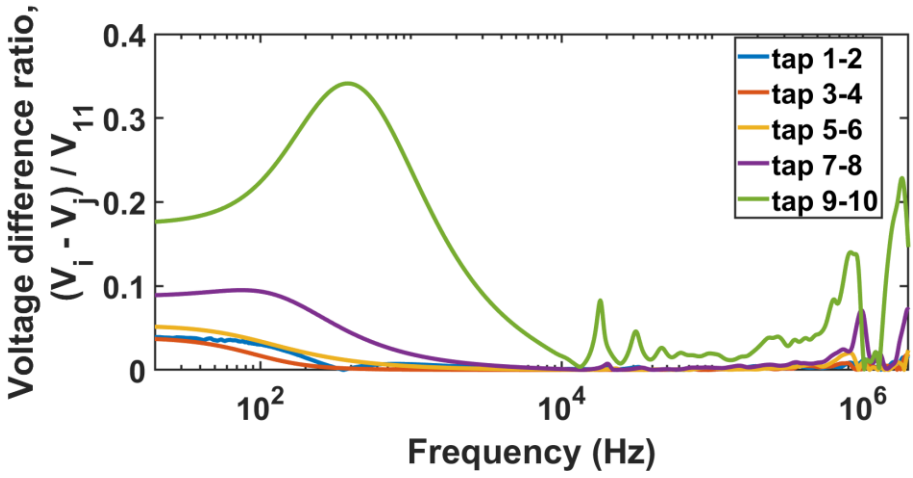

Figure 4.15: Tap-to-tap voltage ratio difference response as a function of applied voltage frequency for Transformer T1.

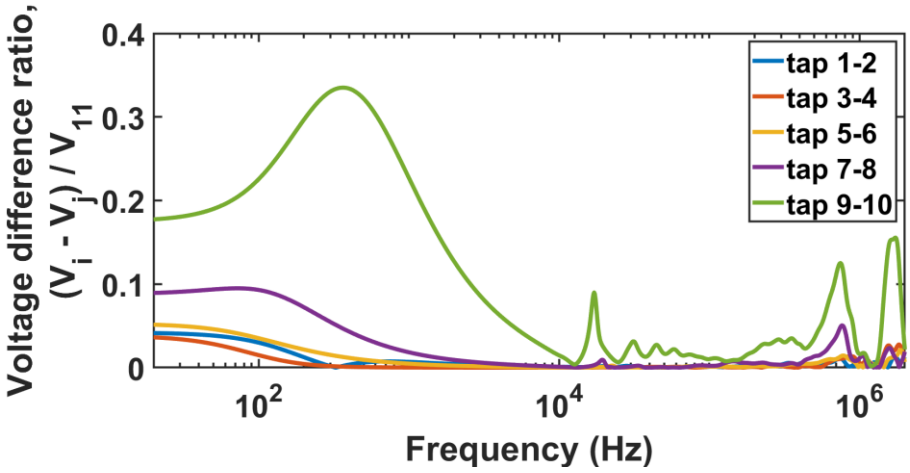

Figure 4.16: Tap-to-tap voltage ratio difference response as a function of applied voltage frequency for Transformer T2.

4.1.2 Transient response measurement

The repetitive transient voltage is applied across transformer line end tap and the transient response of the transformer along the remaining taps were obtained (Figure 3.4). Figure 4.17 show the distribution of transient voltage along the taps of transformer T1, for an input transient voltage of amplitude = 100 V, duty cycle = 10%, switching frequency = 1 kHz, rise time = 260 ns. The amplitude of the transient response increases and the rise time of the response decreases as we move from tap 1 to tap 11 along the transformer winding. This is due to dispersion and attenuation of the transient traveling along the winding. Figure 4.18 show the distribution of transient voltage along the taps of transformer T1, for an input transient voltage of amplitude = 1000 V, duty cycle = 10%, switching frequency = 1 kHz, rise time = 290 ns. Similar to Figure 4.17, the amplitude of the transient response increases and the rise time of the response decreases as we move from core end taps to high voltage terminal taps of the transformer. Thus, the distribution of the transient response along the transformer taps is non-uniform.

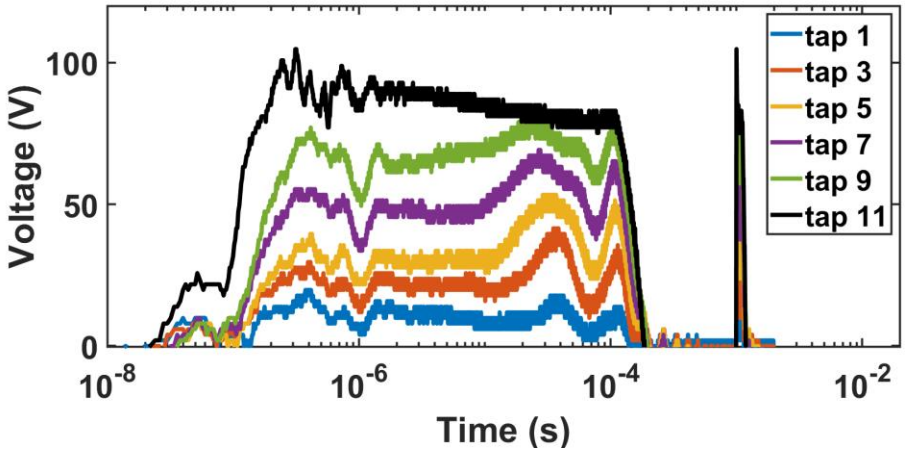

Figure 4.17: Transformer (T1) transient response for an input voltage of amplitude = 100 V, duty cycle = 10%, switching frequency = 1 kHz, rise time = 260 ns.

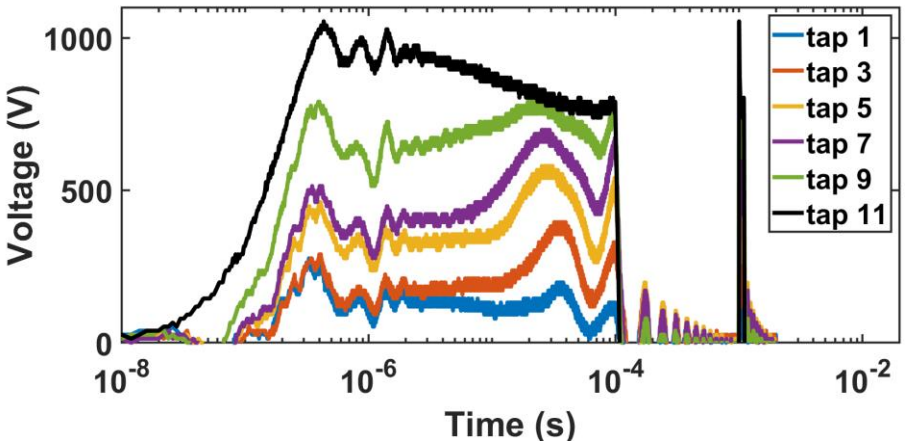

Figure 4.18: Transformer (T1) transient response for an input voltage of amplitude = 1000 V, duty cycle = 10%, switching frequency = 1 kHz, rise time = 290 ns.

The rise time along the taps (taps 10, 6, 3) of Transformers T1 and T2 for the four cases of transient voltage are shown in Table 4.1 and Table 4.2. The lower rise time (faster transient) for tap 10 and tap 6 is obtained for case 3 of the input transient voltage with an amplitude of 1000 V, rise time of 290 ns and duty cycle of 10 %. The transient voltage travel along the winding leading to attenuation and dispersion of the transient surge voltage. Thus, the rise time of the transient voltage decreases with

increase in tap number. For taps 10 and 6, the Transformer, T2 has lower rise time values compared to Transformer, T1. Transformer T1 is aged under sinusoidal voltage, while Transformer T2 is aged under repetitive transients. Considering tap 3 for the transformers, the lowest rise time (faster transient) for Transformer T2 and Transformer T1 is with case 3 and case 2 of the transient voltage respectively.

Table 4.1: Rise time along the taps for Transformer T1 for different cases of transient voltage parameters.

Cases	Tap 10 (ns)	Tap 6 (ns)	Tap 3 (ns)
Case 1	260	28700	46500
Case 2	701	23700	28700
Case 3	232	19100	42100
Case 4	10900	26800	35900

Table 4.2: Rise time along the taps for Transformer T2 for different cases of transient voltage parameters.

Cases	Tap 10 (ns)	Tap 6 (ns)	Tap 3 (ns)
Case 1	280	28600	53700
Case 2	518	19200	31700
Case 3	227	18400	20600
Case 4	9660	21200	38300

The Tap-to-tap voltage difference in per unit for Transformers T1 and T2 under various cases of transient voltage parameters are shown in Figure 4.19 and Figure 4.20, respectively. The figures show that the tap-to-tap voltage difference for both transformers is highest at the end taps. The highest tap-to-tap voltage difference is obtained for case 2 of the transient input voltage with an amplitude of 100

V, a rise time of 290 ns, and duty cycle of 50%. For case 2 of the transient, the input voltage has higher duty cycle and faster rise time, leading to greater stress on the winding due to longer pulse duration and increased dV/dt. The Tap-to-tap voltage difference in per unit for Transformers T1 and T2 for fast Fourier transform (FFT) of transient voltage cases are shown in Figure 4.21 and Figure 4.22, respectively. The tap-to-tap voltage difference shown in Figure 4.21 and Figure 4.22 is at the frequency of 10 kHz. The frequency component of 10 kHz is selected from the tap-to-tap impedance difference frequency response characteristics (Figure 4.11 and Figure 4.12) of the transformers. Very fast transient contains the frequency component ranging from 1 kHz to 1 MHz. The transformer's (T1 and T2) have critical resonance frequency (based on their design) at 10 kHz, and when the resonance frequency of the transformer matches the frequency component of the repetitive transient, it would lead to large voltage amplitudes and rise time, and thus may result in transformer insulation failure. From the figures, (Figure 4.21 and Figure 4.22) it is seen that the highest tap-to-tap voltage difference is obtained in the initial taps of the winding located at the second resonance region of 10 kHz. For Transformer T2, an applied voltage level of 1000 V with rise time of 290 ns lead to resonance amplification at tap 3-4 (Figure 4.22). With an applied voltage of 100 V, the resonance amplification is not observed at tap 3-4. The transient voltage travelling along the tap-to-tap RLC network has caused these observed differences. There are 748 turns between two taps of the model transformers (T1, T2). The network of resistances, inductances and capacitances are formed due to transformer conductors, enamel coating, and paper-oil insulation. Thus, the applied transient voltage with an amplitude of 1000 V and rise of 290 ns, resulted in steeper dV/dt, leading to resonance amplification at tap 3-4 (Figure 4.22) as compared to transient voltage with an amplitude of 100 V. In summary, based on the frequency characteristics of the tap-to-tap RLC network, the difference in rate of rise can lead to resonance amplification at the initial taps of the transformer winding.

The highest tap-to-tap voltage difference for the frequency domain results (Figure 4.21 and Figure 4.22) are seen at the initial taps, tap 1-2; whereas, the highest tap-to-tap voltage difference for the time domain results (Figure 4.19 and Figure 4.20) are seen at the end taps, tap 10-11 of the transformer winding. Thus, if the frequency of the repetitive transient voltage generated by switching operation of circuit breaker matches the transformer's critical resonance frequency, there are possibilities of transient voltage amplification at the initial taps of the transformer winding.

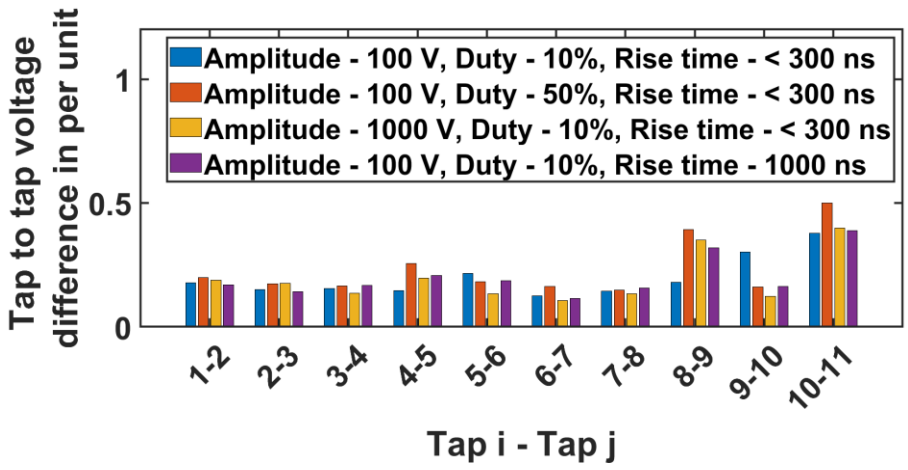

Figure 4.19: Tap-to-tap voltage difference under various cases of transient voltage parameters for Transformer T1.

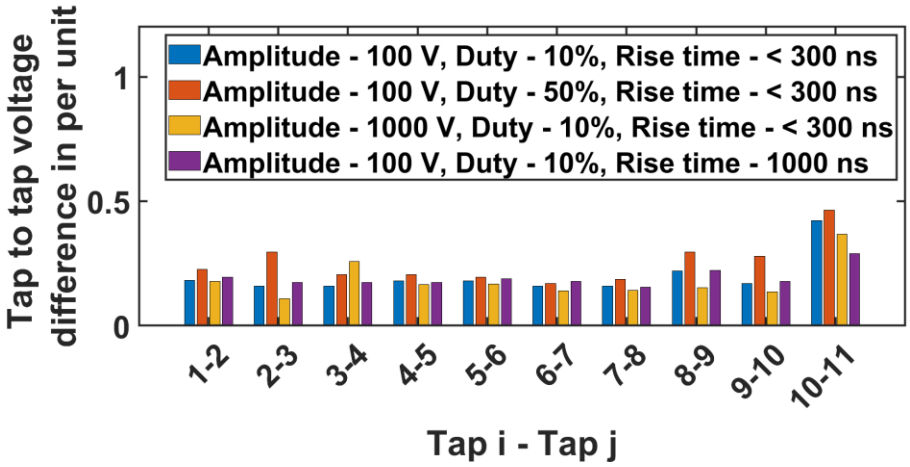

Figure 4.20: Tap-to-tap voltage difference under various cases of transient voltage parameters for Transformer T2.

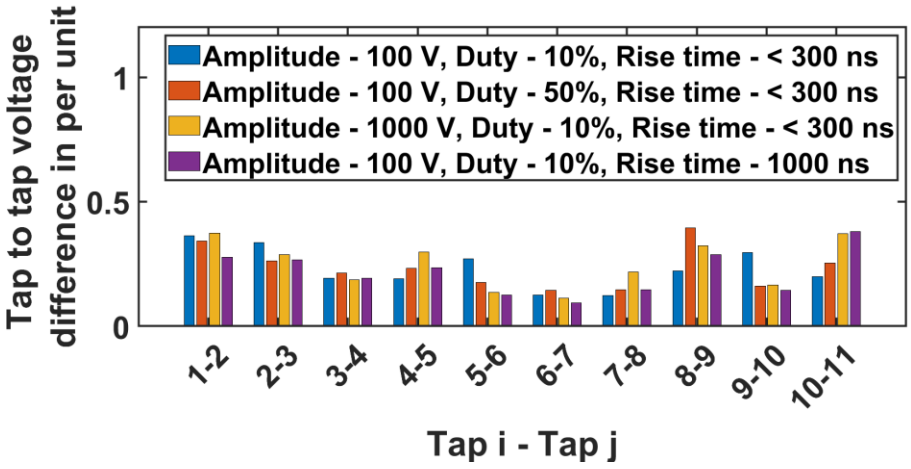

Figure 4.21: Tap-to-tap voltage difference under various cases of transient voltage parameters for Transformer T1 (FFT).

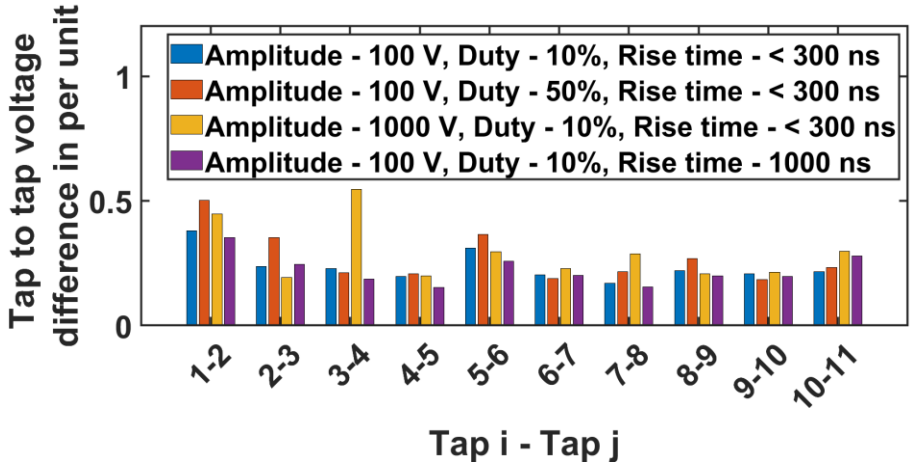

Figure 4.22: Tap-to-tap voltage difference under various cases of transient voltage parameters for Transformer T2 (FFT).

4.2 Influence of repetitive transient voltage on the ageing of paper-oil insulation

The section describes the ageing of the paper-oil insulation under the application of repetitive transient voltage. The ageing of the paper-oil insulation was carried out by using six rod-plane electrode set-up.

The transformer oil considered for the study are Luminol TRi, Voltesso 35 A, and Voltesso 35 B mineral oils. The ageing responses that are used in the analysis are dissipation factor, polarisation current, depolarisation current, and partial discharge activity.

4.2.1 Six rod-plane geometry for paper-oil insulation ageing test

4.2.1.1 AC ageing of Luminol TRi mineral oil

An AC voltage of amplitude = 4 kV rms was applied across the rod-plane electrodes with paper sample sandwiched between the electrodes. The oil used was Luminol TRi mineral oil and the AC ageing was carried out for 440 hours. Figure 4.23 shows the paper aged under AC voltage for a duration of 440 hours. There were no signs of carbon deposition or puncture on the paper, and thus the paper was considered not degraded due to AC ageing with Luminol TRi oil. The long-term ageing of paper-oil insulation was carried out under AC voltage in order to obtain the equivalent voltage level (6 kV) required for ageing of paper-oil insulation under repetitive transient voltage. Accordingly, a pulse with magnitude of 6kV peak has been selected as the test voltage.

Figure 4.23: Aged (440 hours) paper under AC voltage of amplitude = 4 kV rms and frequency = 60 Hz with Luminol TRi oil.

4.2.1.2 Repetitive transient ageing of Luminol TRi mineral oil

A repetitive transient voltage of amplitude = 6 kV, switching frequency = 1 kHz, duty cycle = 50% and rise time = 220 ns was applied across the paper-oil insulation with Luminol TRi oil, and the transient voltage ageing duration was 300 hours. Figure 4.24 shows the repetitive transient voltage waveform applied for the transient ageing of the paper-oil insulation.

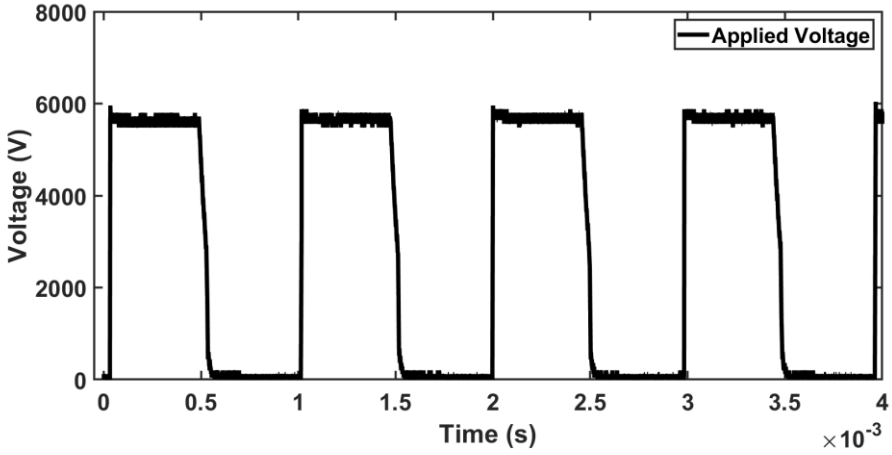

Figure 4.24: Repetitive transient voltage of amplitude = 6 kV, switching frequency = 1 kHz, duty cycle = 50%, and rise time = 220 ns for transient ageing of paper-oil insulation.

The image of the paper aged under repetitive transient voltage for a duration of 300 hours is shown in Figure 4.25. There were no observable signs of carbon deposition or puncture on the paper, thus the paper was not degraded due to transient ageing with Luminol TRi oil.

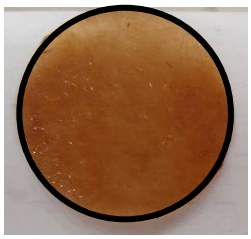

Figure 4.25: Aged (300 hours) paper under repetitive transient voltage of amplitude = 6 kV, switching frequency = 1 kHz, duty cycle = 50%, and rise time = 220 ns with Luminol TRi oil.

4.2.1.2.1 Dielectric frequency response

The dissipation factor as a function of frequency is measured at 65 hours, 130 hours, 195 hours, 260 hours, and 300 hours of ageing period for the paper-oil insulation with Luminol TRi, and the results are presented in Figure 4.26. The ageing responses including the dissipation factor were measured at a

temperature of 23 °C and humidity of 18%. The overall dissipation factor did not increase significantly even with the ageing period of 300 hours.

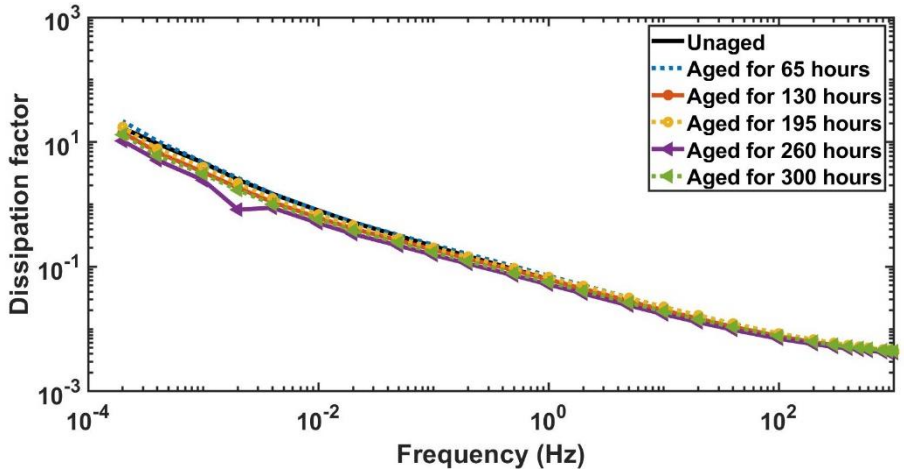

Figure 4.26: Dissipation factor as a function of frequency for ageing of paper-oil insulation with Luminol TRi oil, aged under repetitive transient voltage of amplitude = 6 kV, switching frequency = 1 kHz, duty cycle = 50%, and rise time = 220 ns.

4.2.1.2.2 Polarisation and depolarisation current responses

The measured polarisation currents are presented in Figure 4.27. The polarisation current for the paper-oil insulation with Luminol TRi oil did not increase from unaged to 65 hours of ageing period. From 65 hours of ageing time to 130 hours of ageing period, the polarisation current decreased by a small extent. From 130 hours of ageing time to 195 hours of ageing time, the polarisation current increased by a small extent. From 195 hours of ageing time to 260 hours of ageing time, the polarisation current decreased. The variation in polarisation current with ageing time is not significant, and the transient ageing of paper-oil insulation with Luminol TRi oil did not degrade the oil and paper insulation.

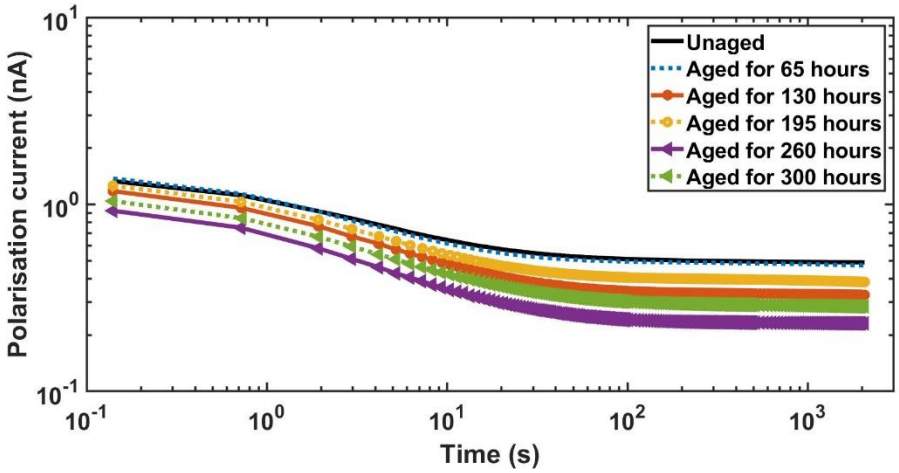

Figure 4.27: Polarisation current response for ageing of paper-oil insulation with Luminol TRi oil, aged under repetitive transient voltage of amplitude = 6 kV, switching frequency = 1 kHz, duty cycle = 50%, and rise time = 220 ns.

The corresponding measured depolarisation currents are presented in Figure 4.28. The variation in depolarisation current with ageing time for transient ageing of paper-oil insulation with Luminol TRi oil is not significant, and thus the transient ageing did not degrade the oil and the paper insulation.

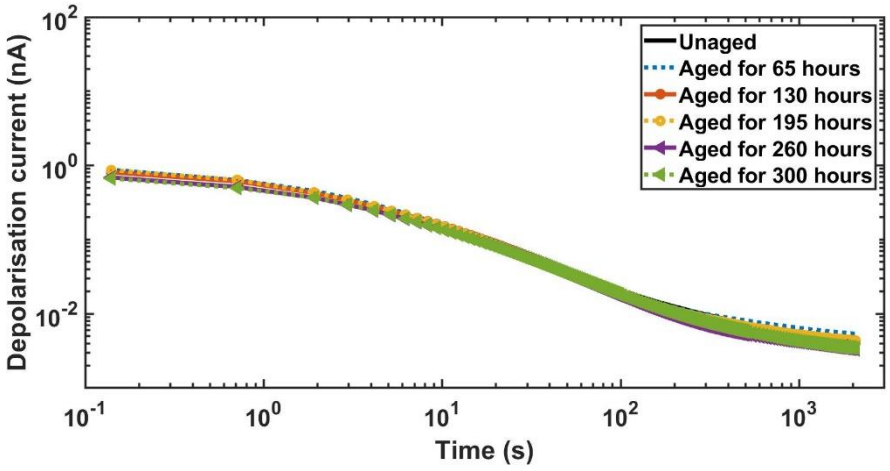

Figure 4.28: Depolarisation current response for ageing of paper-oil insulation with Luminol TRi oil, aged under repetitive transient voltage of amplitude = 6 kV, switching frequency = 1 kHz, duty cycle = 50%, and rise time = 220 ns.

4.2.1.2.3 Additional ageing responses

Table 4.3 shows the ageing response including capacitance, dissipation factor, dissolved hydrogen gas in oil, oil temperature, partial discharge inception voltage (PDIV), and partial discharge extinction voltage (PDEV) measured for the ageing case reported in section 4.2.1.2. The capacitance, dissipation factor, dissolved hydrogen gas in oil, oil temperature, PDIV, and PDEV did not change significantly with the transient ageing of paper immersed in Luminol TRi oil (coefficient of variation = 7 %). Thus, the transient ageing of paper in Luminol TRi oil did not change the chemical property of the oil and the paper.

Table 4.3: Ageing response as a function of time for paper-oil insulation with Luminol TRi oil, aged under repetitive transient voltage of amplitude = 6 kV, switching frequency = 1 kHz, duty cycle = 50%, and rise time = 220 ns.

Ageing response	unaged	65 hours	130 hours	195 hours	260 hours	300 hours
Capacitance in pF @ 60 Hz	41.6	41.8	41.8	42.0	42.0	40.7
Dissipation factor @ 60 Hz	0.0090	0.0098	0.0092	0.0102	0.0083	0.0092
Hydrogen gas amount in ppm	0	1	0	0	0	0
Oil Temperature in °C	19.5	21.6	21.0	25.0	21.0	22.6
Partial discharge inception voltage (PDIV) in kV	6.9	5.4	5.7	5.9	6.7	5.4
Partial discharge extinction voltage (PDEV) in kV	5.2	4.1	4.8	5.0	5.5	4.2

4.2.1.3 Repetitive transient ageing of Voltesso 35 A mineral oil

A repetitive transient voltage of amplitude = 6 kV, switching frequency = 1 kHz, duty cycle = 50%, and rise time = 220 ns was applied across the paper-oil insulation with Voltesso 35 A oil, and the transient voltage ageing duration was 300 hours. The image of the paper aged under repetitive transient voltage for a duration of 300 hours is shown in Figure 4.29. There was dark circular carbon deposition on the paper, indicating that the paper degraded due to transient ageing with Voltesso 35 A oil. The dimension of the circular carbon deposit was similar to the high voltage rod electrode dimension, and the carbon deposit was present on all six samples.

Figure 4.29: Aged (300 hours) paper under repetitive transient voltage of amplitude = 6 kV, switching frequency = 1 kHz, duty cycle = 50%, and rise time = 220 ns with Voltesso 35 A oil.

4.2.1.3.1 Dielectric frequency response

The dissipation factor as a function of frequency is measured at 65 hours, 130 hours, 195 hours, 260 hours, and 300 hours of ageing period for the paper-oil insulation with Voltesso 35 A oil, and the results are presented in Figure 4.30. The ageing responses including the dissipation factor were measured at a temperature of 23.2 °C and humidity of 22%. The dissipation factor increased significantly with ageing time in the frequency range between 0.01 Hz to 1 kHz. The rate of increase in dissipation factor was highest when the paper-oil insulation was aged to 65 hours. The rate of increase in dissipation factor reduced as the ageing time increased from 65 hours to 130 hours. The rate of change in dissipation factor was not significant when the ageing time increased from 130 hours to 300 hours.

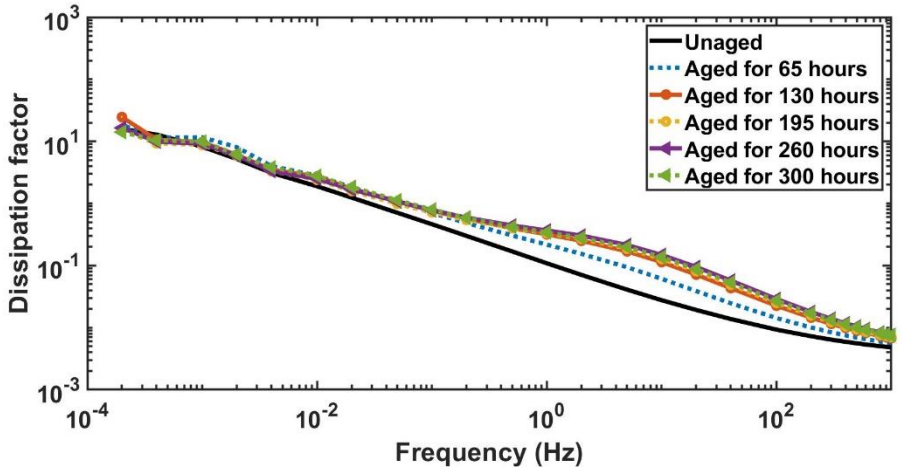

Figure 4.30: Dissipation factor as a function of frequency for ageing of paper-oil insulation with Voltesso 35 A oil, aged under repetitive transient voltage of amplitude = 6 kV, switching frequency = 1 kHz, duty cycle = 50%, and rise time = 220 ns.

4.2.1.3.2 Polarisation and depolarisation current responses

The measured polarisation currents are presented in Figure 4.31. The polarisation current increased significantly with ageing time. The rate of increase in polarisation current was highest when the paper-oil insulation was aged to 65 hours. The rate of increase in polarisation current reduced as the ageing time increased from 65 hours to 130 hours. The rate of change in polarisation current was not significant when the ageing time increased from 130 hours to 300 hours.

The corresponding measured depolarisation currents are presented in Figure 4.32. The depolarisation current increased significantly with ageing time for measurement time ranging from 100 s to 2000 s. The rate of increase in depolarisation current was highest when the paper-oil insulation was aged to 65 hours. The rate of change in depolarisation current was not significant when the ageing time increased from 65 hours to 300 hours.

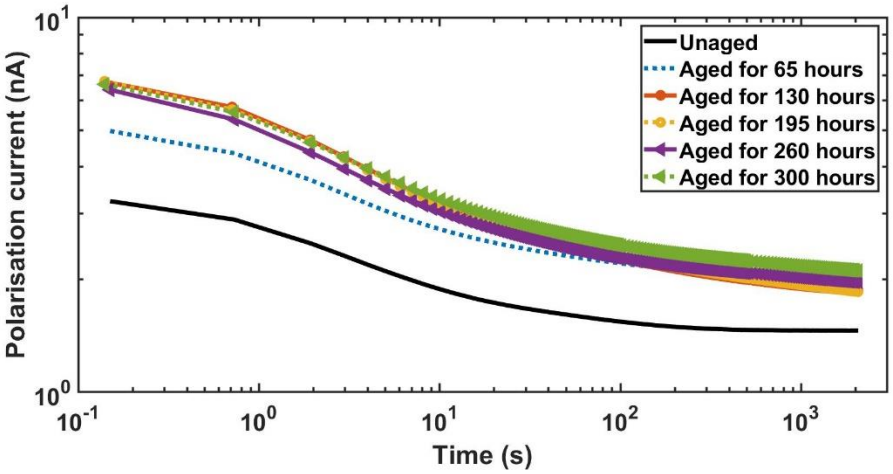

Figure 4.31: Polarisation current response for ageing of paper-oil insulation with Voltesso 35 A oil, aged under repetitive transient voltage of amplitude = 6 kV, switching frequency = 1 kHz, duty cycle = 50%, and rise time = 220 ns.

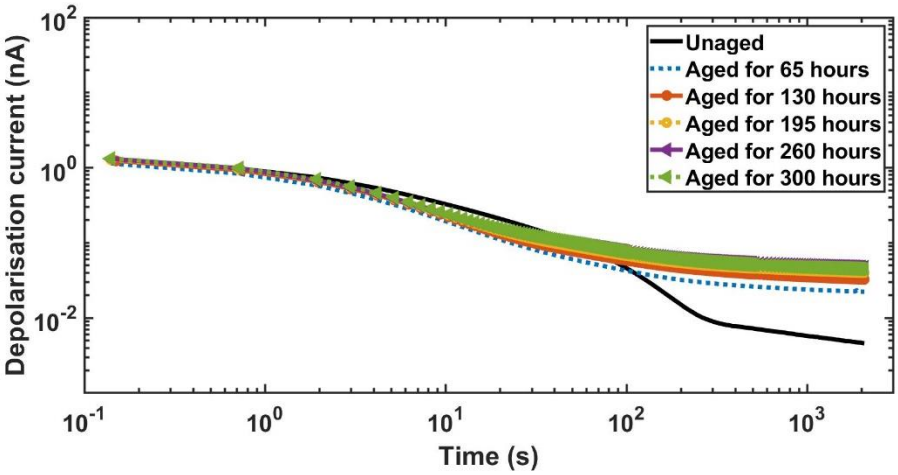

Figure 4.32: Depolarisation current response for ageing of paper-oil insulation with Voltesso 35 A oil, aged under repetitive transient voltage of amplitude = 6 kV, switching frequency = 1 kHz, duty cycle = 50%, and rise time = 220 ns.

4.2.1.3.3 Additional ageing responses

Table 4.4 shows the ageing response including dissipation factor, and insulation resistance measured for the ageing case reported in section 4.2.1.3. The dissipation factor increased almost uniformly with increase in ageing time (coefficient of variation = 40.21 %). The insulation resistance decreased significantly with increase in ageing time up to 130 hours of ageing (coefficient of variation = 20.01 %). However, the insulation resistance did not change significantly for ageing time from 130 hours to 300 hours. The partial discharge inception voltage and the partial discharge extinction voltage were not measured because the samples failed during the inception of partial discharge activity while using Voltesso 35 A as the insulating oil. The measured capacitance, dissolved hydrogen gas in oil, and oil temperature did not change significantly with the transient ageing of paper immersed in Voltesso 35 A oil, thus the corresponding values are not reported in this section. The measured dissolved hydrogen gas in oil did not change significantly because the volume of oil used in the ageing process was huge compared to the high-field test zone (20 litres).

Table 4.4: Ageing response as a function of time for paper-oil insulation with Voltesso 35 A oil, aged under repetitive transient voltage of amplitude = 6 kV, switching frequency = 1 kHz, duty cycle = 50%, and rise time = 220 ns.

Ageing response	unaged	65 hours	130 hours	195 hours	260 hours	300 hours
Dissipation factor @ 60 Hz	0.0116	0.0182	0.0299	0.0334	0.0381	0.0410
Insulation resistance in GΩ @ 60 s	125	88	83	82	84	77

4.2.2 Parallel-plane geometry for ageing response measurement

The ageing response including dissipation factor, polarisation current, depolarisation current, and insulation resistance were measured for the aged paper samples placed in the standard parallel-plane electrode system.

4.2.2.1 Repetitive transient ageing of Voltesso 35 A mineral oil

In order to analyse the changes in paper, all six aged paper samples were sandwiched between parallel-plane electrodes.

4.2.2.1.1 Transient voltage ageing at room temperature

The ageing response is obtained for six aged paper samples placed in between the parallel-plane electrodes. The six paper samples were aged at 300 hours of ageing time under repetitive transient voltage of amplitude = 6 kV, switching frequency = 1 kHz, duty cycle = 50%, and rise time = 220 ns using the six rod-plane electrodes with Voltesso 35 A as the insulating oil.

4.2.2.1.1.1 Dielectric frequency response

The dissipation factor as a function of frequency is measured after 300 hours of ageing period for the six aged paper samples sandwiched between parallel-plane electrodes with Voltesso 35 A as the insulating oil, and the results are presented in Figure 4.33. The ageing responses including the dissipation factor were measured at a temperature of 22.4 °C and humidity of 33%. The dissipation factor of the aged (300 hours) paper-oil insulation is 10 times greater than the dissipation factor of the unaged paper-oil insulation in the frequency range between 0.2 mHz to 10 kHz. There is also a peak seen for aged dissipation factor response at a frequency of 1 mHz. The peak is caused due to interface polarisation along six aged paper samples placed in between the parallel-plane electrode.

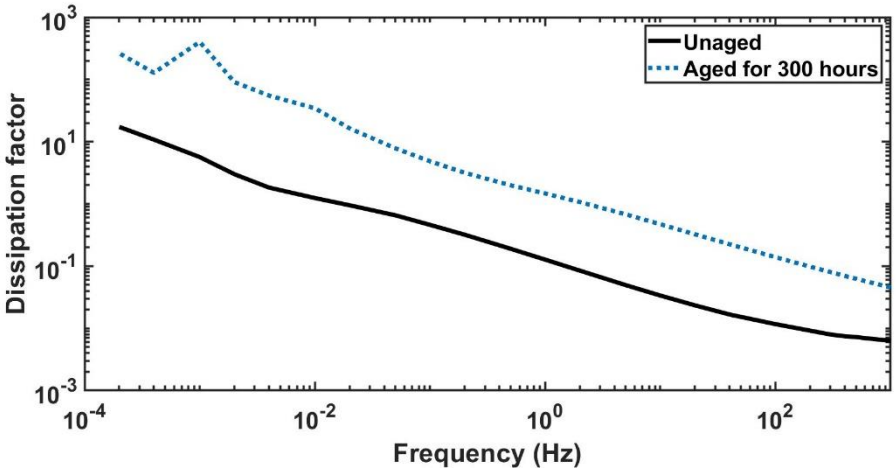

Figure 4.33: Dissipation factor as a function of frequency for ageing of paper-oil insulation with Voltesso 35 A oil, aged under repetitive transient voltage of amplitude = 6 kV, switching frequency = 1 kHz, duty cycle = 50%, and rise time = 220 ns.

4.2.2.1.1.2 Polarisation and depolarisation current responses

The measured polarisation currents are presented in Figure 4.34. The polarisation current of the aged (300 hours) paper-oil insulation is about 40 times greater than the polarisation current of the unaged paper-oil insulation in the time range between 0 – 2000 s.

The corresponding measured depolarisation currents are presented in Figure 4.35. The depolarisation current of the aged (300 hours) paper-oil insulation is 4 times greater than the depolarisation current of the unaged paper-oil insulation in the time range between 0 – 40 s. Between 40 – 2000 s, the depolarisation current of the aged paper-oil insulation is 100 times greater than the depolarisation current of the unaged paper-oil insulation.

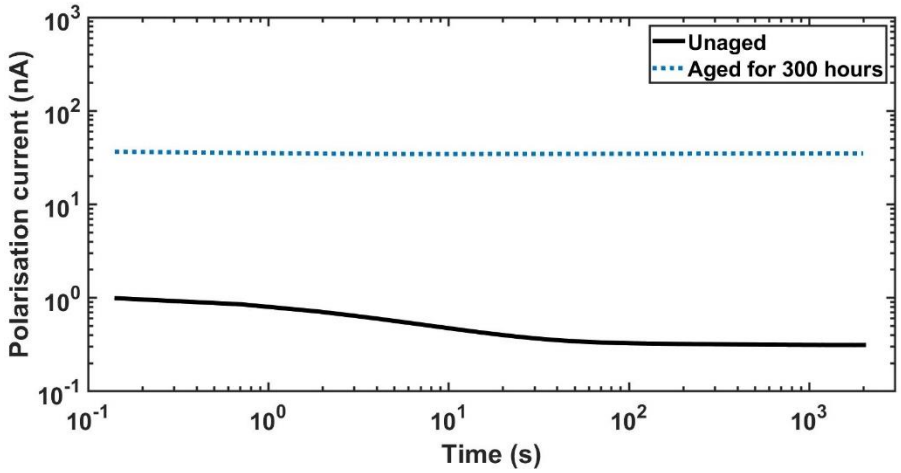

Figure 4.34: Polarisation current response for ageing of paper-oil insulation with Voltesso 35 A oil, aged under repetitive transient voltage of amplitude = 6 kV, switching frequency = 1 kHz, duty cycle = 50%, and rise time = 220 ns.

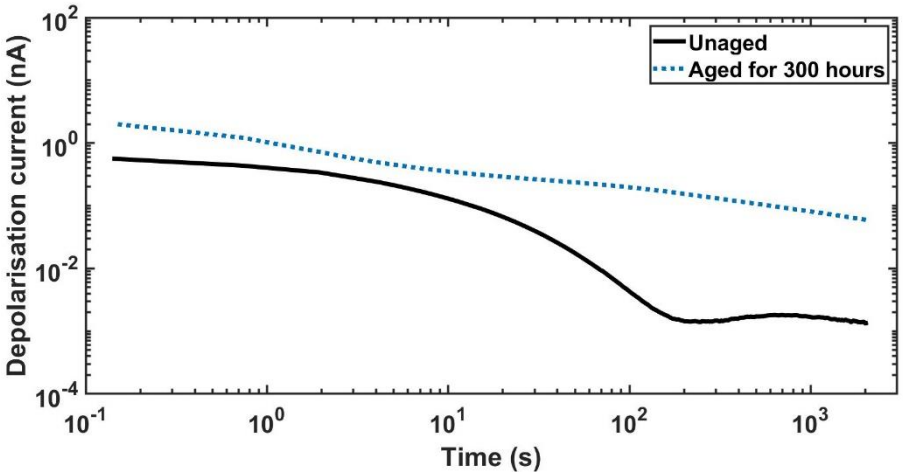

Figure 4.35: Depolarisation current response for ageing of paper-oil insulation with Voltesso 35 A oil, aged under repetitive transient voltage of amplitude = 6 kV, switching frequency = 1 kHz, duty cycle = 50%, and rise time = 220 ns.

4.2.2.1.1.3 Additional ageing responses

Table 4.5 presents the ageing (300 hours) response including capacitance, dissipation factor, and insulation resistance for the ageing case reported in section 4.2.2.1.1. The capacitance value of the aged paper-oil insulation increased by 23.06% as compared to the capacitance value of the unaged paper-oil insulation. The dissipation factor of the aged paper-oil insulation increased by 170.26% as compared to the dissipation factor of the unaged paper-oil insulation. The insulation resistance of the unaged paper-oil insulation is greater than aged paper-oil insulation by 196.14%.

Table 4.5: Ageing response as a function of time for paper-oil insulation with Voltesso 35 A oil, aged under repetitive transient voltage of amplitude = 6 kV, switching frequency = 1 kHz, duty cycle = 50%, and rise time = 220 ns.

Ageing response	Unaged	Aged for 300 hours	Percentage difference
Capacitance in pF @ 60 Hz	12.0	15.1	23.06
Dissipation factor @ 60 Hz	0.0147	0.1830	170.26
Insulation resistance in GΩ @ 60 s	592	6	-196.14

4.2.2.1.2 Transient voltage ageing at temperature of 50° C

The six paper samples were aged for 70 hours of ageing time under repetitive transient voltage of amplitude = 6 kV, switching frequency = 1 kHz, duty cycle = 50%, and rise time = 220 ns at oil temperature of 50° C using the six rod-plane electrodes with Voltesso 35 A as the insulating oil. The image of the paper aged under repetitive transient voltage for a duration of 70 hours at temperature of 50° C is shown in Figure 4.36. There was dark circular carbon deposition on the paper, indicating that the paper degraded due to transient ageing with Voltesso 35 A oil at temperature of 50° C. The dimension of the circular carbon deposit was similar to the high voltage rod electrode dimension, and the paper degradation was extreme in nature.

Figure 4.36: Aged paper under repetitive transient voltage of amplitude = 6 kV, switching frequency = 1 kHz, duty cycle = 50%, and rise time = 220 ns with Voltesso 35 A oil, aged for 70 hours at temperature of 50 °C.

4.2.2.1.2.1 Dielectric frequency response

The dissipation factor as a function of frequency is measured after 70 hours of ageing period for the six aged paper samples sandwiched between parallel-plane electrodes with Voltesso 35 A as the insulating oil, and the results are presented in Figure 4.37. The ageing responses including the dissipation factor were measured at a temperature of 22.4 °C and humidity of 31%.

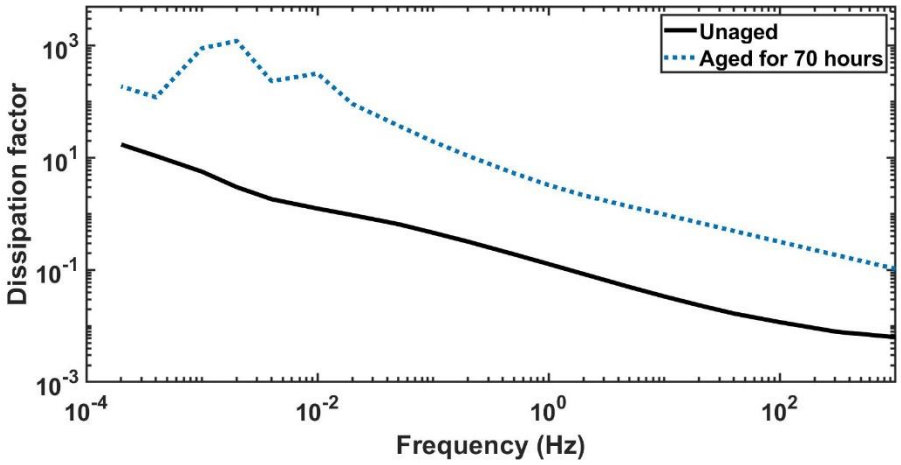

Figure 4.37: Dissipation factor as a function of frequency for ageing of paper-oil insulation with Voltesso 35 A oil, aged under repetitive transient voltage of amplitude = 6 kV, switching frequency = 1 kHz, duty cycle = 50%, rise time = 220 ns, and temperature of 50 °C.

The dissipation factor of the aged (70 hours) paper-oil insulation is about 30 times greater than the dissipation factor of the unaged paper-oil insulation in the frequency range between 0.1 mHz to 10 kHz.

There were two peaks seen for aged dissipation factor response at frequencies of 0.01 Hz and 0.002 Hz. The two peaks are caused due to interface polarisation along six aged paper samples placed in between the parallel-plane electrodes.

4.2.2.1.2.2 Polarisation and depolarisation current responses

The measured polarisation currents are presented in Figure 4.38. The polarisation current of the aged (70 hours) paper-oil insulation is 200 times greater than the polarisation current of the unaged paper-oil insulation in the time range between 0 – 2000 s.

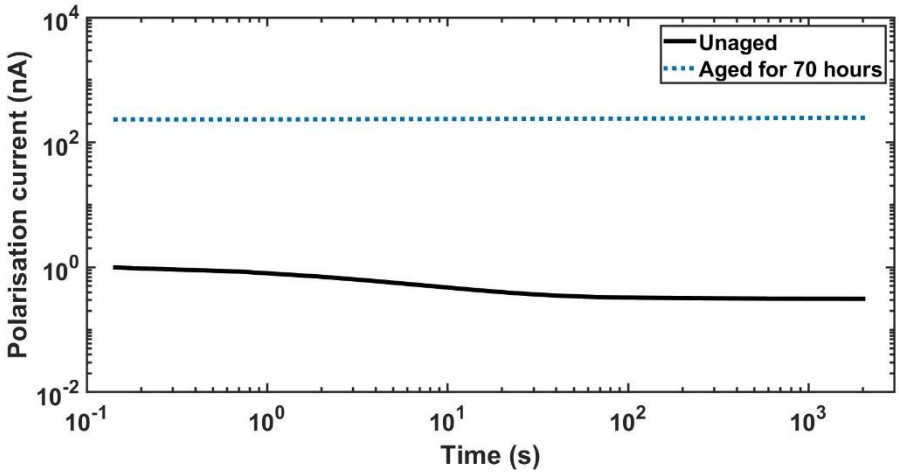

Figure 4.38: Polarisation current response for ageing of paper-oil insulation with Voltesso 35 A oil, aged under repetitive transient voltage of amplitude = 6 kV, switching frequency = 1 kHz, duty cycle = 50%, rise time = 220 ns, and temperature of 50 °C.

The corresponding measured depolarisation currents are presented in Figure 4.39. The depolarisation current of the aged (70 hours) paper-oil insulation is 9 times greater than the depolarisation current of the unaged paper-oil insulation in the time range between 0 – 50 s. Between 40 – 2000 s, the depolarisation current of the aged paper-oil insulation is about 300 times greater than the depolarisation current of the unaged paper-oil insulation.

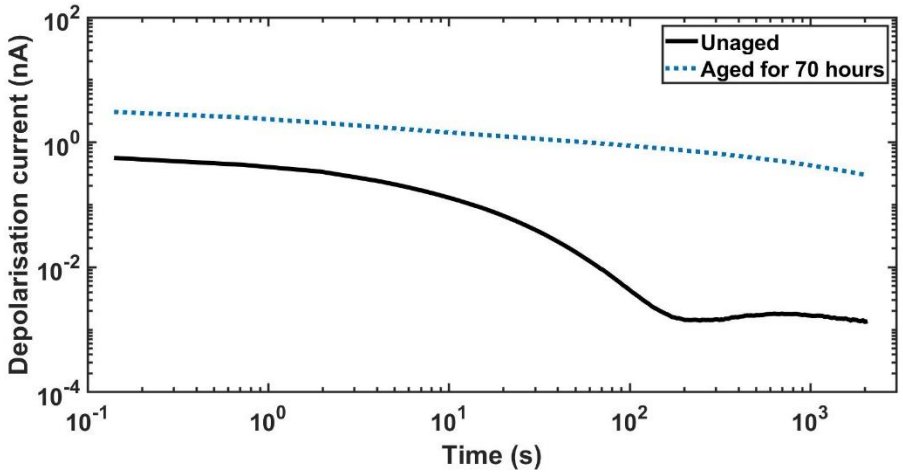

Figure 4.39: Depolarisation current response for ageing of paper-oil insulation with Voltesso 35 A oil, aged under repetitive transient voltage of amplitude = 6 kV, switching frequency = 1 kHz, duty cycle = 50%, rise time = 220 ns, and temperature of 50 °C.

4.2.2.1.2.3 Additional ageing response

Table 4.6 presents the ageing (70 hours) response including capacitance, dissipation factor, and insulation resistance for the ageing case reported in section 4.2.2.1.2. The capacitance value of the aged paper-oil insulation increased by 46.98% as compared to the capacitance value of the unaged paper-oil insulation.

Table 4.6: Ageing response as a function of time for paper-oil insulation with Voltesso 35 A oil, aged under repetitive transient voltage of amplitude = 6 kV, switching frequency = 1 kHz, duty cycle = 50% and rise time = 220 ns, and temperature of 50 °C.

Ageing response	Unaged	Aged for 70 hours	Percentage difference
Capacitance in pF @ 60 Hz	12.0	19.3	46.98
Dissipation factor @ 60 Hz	0.0147	0.4300	186.78
Insulation resistance in GΩ @ 60 s	592	1	-199.37

The dissipation factor of the aged paper-oil insulation increased by 186.78% as compared to the dissipation factor of the unaged paper-oil insulation. The insulation resistance of the unaged paper-oil insulation is greater than aged paper-oil insulation by 199.37%.

4.2.2.2 Repetitive transient ageing of Voltesso 35 B mineral oil

The current section presents result pertaining to the influence of repetitive transient voltage parameters including rise time and switching frequency on the ageing of the paper-oil insulation. Six paper samples were aged at 130 hours of ageing time under various cases of repetitive transient voltage parameters using the six rod-plane electrodes with Voltesso 35 B as the insulating oil. The repetitive transient voltage cases are presented in Table 4.7. The amplitude and the duty cycle for the transient voltage are fixed at 6 kV and 50% respectively. The ageing time of 130 hours is selected because the rate of change in ageing responses was not significant for ageing duration above 130 hours (refer to section 4.2.1.3).

Table 4.7: Repetitive transient voltage cases for ageing paper-oil insulation with Voltesso 35 B oil having fixed transient voltage amplitude of 6 kV and duty cycle of 50%.

Cases	Rise time (ns)	Switching frequency (kHz)
Case 1	220	1
Case 2	220	3
Case 3	650	1
Case 4	650	3

The image of the paper aged under case 1 of repetitive transient voltage having amplitude = 6 kV, switching frequency = 1 kHz, duty cycle = 50%, and rise time = 220 ns with Voltesso 35 B as the insulating oil for ageing duration of 130 hours is shown in Figure 4.40. There was circular carbon deposition on the paper for transient voltage ageing, indicating that the paper degraded due to transient ageing with Voltesso 35 B oil. Additionally, the aged paper had circular punctures due to transient voltage ageing.

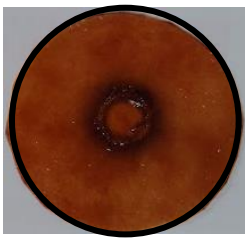

Figure 4.40: Aged (130 hours) paper under repetitive transient voltage of amplitude = 6 kV, switching frequency = 1 kHz, duty cycle = 50%, and rise time = 220 ns (case 1) with Voltesso 35 B oil.

4.2.2.2.1 Dielectric frequency response

The dissipation factor as a function of frequency is measured after 130 hours of ageing period for the three aged paper samples sandwiched between parallel-plane electrodes with Voltesso 35 B as the insulating oil, and the results are presented in Figure 4.41. The ageing responses including the dissipation factor were measured at a temperature of 22.9 °C and humidity of 34%. Six paper samples were aged under various cases of repetitive transient voltage shown in Table 4.7 using the six rod-plane electrodes with Voltesso 35 B as the insulating oil. Three aged samples were sandwiched between the parallel-plane electrodes instead of six samples. The purpose of using three samples was to obtain two measurements for each case of repetitive transient voltage ageing. For all four cases of the transient voltage ageing, the dissipation factor of the aged (130 hours) paper-oil insulation is about 10 to 100 times greater than the dissipation factor of the unaged paper-oil insulation in the frequency range between 0.1 mHz to 10 kHz. Among the four cases of transient voltage ageing, the case 2 with transient voltage amplitude = 6 kV, rise time = 220 ns, switching frequency = 3 kHz, and duty cycle = 50% has the highest increase in the dissipation factor of the aged paper-oil insulation compared to the dissipation factor of the unaged paper-oil insulation. Also, case 2 has the highest number of peaks and valleys for aged (130 hours) dissipation factor response at the measured frequency range. The peaks/valleys are caused due to interface polarisation along the three aged paper samples placed in between the parallel-plane electrode.

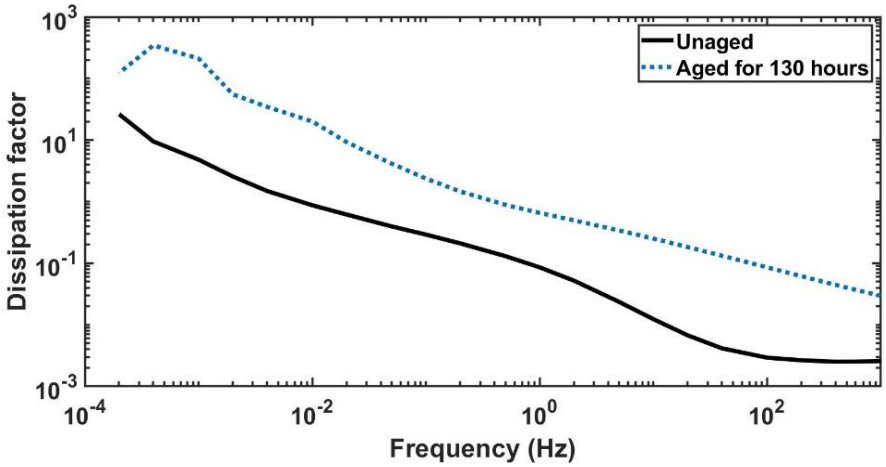
Unaged
Aged for 130 hours
Dissipation factor
Frequency (Hz)
10^{3}
10^{1}
10^{-1}
10^{-3}
10^{-4}
10^{-2}
10^{0}
10^{2}

(a)

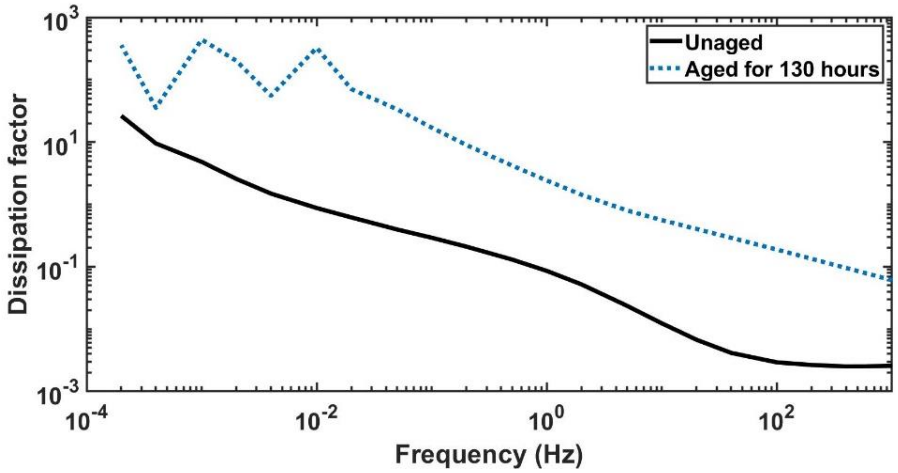
Unaged
Aged for 130 hours
Dissipation factor
Frequency (Hz)
10^{3}
10^{1}
10^{-1}
10^{-3}
10^{-4}
10^{-2}
10^{0}
10^{2}

(b)

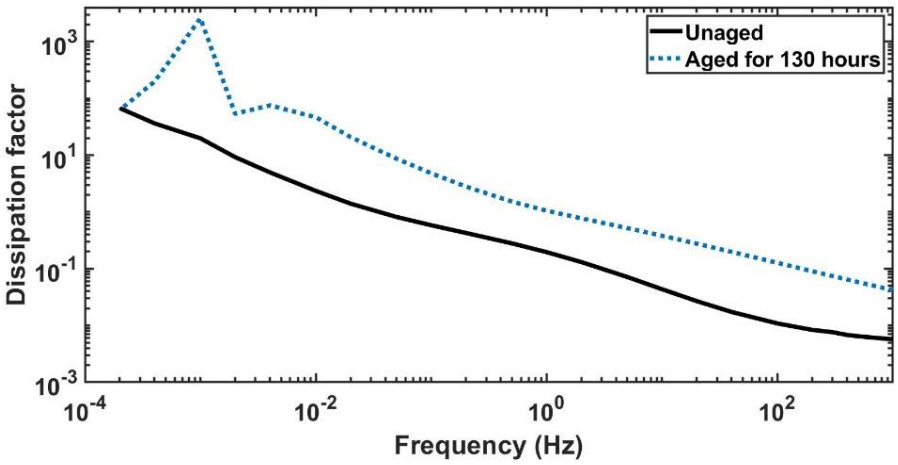

(c)

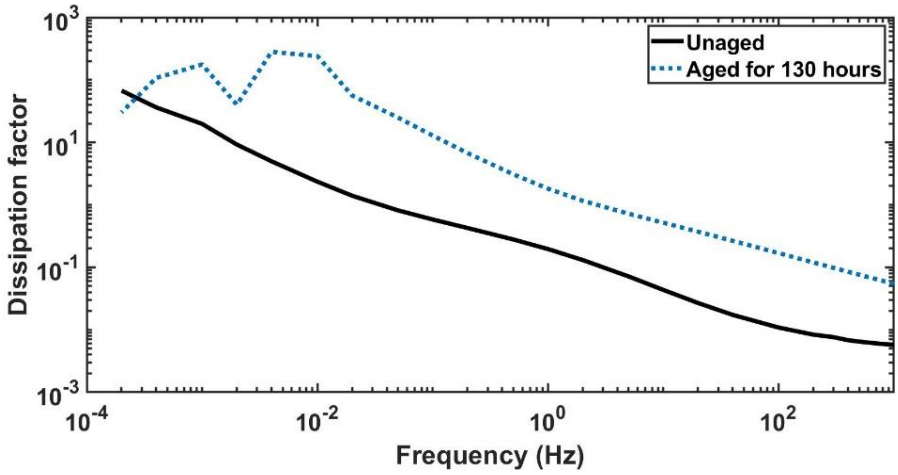

(d)

Figure 4.41: Dissipation factor as a function of frequency for various cases of transient voltage ageing of paper-oil insulation with Voltesso 35 B oil: (a) Case 1, (b) Case 2, (c) Case 3, and (d) Case 4.

The dissipation factor difference in per unit as a function of frequency for paper-oil insulation ageing (130 hours) under various cases of repetitive transient voltage (Table 4.7) for the three aged paper samples sandwiched between parallel-plane electrodes with Voltesso 35 B as the insulating oil is

presented in Figure 4.42. The dissipation factor difference is obtained by subtracting the dissipation factor of unaged paper-oil insulation from the dissipation factor of aged (130 hours) paper-oil insulation. From the Figure 4.42, it can be seen that the order of dissipation factor difference from highest to lowest in the frequency range between 10 Hz to 1000 Hz.is as followed: case 2 > case 1 > case 4 > case 3.

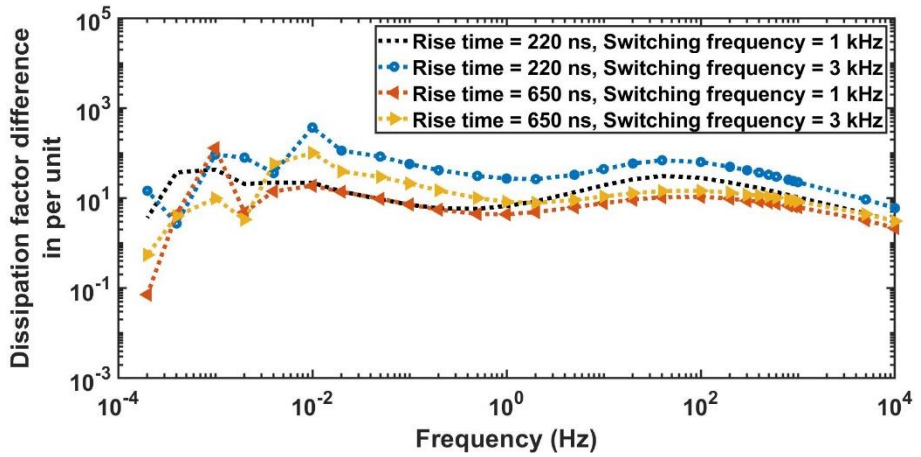

Figure 4.42: Dissipation factor difference as a function of frequency for various cases of transient voltage ageing (130 hours) of paper-oil insulation with Voltesso 35 B oil.

4.2.2.2.2 Polarisation and depolarisation current responses

The measured polarisation currents are presented in Figure 4.43. For all four cases of the transient voltage ageing, the polarisation current of the aged (130 hours) paper-oil insulation is about 20 to 600 times greater than the polarisation current of the unaged paper-oil insulation in the time range between 0 – 2000 s. Among the four cases of transient voltage ageing, the case 2 with transient voltage amplitude = 6 kV, rise time = 220 ns, switching frequency = 3 kHz, and duty cycle = 50% has the highest increase in the polarisation current for the aged paper-oil insulation compared to the polarisation current for the unaged paper-oil insulation.

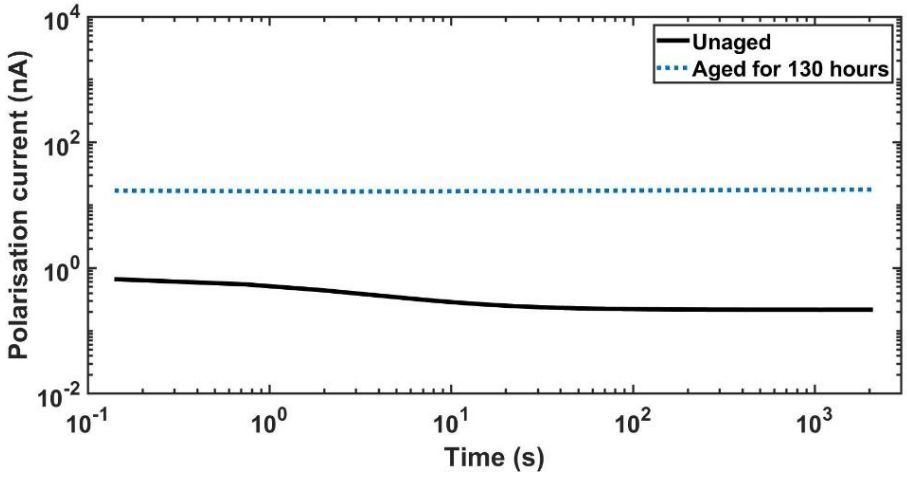
Unaged
Aged for 130 hours
Polarisation current (nA)
Time (s)

(a)

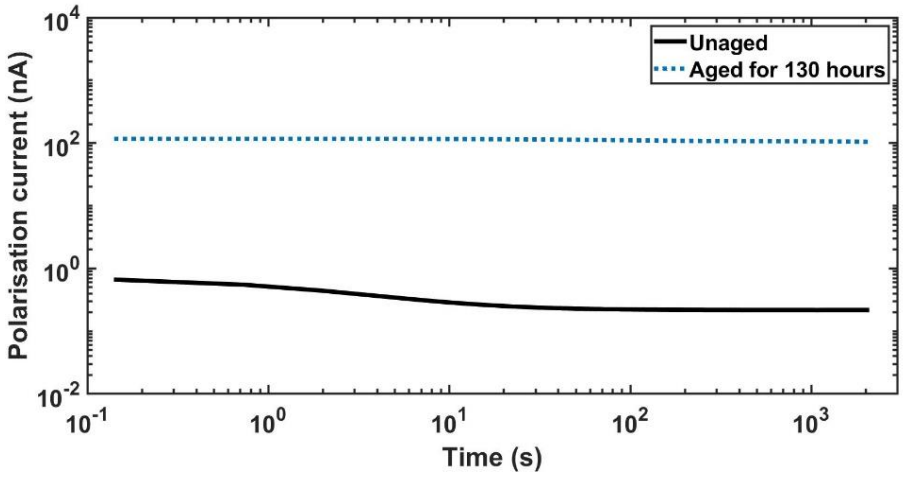
Unaged
Aged for 130 hours
Polarisation current (nA)
Time (s)

(b)

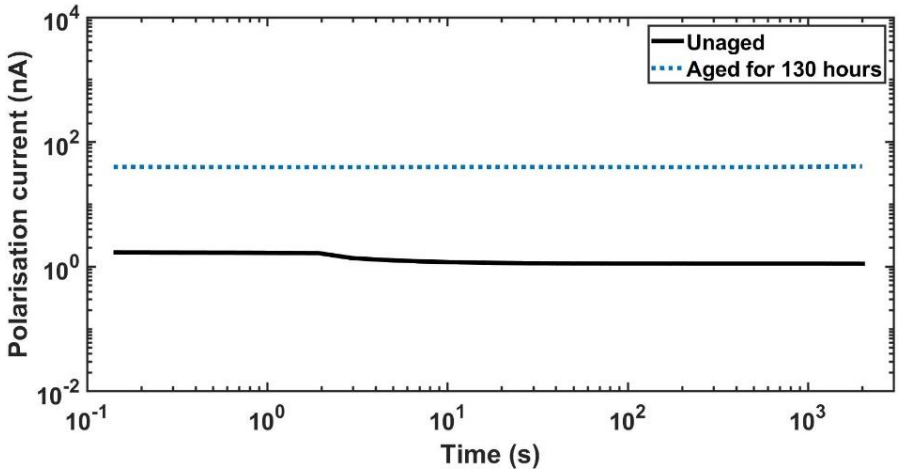

(c)

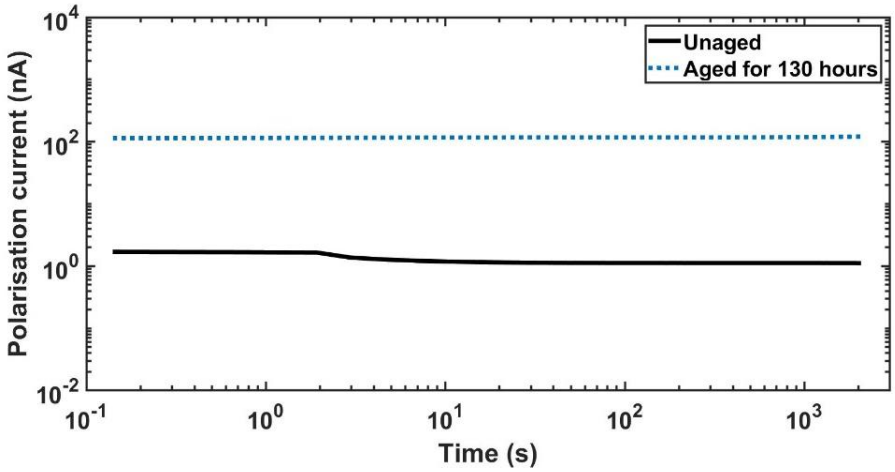

(d)

Figure 4.43: Polarisation current response for various cases of transient voltage ageing of paper-oil insulation with Voltesso 35 B oil: (a) Case 1, (b) Case 2, (c) Case 3, and (d) Case 4.

The polarisation current difference in per unit is obtained by subtracting the polarisation current of unaged paper-oil insulation from the polarisation current of aged (130 hours) paper-oil insulation, and is presented in Figure 4.44. From the Figure 4.44, it can be seen that the order of polarisation current

difference from highest to lowest in the time range between 100 s to 2000 s is as followed: case 2 > case 4 = case 1 > case 3.

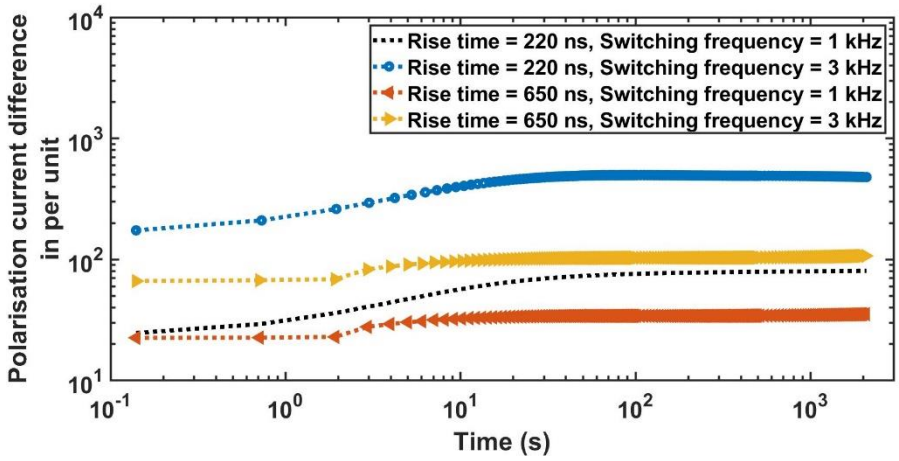

Figure 4.44: Polarisation current difference for various cases of transient voltage ageing (130 hours) of paper-oil insulation with Voltesso 35 B oil.

The corresponding measured depolarisation currents are presented in Figure 4.45. For all four cases of the transient voltage ageing, the depolarisation current of the aged (130 hours) paper-oil insulation is about 2 to 7 times greater than the depolarisation current of the unaged paper-oil insulation in the time range between 0 to 50 s. Between the time range of 50 to 2000 s, the depolarisation current of the aged (130 hours) paper-oil insulation is about 10 to 100 times greater than the depolarisation current of the unaged paper-oil insulation. Among the four cases of transient voltage ageing, the case 2 with transient voltage amplitude = 6 kV, rise time = 220 ns, switching frequency = 3 kHz, and duty cycle = 50% has the highest increase in the depolarisation current for the aged paper-oil insulation compared to the depolarisation current for the unaged paper-oil insulation.

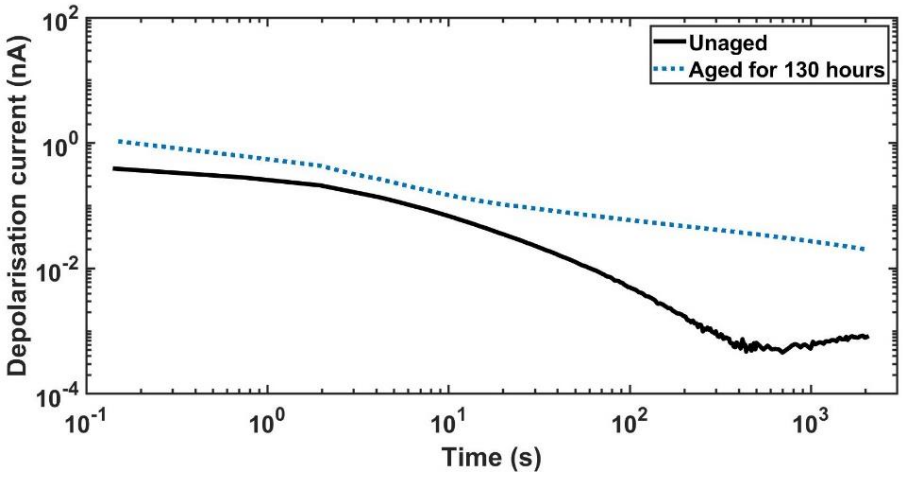
Unaged
Aged for 130 hours
Depolarisation current (nA)
Time (s)

(a)

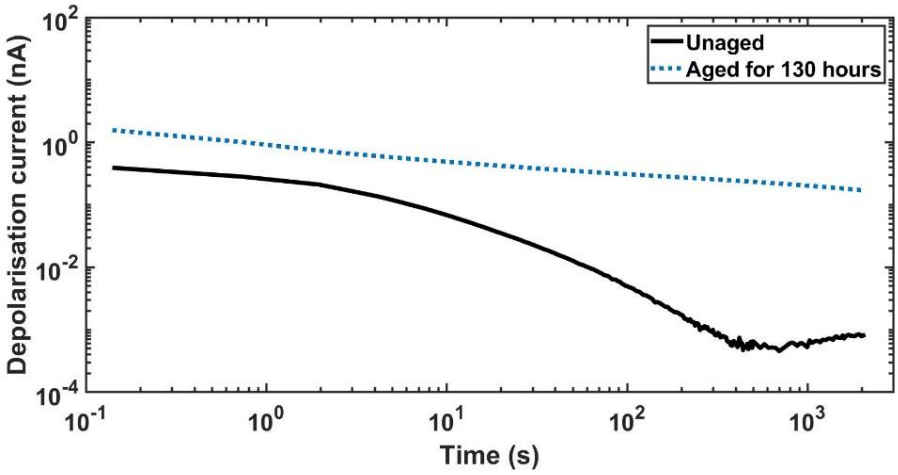
Unaged
Aged for 130 hours
Depolarisation current (nA)
Time (s)

(b)

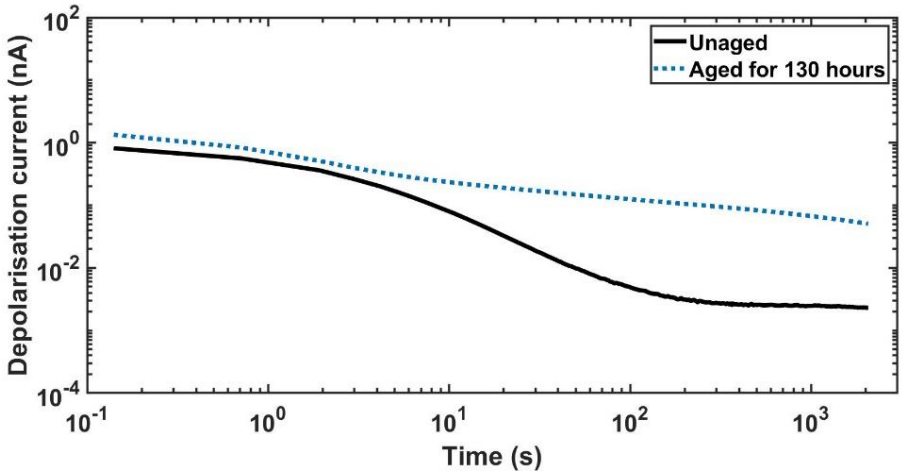

(c)

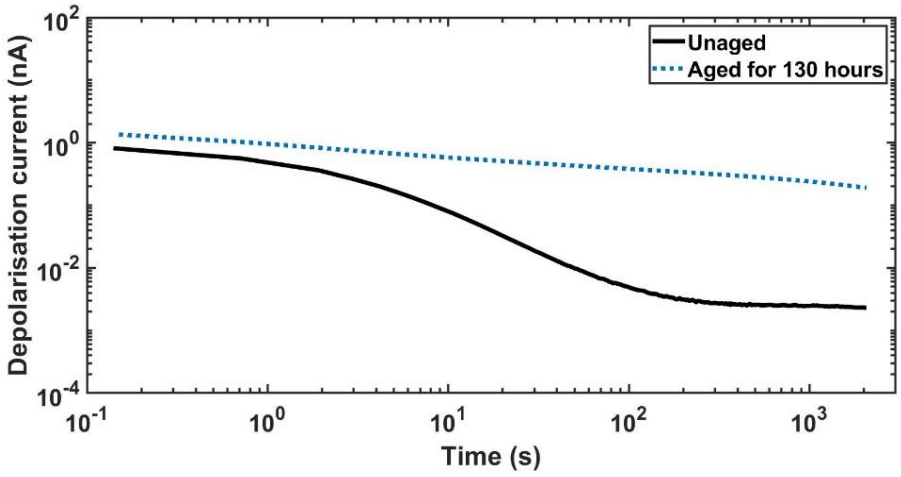

(d)

Figure 4.45: Depolarisation current response for various cases of transient voltage ageing of paper-oil insulation with Voltesso 35 B oil: (a) Case 1, (b) Case 2, (c) Case 3, and (d) Case 4.

The depolarisation current difference in per unit is obtained by subtracting the depolarisation current of unaged paper-oil insulation from the depolarisation current of aged (130 hours) paper-oil insulation, and is presented in Figure 4.46. From the Figure 4.46, it can be seen that the order of depolarisation

current difference from highest to lowest in the setting time region (> 300 s) is as followed: case 2 > case 4 = case 1 > case 3.

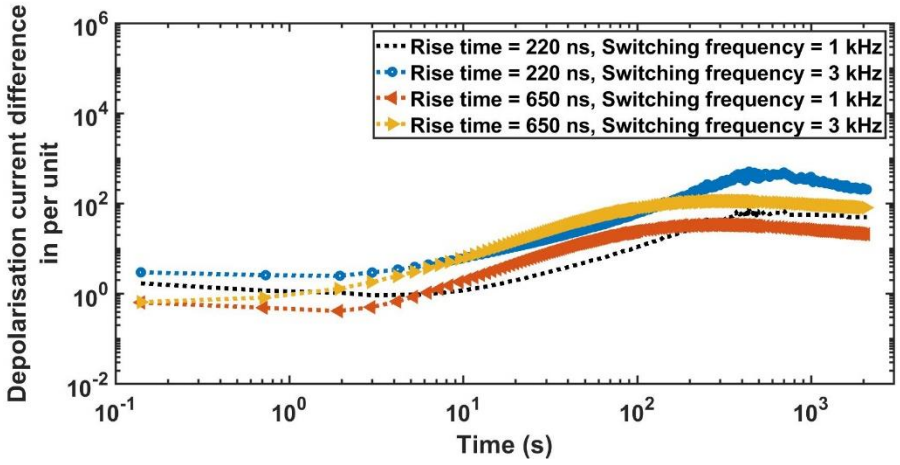

Figure 4.46: Depolarisation current difference for various cases of transient voltage ageing (130 hours) of paper-oil insulation with Voltesso 35 B oil.

4.2.2.2.3 Additional ageing response

The ageing (130 hours) responses including dissipation factor, and insulation resistance for the ageing case reported in section 4.2.2.2. are presented in Table 4.8, and Table 4.9 respectively. For the four cases of the transient voltage ageing, the dissipation factor of the aged paper-oil insulation is about 1.69 to 1.94 higher than the dissipation factor of the unaged paper-oil insulation. Among the four cases of the transient voltage ageing, the case 2 with transient voltage amplitude = 6 kV, rise time = 220 ns, switching frequency = 3 kHz, and duty cycle = 50% has the highest increase (1.94 times) in the dissipation factor for the aged paper-oil insulation compared to the dissipation factor for the unaged paper-oil insulation. For the four cases of the transient voltage ageing, the insulation resistance of the unaged paper-oil insulation is about 1.89 to 1.99 higher than the insulation resistance of the aged paper-oil insulation. Case 2 has the highest reduction (1.99 times) in the insulation resistance for the aged paper-oil insulation compared to the insulation resistance for the unaged paper-oil insulation.

Table 4.8: Dissipation factor (@ 60 Hz) for various cases (shown in Table 4.7) of transient voltage ageing of paper-oil insulation with Voltesso 35 B oil.

Cases	Unaged	Aged for 130 hours	Percentage difference
Case 1	0.0035	0.0970	186.07
Case 2	0.0035	0.2480	194.43
Case 3	0.0140	0.1670	169.06
Case 4	0.0140	0.2350	177.51

Table 4.9: Insulation resistance (@ 60 s) in GΩ for various cases (shown in Table 4.7) of transient voltage ageing of paper-oil insulation with Voltesso 35 B oil.

Cases	Unaged (GΩ)	Aged for 130 hours (GΩ)	Percentage difference
Case 1	883	12.0	-194.74
Case 2	883	1.8	-199.19
Case 3	177	5.0	-188.96
Case 4	177	1.7	-196.19

Chapter 5
Discussion

The chapter describes the discussion of the results obtained during the current research work. The discussion is divided into four sections. The first section discusses about the results of the transient voltage distribution along the transformer winding as a function of transient voltage parameters. The related transient ageing of the paper-oil insulation is discussed in the second section. The results pertaining to the influence of the transient voltage parameters on ageing of the paper-oil insulation is discussed in the third section. Final section compares the transient voltage ageing results obtained for two transformer oils, namely: Luminol TRi oil and Voltesso 35 oil.

5.1 Transient voltage distribution along the transformer winding

The results for three types of transfer function frequency response for two transformers, T1 and T2 are presented in section 4.1.1. The transformer T1 (rating, 1 kVA) was aged under the application of sinusoidal voltage and transformer T2 was aged under the application of repetitive transient voltage. The three transfer function frequency responses were magnitude of voltage difference response in dB, impedance difference response, and voltage ratio difference response. The magnitude of voltage difference response in dB (Figure 4.3, and Figure 4.4) and impedance difference response (Figure 4.11 and Figure 4.12) showed the highest tap-to-tap frequency response difference in the initial taps (tap 1-2) of the transformer winding. Additionally, the magnitude of voltage difference response in dB displayed the distinction in frequency response between aged transformers, T1 and T2. The voltage ratio difference response (Figure 4.15 and Figure 4.16) did not show the highest difference in the initial taps (tap 1-2) of the transformer winding, and it was unable to show the distinction between aged transformers, T1 and T2.

Both the magnitude of voltage difference response in dB and voltage ratio difference response are mainly governed by the self-inductance and series capacitance of the transformer winding. But for the magnitude of voltage difference response in dB, the representation in decibel helped in amplifying the frequency response in the resonance region. Thus the magnitude of voltage difference response in dB is able to show the difference between aged transformers, T1 and T2. The impedance difference response is mainly governed by the total inductance and series capacitance of the transformer winding.

The impedance difference response showed the highest difference in the initial taps (tap 1-2) of the transformer winding, but it was unable to show the distinction between aged transformers, T1 and T2. This was because the impedance difference response was not obtained from the decibel representation of the transfer function. Thus, we can conclude that the measurement connections to obtain the transfer function, and the representation of the transfer function is crucial in obtaining the tap-to-tap frequency response difference. Care must be taken in measuring and representing these transfer function frequency responses used for designing the tap-to-tap winding insulation to prevent resonance voltage along the transformer windings.

In [99], Jayasinghe et al. simulated various mechanical defects including axial displacement, radial displacement, and forced buckling of the transformer windings. They obtained and compared the sensitivity of various frequency response measurement connections in detecting the mechanical defects along the transformer winding. The frequency response measurement connections used include end-to-end voltage ratio, transfer voltage ratio, and input admittance measurements. The end-to-end voltage ratio measurement connection by Jayasinghe et al. was similar to the impedance difference response measurement connection presented in the current research work. The authors showed that the end-to-end voltage ratio frequency response and transfer voltage ratio frequency response are sensitive in detecting the transformers mechanical defects, but the input admittance frequency response is least sensitive in detecting the mechanical defects.

The research aimed to obtain the sensitivity of various transfer function frequency responses in identifying the resonance of transformer's tap-to-tap voltage. The analysis of the resonance region for the transformer tap-to-tap frequency response will help in understanding the transient voltage amplification along the transformer winding. Jayasinghe et al. studied the sensitivity of various transfer functions in identifying the transformers mechanical defect through their simulation study. Thus from both the studies, it can be concluded that measurement connections to obtain the transfer function and the representation of the transfer function is crucial for sensitivity analysis of transfer function frequency response.

The results pertaining to the distribution of transient voltage along the transformer winding as a function of transient voltage parameters including rise time, duty cycle, and applied voltage amplitude were presented in section 4.1.2. The highest tap-to-tap voltage difference (Figure 4.19 and Figure 4.20)

along the transformer winding were obtained for the case with transient voltage of amplitude = 100 V, rise time < 300 ns, and duty cycle = 50%. The reason for the highest tap-to-tap voltage difference at shorter rise time (<300 ns) is because shorter rise time led to increase in rate of rise of the transient voltage. The transformer windings are a network of resistance (R), inductance (L), and capacitance (C), and the increase in rate of rise caused non-linear distribution of the transient voltage along the RLC network of the transformer winding. Thus, the non-linear distribution of transient voltage gave rise to increase in tap-to-tap voltage difference along the transformer winding. Also, the highest tap-to-tap voltage difference is seen in the line end (tap 10-11) of the transformer winding. The results obtained in this research match with the findings obtained by Abdulahovic [37]; where it has been shown that shorter rise time (35 ns) of the transient voltage led to the highest turn-to-turn voltage, and its voltage derivative at the line end of the transformer winding. This was because very short rise time can lead to the interlayer resonance that can cause very high voltage at the initial turns of the winding. But Adbulahovi studied the distribution of transient voltage for a single step voltage with rise time ranging from 35 ns to 500 ns. The current work obtained the distribution of the repetitive square wave voltage with rise time of 290 ns and 1000 ns, switching frequency of 1kHz, and duty cycle of 10% and 50%. Comparing duty cycles of 10% and 50%, it was seen that duty cycle of 50% had the highest tap-to-tap transient voltage difference because duty cycle of 50% has long duration of pulse, and thus higher energy spectrum. Therefore, the transient voltage with duty cycle of 50% and rise time < 300 ns had the highest tap-to-tap voltage difference. The current study help to identify the transient voltage with highest impact on the transformer winding insulation under repetitive pulses.

Based on the design parameters of the transformers, T1 and T2, the critical resonance frequency of the transformers is 10 kHz (Figure 4.9 and Figure 4.10). The fast Fourier transform (FFT) of the transient voltage distribution along the transformer winding is taken, and the tap-to-tap voltage difference at frequency of 10 kHz for various cases of transient voltage parameters were obtained in Figure 4.21 and Figure 4.22. The results showed that shorter rise time led to higher tap-to-tap voltage difference along the transformer winding. But the highest tap-to-tap voltage difference were obtained at the ground end (tap 1-2) of the transformer winding. At the critical frequency of 10 kHz, the resonance led to higher tap-to-tap voltage difference at the tap 1-2. The resonance region can also be observed in the impedance difference response presented in Figure 4.11 and Figure 4.12.

5.2 Transient voltage ageing of the transformer paper-oil insulation

The AC ageing of paper-oil insulation was carried out with Luminol TRi as the insulating oil to obtain the influence of the AC voltage on the long-term ageing (440 hours) of the transformer paper-oil insulation (section 4.2.1.1). There were no signs of deposition of carbon particles on the paper sample (Figure 4.23). The observed negligible degradation of the insulation can be correlated to lack of PD activity under AC ageing. In [48], Khanali et al. obtained the influence of AC voltage on the long-term ageing (500 hours) of the transformer paper-oil insulation with Voltesso 35 as the insulating oil. The authors confirmed that there were no changes in the dielectric property of the transformer paper-oil insulation aged under AC voltage with Voltesso 35 oil as the insulating oil [48].

The repetitive transient voltage ageing of the paper-oil insulation was carried out with Luminol TRi as the insulating oil to obtain the influence of the transient voltage on the long-term ageing (300 hours) of the transformer paper-oil insulation (section 4.2.1.2). The dissipation factor (Figure 4.26) and depolarisation current (Figure 4.28) did not change significantly with long-term ageing of the insulation with Luminol TRi oil. There were changes in polarisation current (Figure 4.27) with ageing time, but the changes were not significant, and negligible degradation of the paper-oil insulation were observed. In addition, there were no carbon deposits on the paper samples. Thus, neither the paper, nor the oil had any changes in their responses due to transient voltage ageing. The reason is Luminol TRi oil has higher resistance to electrical breakdown than Voltesso 35 oil and is stable towards chemical and electrical ageing (Table 3.4).

The ageing of the paper-oil insulation under repetitive transient voltage with Voltesso 35 A as the insulating oil were carried out to analyse the influence of the transient voltage on the long-term ageing (300 hours) of paper-oil insulation with Voltesso 35 A oil (4.2.1.3). The paper aged significantly, and there was a circular carbon deposit on the paper sample indicating the degradation of the paper due to transient voltage ageing (Figure 4.29). The dissipation factor in Figure 4.30 increased with ageing time in the frequency range between 0.01 Hz to 1000 Hz. In [73], [100], it was shown that the ageing of paper (cellulose insulation) led to changes in dissipation factor in the frequency range between 10 Hz to 1000 Hz. The ageing of oil led to changes in dissipation factor in the frequency range between 0.01 Hz to 10 Hz. Thus, it is clear from the dissipation factor measurements that both the paper and oil degraded due to the transient voltage ageing. The conductivity of the oil is increased due to the

development of carbon particles and soot during the ageing process leading to increase in dissipation factor in the frequency region between 0.01 Hz to 10 Hz. The rate of increase in dissipation factor was highest when the paper-oil insulation was aged to 65 hours. The rate of increase in dissipation factor reduced as the ageing time increased from 65 hours to 130 hours. The rate of change in dissipation factor was not significant when the ageing time increased from 130 hours to 300 hours. The insignificant rate of change in dissipation factor with increase in ageing time is due to conditioning of the paper-oil insulation with time. The conditioning of the insulation led to saturation of charge carriers, thus, the rate of change in dissipation factor saturated after 130 hours of ageing time. The polarisation current (Figure 4.31) increased with increase in ageing time in the complete measurement time range. The initial part (value at initial time) of the polarisation current reflects the changes in oil conductivity due to ageing process [100]. The final part (value at longer time) of the polarisation current reflects the changes in the molecular structure of the paper due to ageing process (carbon deposits) [100]. The increase in oil conductivity due to ageing saturated after ageing time of 130 hours. The increase in carbon deposits (paper degradation) due to ageing saturated with the ageing time of 65 hours. The rate of increase in ageing factor saturated due to conditioning of the paper-oil insulation. The depolarisation current (Figure 4.32) increased with increase in ageing time at the measurement time range of 100 s to 2000 s. The increase in depolarisation current during ageing process is due to increase in degradation level of the paper leading to increase in charge traps on the paper sample. The final part (100 s to 2000 s) of the depolarisation current reflects the ageing of paper sample. The increase in depolarisation current saturated with ageing time of 65 hours. Thus the deposition level of the carbon particles on the paper sample saturated after the ageing time of 65 hours. During the ageing process, the oil temperature was constant at room temperature. Thus, the transient ageing of the paper-oil insulation did not lead to oxidation of the oil. The amount of dissolved hydrogen gas in oil did not increase with the long-term ageing of the paper-oil insulation. In [51], Khanali obtained significant amount of increase in dissolved hydrogen gas in oil during the transient voltage ageing of the paper-oil insulation. The reason for insignificant dissolved hydrogen gas amount in the present research work is because the volume of oil used in the ageing process was huge (20 litres), and the dissolved hydrogen gas may not be significant enough to be shown in the measurement device. Additionally, the research focused on ageing degradation at the region of paper sample that is in contact with the rod-plane electrode. Thus, the

ageing responses including dielectric frequency response, polarisation current, and depolarisation current are used to analyse the ageing level of the transformer paper-oil insulation.

The ageing of paper-oil insulation under repetitive transient voltage at room temperature and elevated temperature of 50°C were presented as two cases in section 4.2.2.1. The first case was transient voltage ageing of paper-oil insulation for ageing duration of 300 hours at room temperature (section 4.2.2.1.1). The second case was transient voltage ageing of paper-oil insulation for ageing duration of 70 hours at temperature of 50° C (4.2.2.1.2). Both the cases used Voltesso 35 A oil as the insulating oil for the ageing process. The dissipation factor, polarisation current, and depolarisation current of the paper-oil insulation aged for 300 hours at room temperature is 10, 40, 100 times greater than the respective dissipation factor, polarisation current, and depolarisation current of the unaged paper-oil insulation (Figure 4.33, Figure 4.34, and Figure 4.35). The dissipation factor, polarisation current, and depolarisation current of the paper-oil insulation aged for 70 hours at temperature of 50° C is 30, 200, 300 times greater than the respective dissipation factor, polarisation current, and depolarisation current of the unaged paper-oil insulation (Figure 4.37, Figure 4.38, and Figure 4.39). It is evident from the results that the insulation aged under transient voltage for 70 hours at temperature of 50° C has higher ageing effects compared to the insulation aged under transient voltage for 300 hours at room temperature. Even though the high temperature ageing involved considerably lower ageing time compared to room temperature ageing, the ageing response had an exponential increase for elevated temperature ageing. The oil used for the current ageing study is Voltesso 35 A oil, and the Voltesso 35 A oil contains moisture, and other ionic contaminants dissolved in it. Also, the electrical conductivity of Voltesso 35 A oil is significantly high with a value of 24.7 pS/m (Table 3.5). Thus, the contaminants led to degradation of the paper-oil insulation due to hydrolysis and oxidation process at increased temperature. Furthermore, the increase in temperature will lead to increase in the ageing rate of the paper-oil insulation. The increase in temperature causes increase in reaction rate for the oxidation and hydrolysis of the insulation [101]. Thus, the ageing rate accelerates with increase in temperature leading to considerable increase in the ageing process for transient voltage ageing of the paper-oil insulation at the elevated temperature of 50° C. In [71], Koltunowicz aged the paper-oil insulation with repetitive transient voltage of amplitude = 1kV superimposed on an AC voltage of amplitude = 2.22 kV for temperatures ranging from 40° C to 80° C. The author found that the increase in temperature did not increase the dissipation factor for the paper-oil insulation aged under repetitive transient voltage. The

ageing time (22 hours), and the amplitude of the applied voltage were low and also, the paper sample were not degraded significantly. The current work used Voltesso 35 A oil for the ageing process, and the ageing was done for a longer duration with six rod-plane electrodes. The conditions are closed to those encountered in transformers in service, introducing non-uniformity in geometries, contaminants and elevated temperature. Thus, there was significant variation in the ageing response due to transient voltage ageing carried out at an elevated temperature of 50° C. Therefore, the ageing of the paper-oil insulation under elevated temperature is analysed to obtain the influence of temperature on the transient voltage ageing of the paper-oil insulation.

5.3 Influence of the transient voltage parameters on ageing of the paper-oil insulation

The present section discusses the result pertaining to the influence of the transient voltage parameters including rise time and switching frequency on the ageing of the paper-oil insulation. In literature, there were a few contradictions about the influence of transient voltage parameters on the ageing of the transformer paper-oil insulation. In [51], Khanali et al. claimed that the faster rise time lead to increase in partial discharge inception voltage (PDIV) for the paper-oil insulation under the application of transient voltage; whereas, Koltunowicz [71] obtained that the faster rise time decreased PDIV for the paper-oil insulation under the application of transient voltage. However, Khanali et al. also obtained that the energy of the partial discharge activity were higher with faster rise time of the transient voltage [51]. In [71], the breakdown voltage for the paper-oil insulation decreased with an increase in repetition frequency of the transient voltage in the frequency range of 1 kHz to 10 kHz; whereas, in [66], the breakdown voltage for the paper-oil insulation increased with an increase in oscillation frequency in the frequency range of 600 Hz – 1 kHz. Previous research work focussed on the influence of the transient voltage parameter on the short-term ageing of the paper-oil insulation. Thus, the current research work clarifies the effect of transient voltage parameters including rise time and switching frequency on the long-term ageing of the paper-oil insulation.

Section 4.2.2.2 presents the result for ageing of the paper-oil insulation under various cases of the repetitive transient voltage shown in Table 4.7 with Voltesso 35 B mineral oil as the insulating oil. The four cases in Table 4.7 are based on two parameters of the repetitive square wave (transient) voltage; they are rise time and switching frequency. The amplitude and the duty cycle for the transient voltage

are fixed at 6 kV and 50% respectively. The ageing lead to deposition of carbon on the paper sample, and the paper sample severely degraded. The dissipation factor, polarisation current, and depolarisation current of the aged (130 hours) paper-oil insulation is about 25, 174, 76 times greater than the respective dissipation factor, polarisation current, and depolarisation current of the unaged paper-oil insulation (Figure 4.41, Figure 4.43, and Figure 4.45). The average value of all four cases of transient voltage ageing response is considered when obtaining the above mentioned ratio between aged and unaged paper-oil insulation. Among the four cases of transient voltage ageing, case 2 with transient voltage amplitude = 6 kV, rise time = 220 ns, switching frequency = 3 kHz, and duty cycle = 50% has the highest increase in dissipation factor, polarisation current, and depolarisation current for the aged paper-oil insulation compared to the unaged paper-oil insulation. This is because the transient voltage with rise time = 220 ns and switching frequency = 3 kHz has the highest voltage energy spectrum leading to higher degradation of the aged paper-oil insulation.

The percentage difference between the aged and unaged paper-oil insulation for dissipation factor (@ 60 Hz) under various cases of transient voltage ageing is shown in Table 5.1. The dissipation factor at 60 Hz for various cases of transient voltage ageing was obtained from Table 4.8. From Table 5.1, it was seen that the order of dissipation factor percentage difference from highest to lowest was as followed: case 2 > case 1 > case 4 > case 3. The above order is similar to the order of dissipation factor difference in the frequency range between 10 Hz to 1000 Hz obtained in Figure 4.42. The effects of transient voltage rise time and duty cycle on the dissipation factor percentage difference of the aged paper-oil insulation is analysed by using two-level, two-factor design of experiments for the transient voltage parameters. Table 5.2 shows the effects of transient voltage parameter on the dissipation factor percentage difference. Two replicates were obtained for each of the cases shown in Table 5.1, and the error for dissipation factor percentage difference is 1.00. From Table 5.2, it can be seen that the effect for ‘rise time x switching frequency’ interaction is 0.04, and can be neglected because the interaction effect is lower than the error. The effect of rise time is -16.96, which means faster rise time (220 ns) has higher percentage difference for dissipation factor. Thus, faster rise time led to higher damage to the paper insulation under transient voltage ageing. The research results match with Koltunowicz [71], where the author says that the faster rise leads to decrease in PDIV. The faster rise time led to higher ageing because the faster rise time causes increase in partial discharge, and also leads to increase in space charge accumulation, thus resulting in higher degradation of the paper-oil insulation. The effect

of switching frequency is 8.40, which means higher switching frequency (3 kHz) has higher percentage difference for dissipation factor. Thus, higher switching frequency led to higher damage to the paper insulation under transient voltage ageing. The higher switching frequency will increase the rate of partial discharge on the paper-oil insulation during the ageing process, thus leading to faster degradation of the paper-oil insulation. The 95 % confidence interval for the effects of transient voltage parameters on the dissipation factor percentage difference is shown in Table 5.2. From Table 5.2, it can be seen that the confidence interval for the 'rise time x switching frequency' interaction effect has zero in the interval; whereas, the confidence interval for rise time effects and switching frequency effects does not have zero in their interval. Thus, the 'rise time x switching frequency' interaction effect on the dissipation factor percentage difference can be neglected.

Percentage difference between dissipation factor (@ 60 Hz) of aged and unaged paper-oil insulation is plotted with switching frequency on the x-axis, and rise time as the legend in Figure 5.1. It is seen from Figure 5.1 that the two lines corresponding to rise time of 220 ns and 650 ns are parallel to each other, indicating that there is no interaction effect between the rise time and the switching frequency. The effect of rise time is obtained by the value of perpendicular distance between the two parallel lines. The effect of switching frequency is obtained by the average of slopes of the two lines. The effect of rise time is higher than the effect of switching frequency for the long-term ageing of the transformer paper-oil insulation. In [102], Jarrar et al. studied the influence of repetitive transient voltage parameters including rise time (0.3 ns and 0.5 ns), switching frequency (1 kHz and 4 kHz), and overshoot (0 and 30 %) on the partial discharge rate during the transient ageing of the type II Turn-to-Turn motor insulation. They found that the overshoot and switching frequency of the transient voltage had a significant impact on the average PD rate from the motor insulation ageing, whereas; rise time did not have significant effect on the average PD rate for the motor insulation ageing. In the current research work, both rise time and the switching frequency had significant effect on the ageing of the paper-oil insulation. In [102], the authors worked on motor insulation, which is a solid structure; whereas, in the current work, the ageing is carried out for transformer paper-oil insulation, which is solid-liquid insulation. Thus, the presence of the solid-liquid interface can lead to higher amount of polarisation and change in space charge accumulation dynamics during the ageing process.

Table 5.1: Dissipation factor (@ 60 Hz) for various cases of transient voltage ageing of paper-oil insulation with Voltesso 35 B oil.

Cases	Rise time (ns)	Switching frequency (kHz)	Unaged	Aged for 130 hours	Percentage Difference
Case 1	220 (-)	1 (-)	0.0035	0.0970	186.07
Case 2	220 (-)	3 (+)	0.0035	0.2480	194.43
Case 3	650 (+)	1 (-)	0.0140	0.1670	169.06
Case 4	650 (+)	3 (+)	0.0140	0.2350	177.51

Table 5.2: Parameter effects for dissipation factor percentage difference under transient voltage ageing (130 hours) of the paper-oil insulation.

Effects	Percentage Difference	95 % Confidence Interval for Percentage Difference
Rise time	-16.96	(-17.94, -15.98)
Switching Frequency	8.40	(7.42, 9.38)
Interaction	0.04	(-0.94, 1.02)

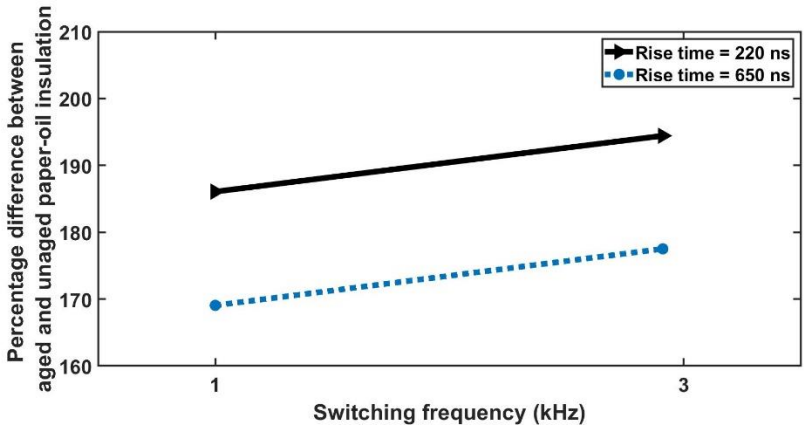

Figure 5.1: Percentage difference between dissipation factor (@ 60 Hz) of aged and unaged paper-oil insulation for ageing carried out (130 hours) under various cases of transient voltage parameters.

5.4 Comparison of transient voltage ageing of Luminol TRi and Voltesso 35 oils

There were large differences in ageing response for the paper-oil insulation with Voltesso 35 oil (section 4.2.1.3 and section 4.2.2) compared to the ageing responses for the paper-oil insulation with Luminol TRi oil (section 4.2.1.2). The reason for above findings are the following (Table 3.4 and Table 3.5):

- The power factor and the electrical conductivity for the Voltesso 35 oil is greater than the power factor and the electrical conductivity for the Luminol TRi oil. Thus Luminol TRi oil has lower losses compared to the Voltesso 35 oil.
- The tendency for gassing (ASTM D2300) for Luminol TRi oil is -10 µl/min, and for Voltesso 35 oil is 30 µl/min. Thus, there was insignificant partial discharge activity for ageing with Luminol TRi oil leading to a negative gassing tendency. Thus, the ageing level of paper-oil insulation with Luminol TRi reduced due to insignificant partial discharge.
- During oxidation process (ASTM D2440), the formation of sludge for Luminol TRi oil is 20 times lower than the sludge formation for Voltesso 35 oil. The formation of acid during oxidation process for Luminol TRi oil is 50 times lower than the acid formation for Voltesso 35 oil. Thus, during the ageing process, the Voltesso 35 oil has higher rate of sludge and acid formation by oxidation reaction compared to the Luminol TRi oil.

Therefore, for the transient voltage ageing conducted in the current research work, the Luminol TRi oil performed better compared to the Voltesso 35 oil.

Chapter 6
Summary and Conclusion

6.1 Summary

The generation of electricity by wind energy source is gaining popularity in the recent times especially in renewable friendly countries including Canada. The operation of circuit breakers and power electronic converters in a wind farm leads to generation of high-frequency repetitive transient voltages at the wind turbine transformer terminals. These high-frequency transients are detrimental to the winding insulation of the transformer. Thus, the distribution of such transients using a square wave voltage along the transformer winding is studied to analyse the inter-winding voltage along the transformer. The repetitive transients generated by the breaker and converter operations can have variations in their rise time, duty cycle, amplitude and switching frequency. Thus, the influence of the transient voltage parameter including rise time, duty cycle and amplitude on its distribution along the windings are obtained for two model transformers and also from a PSCAD simulated transformer equivalent circuit. The repetitive transient voltage travel along the transformer windings and these transients can amplify based on the inter-winding resonance of the transformer. The transfer function frequency responses for the two model transformers are obtained to evaluate the resonance region for the transformers. Three transfer function frequency responses including the magnitude of voltage difference response in dB, impedance difference response, and voltage ratio difference response are compared to assess the ability of the above mentioned transfer function to recognize and distinguish the inter-winding resonance for the two model transformers. On the other, as the paper-oil composite is extensively used in transformers, some fundamental studies are carried out to understand the effect of long-term ageing of the paper-oil insulation under the repetitive transient voltage. Two-level, two-factor design of experiments are used to obtain the effects of rise time and switching frequency on the ageing response of the paper-oil insulation. The ageing responses measured in the current research are dissipation factor, polarisation current and depolarisation current to compare the degradation level of aged paper-oil insulation with an unaged paper-oil insulation. Furthermore, the transient voltage ageing for paper immersed in two different mineral oils are compared. The two oils were Luminol TRi oil and Voltesso 35 oil with difference in their electrical and chemical properties. Finally, the paper-oil insulation is aged under combined electrical and thermal stresses to obtain the influence of increase in

temperature on the ageing of paper-oil insulation. The wind turbine step-up transformers are subjected to thermal stresses due to loading cycle and harmonics, and they are subjected to electrical stresses due to transients generated from operation of breakers and converters, thus the ageing under combined stresses will be helpful for the manufacturers to design the insulation for these transformers.

6.2 **Conclusion**

The distribution of transient voltage along the transformer winding for two model transformers, T1 and T2 are obtained, and the following conclusions are derived:

- The tap-to-tap transient voltage difference along the transformer winding depends on the rise time and duty cycle of the applied transient voltage.
- The transient voltage case with amplitude of 100 V, rise time of 290 ns, and duty cycle of 50 % had the highest tap-to-tap transient voltage difference along the transformer winding. Thus, higher duty cycle and faster rise time led to the highest tap-to-tap voltage difference.
- The transient voltage distribution analysed for transformer equivalent circuit designed in PSCAD simulation software also showed the highest tap-to-tap voltage difference for transient input voltage with an amplitude of 100 V, rise time of 200 ns, and duty cycle of 50 %.

The frequency response for the two model transformers, T1 and T2 are measured and the comparison of three transfer function frequency responses led to the following conclusion:

- Initial taps (tap 1-2) had the highest tap-to-tap difference for the following two transfer functions: magnitude of voltage difference response in dB and impedance difference response. The voltage ratio difference response did not show the highest tap-to-tap difference at the initial taps.
- The distinction between frequency response of aged transformers, T1 and T2 were obtained by the magnitude of voltage difference response in dB. There was no distinction between frequency response of transformers, T1 and T2 for both voltage ratio difference response and the impedance difference response.
- Based on the above observations, it is recommended that the measurement connections to obtain the transfer function and the representation of the transfer function are crucial in

obtaining the tap-to-tap frequency response differences and to distinguish between the transformers.

Based on the long-term ageing of the transformer paper-oil insulation under repetitive transient voltage, the research work concluded the following:

- For long-term ageing (300 hours) of transformer paper-oil insulation, the rate of increase in ageing responses (dissipation factor, polarisation current, and depolarisation current) saturated at ageing time above 130 hours.
- The increase in ageing response for paper-oil insulation stressed under combination of transient voltage stress and thermal stress was significantly higher than the increase in ageing response for paper-oil insulation stressed at room temperature.
- Between, Luminol TRi oil and Voltesso 35 oil, the transient voltage ageing with Voltesso 35 oil had noticeable degradation of paper compared to paper aged with Luminol TRi oil. In fact, paper aged with Luminol TRi oil had shown no signs of degradation. Thus, Luminol TRi oil performed better for the transient voltage ageing studied in the current research work.

Comparing the paper-oil insulation ageing under repetitive transient voltage and sinusoidal voltage, it was seen that the ageing response and degradation level were significantly higher for paper-oil insulation aged under repetitive transient voltage. For ageing of paper-oil insulation under repetitive transient voltage of amplitude = 6 kV, switching frequency = 1 kHz, duty cycle = 50%, and rise time = 220 ns, it was seen that the Luminol TRi oil performed better as an insulating oil compared to the Voltesso 35 oil. However, it is necessary to compare the long-term ageing of paper-oil insulation under repetitive transient voltage, considering the thermal stresses due to load cycling effects for designing the insulation of the wind turbine step-up transformers.

Finally, the influence of transient voltage parameters including rise time and switching frequency on ageing response of the transformer paper-oil insulation is evaluated for transient voltage ageing duration of 130 hours. The ageing duration of 130 hours is selected because the increase in ageing responses saturated at ageing time of 130 hours. The conclusions for the influence of transient voltage parameters on ageing of the paper-oil insulation is as followed:

- The faster rise time and higher switching frequency of the transient voltage led to higher ageing degradation level for the paper-oil insulation.
- Comparing rise time and switching frequency of the transient voltage, the rise time had higher effect on the ageing response compared to the switching frequency.
- There were no interaction effects between the rise time and switching frequency on the transient ageing of the transformer paper-oil insulation. Thus, it can be concluded that the effects due to both the parameters were independent of each other.

6.3 **Potential contribution**

The purpose of the current research is to evaluate the transformer paper-oil insulation under high-frequency repetitive transient voltage and to obtain the best solution to reduce the transformer insulation degradation under these transients. The following are the contributions from the thesis:

- The distribution of transient voltage along the transformer winding with varying transient parameters was analysed. The inter-winding transient voltage distribution will help in designing the transformer insulation and winding subjected to high-frequency repetitive transient voltage.
- The capability of transfer function frequency response to detect the potential inter-tap resonance that can lead to dangerously high transient voltages along the transformer winding was delineated. Selecting the most beneficial transfer function frequency response is required to obtain all the important inter-tap resonance region, so that appropriate RC filters can be designed at the transformer terminals to mitigate these resonance overvoltages.
- The effects of transient voltage parameters including rise time and switching frequency on the ageing of paper-oil insulation under repetitive transient volage were obtained using two-level, two-factor design of experiments. It is difficult to design RC filters that can completely reduce the transient voltages along the transformer winding. Thus, understanding the degradation level of paper-oil insulation will help in designing transformer insulation that is able to withstand the transient voltage having the worst case scenario for rise time and switching frequency.

- The transient voltage ageing of the paper-oil insulation with added stress of elevated temperature have been highlighted in the research work. The combined analysis of the transient voltage stress and thermal stress can help in designing the transformer insulation that faces the variation in load cycle, harmonics, and transient voltage due to switching operation of circuit breakers and converters.
- The comparison of two mineral oils, namely Luminol TRi oil and Voltesso 35 oil to withstand the transient voltage stress for long duration can help the manufacturers in deciding the oil that is best suited for the transformers facing continuous high-frequency repetitive transient voltage.

6.4 Future work

1. In the current research work, the two transient voltage factors (parameters) used for ageing were rise time and switching frequency with two levels for each factor. It would be interesting to include duty cycle as an additional ageing factor. Thus, three levels for each of the three factors (rise time, duty cycle, and switching frequency) of the transient voltage could be used to obtain the effects of transient voltage parameters on the ageing of transformer paper-oil insulation.
2. The combined transient voltage stress and thermal stress was applied on the paper-oil insulation with Voltesso 35 A oil as the test oil. The temperature was elevated to 50°C in the current research work. It would be helpful for the transformer industry to extend the study for higher temperature like 80°C to obtain the high temperature influence on the transient voltage ageing. The high temperature ageing would help in designing transformers with varying load cycles and voltage harmonics.
3. The transient voltage ageing of transformer paper-oil insulation was carried out for six paper samples placed individually between six rod-plane electrodes. It is recommended to extend the study with multi-layer insulation and full winding insulation test samples to include the effects of interfaces and winding designs.
4. The distribution of transient voltage along the transformer winding was analysed for two model transformers. The transient voltage distribution can be extended to transformers of different designs and makes to obtain a design that is best suited to withstand the transient voltage

stresses. Additionally, the comparison of three transfer function frequency responses can be extrapolated to other transformer designs to obtain a complete database for the transformers internal frequency resonance region for various transfer function frequency responses.

5. The PSCAD simulation was carried out for a simple equivalent circuit of the transformer winding to obtain the influence of the transient voltage parameters on its distribution along the transformer winding. The simulation can be further extended to design a complete wind farm chain to obtain the transient distribution along all the transformers in the wind farm chain. This will help in finding the critical transformers in the wind farm network that face the maximum stress under high-frequency repetitive transient voltage.

Bibliography

[1] *Wind energy*. Available: https://renewablesassociation.ca/wind-energy/.

[2] M. Devgan, "Investigation of High Frequency Switching Transients on Wind Turbine Step Up Transformers." , University of Waterloo Thesis, Canada, 2015.

[3] D. N. Hussein, M. Matar and R. Iravani, "A Type-4 Wind Power Plant Equivalent Model for the Analysis of Electromagnetic Transients in Power Systems," *IEEE Transactions on Power Systems,* vol. 28, *(3),* pp. 3096-3104, 2013. . DOI: 10.1109/TPWRS.2012.2227845.

[4] T. Bengtsson *et al*, "Repetitive fast voltage stresses-causes and effects," *IEEE Electrical Insulation Magazine,* vol. 25, *(4),* pp. 26-39, 2009. . DOI: 10.1109/MEI.2009.5191414.

[5] P. Jain, "Addressing Premature Failure of Pad Mount Transformers at Wind Farms," Aug 6, 2013.

[6] P. Dvorak, "Gassing in wind-farm transformers," April 23, 2012.

[7] "IEEE Guide for the Interpretation of Gases Generated in Oil-Immersed Transformers," *IEEE Std C57. 104-2008 (Revision of IEEE Std C57. 104-1991),* pp. 1-36, 2009. . DOI: 10.1109/IEEESTD.2009.4776518.

[8] G. Jose and R. Chacko, "A review on wind turbine transformers," in - *2014 Annual International Conference on Emerging Research Areas: Magnetics, Machines and Drives (AICERA/iCMMD),* 2014. . DOI: 10.1109/AICERA.2014.6908172.

[9] B. Gustavsen, "Study of Transformer Resonant Overvoltages Caused by Cable-Transformer High-Frequency Interaction," *IEEE Transactions on Power Delivery,* vol. 25, *(2),* pp. 770-779, 2010. . DOI: 10.1109/TPWRD.2010.2040292.

[10] S. M. Wong, L. A. Snider and E. W. C. Lo, "Overvoltages and reignition behavior of vacuum circuit breaker," in - *2003 Sixth International Conference on Advances in Power System Control, Operation and Management ASDCOM 2003 (Conf. Publ. no. 497),* 2003. . DOI: 10.1049/cp:20030663.

[11] P. Picot, "Cahier technique no. 198 - Vacuum switching," pp. 1-36, 06/03/2000.

[12] D. D. Shipp *et al*, "Transformer failure due to circuit breaker induced switching transients," *2011 IEEE Industrial and Commercial Power Systems Technical Conference,* pp. 1-10, 2011. . DOI: 10.1109/ICPS.2011.5890893.

[13] C. Vollet and B. de Metz Noblat, "Protecting High-Voltage Motors Against Switching Overvoltages," *2007 4th European Conference on Electrical and Instrumentation Applications in the Petroleum & Chemical Industry,* pp. 1-7, 2007. . DOI: 10.1109/PCICEUROPE.2007.4354001.

[14] A. Cavallini, D. Fabiani and G. C. Montanari, "Power electronics and electrical insulation systems ☍ Part 1: Phenomenology overview," *IEEE Electrical Insulation Magazine,* vol. 26, *(3),* pp. 7-15, 2010. . DOI: 10.1109/MEI.2010.5482783.

[15] M. Khanali, "Effects of Distorted Voltages on the Performance of Renewable Energy Plant Transformers," University of Waterloo Thesis, Canada, 2017. Available: http://hdl.handle.net/10012/12368.

[16] "IEC/IEEE International Draft Standard - Power Transformers - Part 16: Transformers for Wind Turbine Application," *Ieee P60076-16_d1,* pp. 1, 2015.

[17] D. Smugala *et al*, "Wind Turbine Transformers Protection Method Against High-Frequency Transients," *IEEE Transactions on Power Delivery,* vol. 30, *(2),* pp. 853-860, 2015. . DOI: 10.1109/TPWRD.2014.2343261.

[18] G. Liu *et al*, "Analysis of Switching Transients during Energization in Large Offshore Wind Farms," *Energies,* vol. 11, *(2),* 2018. Available: https://www.mdpi.com/1996-1073/11/2/470. DOI: 10.3390/en11020470.

[19] Y. L. Xin *et al*, "Sensitivity analysis of reignition overvoltage for vacuum circuit breaker in offshore wind farm using experiment-based modeling," *Electr. Power Syst. Res.,* vol. 172, pp. 86-95, 2019. . DOI: https://doi.org/10.1016/j.epsr.2019.02.008.

[20] Q. Zhou *et al*, "Analysis of Restrike Overvoltage of Circuit Breakers in Offshore Wind Farms," *IEEE Transactions on Applied Superconductivity,* vol. 26, *(7),* pp. 1-5, 2016. . DOI: 10.1109/TASC.2016.2594830.

[21] J. Zhou *et al*, "Investigation on switching overvoltage in an offshore wind farm and its mitigation methods based on laboratory experiments," in - *2018 IEEE PES Asia-Pacific Power and Energy Engineering Conference (APPEEC),* 2018. . DOI: 10.1109/APPEEC.2018.8566662.

[22] J. Zhou *et al*, "Impact Factor Identification for Switching Overvoltage in an Offshore Wind Farm by Analyzing Multiple Ignition Transients," *IEEE Access,* vol. 7, pp. 64651-64662, 2019. . DOI: 10.1109/ACCESS.2019.2916952.

[23] S. Ghasemi *et al*, "Probabilistic analysis of switching transients due to vacuum circuit breaker operation on wind turbine step-up transformers," *Electr. Power Syst. Res.,* vol. 182, pp. 106204, 2020. . DOI: https://doi.org/10.1016/j.epsr.2020.106204.

[24] Y. Guo *et al*, "Reignition overvoltages induced by vacuum circuit breakers and its suppression in offshore wind farms," *International Journal of Electrical Power & Energy Systems,* vol. 122, pp. 106227, 2020. . DOI: https://doi.org/10.1016/j.ijepes.2020.106227.

[25] Y. L. Xin *et al*, "Overvoltage protection on high-frequency switching transients in large offshore wind farms," in - *2016 IEEE Power and Energy Society General Meeting (PESGM)*, 2016. . DOI: 10.1109/PESGM.2016.7741642.

[26] "IEEE Guide to Describe the Occurrence and Mitigation of Switching Transients Induced by Transformers, Switching Device, and System Interaction," *IEEE Std C57. 142-2010*, pp. 1-56, 2011. . DOI: 10.1109/IEEESTD.2011.5759579.

[27] X. Zhao *et al*, "Performance evaluation of online transformer internal fault detection based on transient overvoltage signals," *IEEE Transactions on Dielectrics and Electrical Insulation*, vol. 24, *(6)*, pp. 3906-3915, 2017. . DOI: 10.1109/TDEI.2017.006772.

[28] M. Kuniewski and P. Zydron, "Analysis of the applicability of various excitation signals for FRA diagnostics of transformers," in - *2018 IEEE 2nd International Conference on Dielectrics (ICD)*, 2018. . DOI: 10.1109/ICD.2018.8514677.

[29] "IEEE Guide for Conducting a Transient Voltage Analysis of a Dry-Type Transformer Coil," *IEEE Std C57. 12. 58-2017 (Revision of IEEE Std C57. 12. 58-1991)*, pp. 1-30, 2017. . DOI: 10.1109/IEEESTD.2017.8126273.

[30] A. H. Soloot, H. K. Høidalen and B. Gustavsen, "Influence of the winding design of wind turbine transformers for resonant overvoltage vulnerability," *IEEE Transactions on Dielectrics and Electrical Insulation*, vol. 22, *(2)*, pp. 1250-1257, 2015. . DOI: 10.1109/TDEI.2015.7076828.

[31] A. H. Soloot, H. K. Høidalen and B. Gustavsen, "Modeling of wind turbine transformers for the analysis of resonant overvoltages," *Electr. Power Syst. Res.*, vol. 115, pp. 26-34, 2014. . DOI: https://doi.org/10.1016/j.epsr.2014.03.004.

[32] M. Khanali and S. H. Jayaram, "Effectiveness of electrostatic shielding in suppressing the impact of fast transients on transformer insulation," in - *2015 IEEE Conference on Electrical Insulation and Dielectric Phenomena (CEIDP)*, 2015. . DOI: 10.1109/CEIDP.2015.7352146.

[33] P. Elhaminia, M. Vakilian and M. Lehtonen, "Wind turbine transformer improved design method entailing resonance blocking," *IET Electric Power Applications*, vol. 12, *(9)*, pp. 1337-1343, 2018. Available: https://ietresearch.onlinelibrary.wiley.com/doi/abs/10.1049/iet-epa.2018.5165. DOI: https://doi.org/10.1049/iet-epa.2018.5165.

[34] S. Sriyono, U. Khayam and S. Suwarno, "SFRA characteristics of power transformer internal winding considering the resonant effect," in - *2020 8th International Conference on Condition Monitoring and Diagnosis (CMD)*, 2020. . DOI: 10.1109/CMD48350.2020.9287194.

[35] E. O. Hassan, E. A. Badran and F. M. H. Youssef, "Effect of lightning impulses on the resonance stresses in the high voltage power transformers," in - *2017 Nineteenth International Middle East Power Systems Conference (MEPCON)*, 2017. . DOI: 10.1109/MEPCON.2017.8301226.

[36] Q. Yang *et al*, "Measurement and analysis of transient overvoltage distribution in transformer windings based on reduced-scale model," *Electr. Power Syst. Res.*, vol. 140, pp. 70-77, 2016. . DOI: https://doi.org/10.1016/j.epsr.2016.06.039.

[37] T. Abdulahovic, "Analysis of high-frequency electrical transients in offshore wind parks," Chalmers University of Technology Thesis, Sweden, 2011.

[38] M. Z. A. Ansari and J. Akhtar, "Time domain analysis of a 12 coil section and 18 coil section transformer model winding subjected to a variety of surge voltages," in - *2015 International Conference on Power and Advanced Control Engineering (ICPACE)*, 2015. . DOI: 10.1109/ICPACE.2015.7274981.

[39] L. Liu *et al*, "Analysis of lightening impulse response of cast resin dry-type transformer," in - *2018 12th International Conference on the Properties and Applications of Dielectric Materials (ICPADM)*, 2018. . DOI: 10.1109/ICPADM.2018.8401168.

[40] M. Florkowski *et al*, "Comparison of transformer winding responses to standard lightning impulses and operational overvoltages," *IEEE Transactions on Dielectrics and Electrical Insulation*, vol. 25, *(3)*, pp. 965-974, 2018. . DOI: 10.1109/TDEI.2018.007001.

[41] M. Florkowski, J. Furgał and M. Kuniewski, "Propagation of overvoltages in distribution transformers with silicon steel and amorphous cores," *IET Gener. Transm. Distrib.*, vol. 9, *(16)*, pp. 2736-2742, 2015. Available: https://doi.org/10.1049/iet-gtd.2015.0395. DOI: https://doi.org/10.1049/iet-gtd.2015.0395.

[42] M. Bagheri, B. T. Phung and M. S. Naderi, "Impulse voltage distribution and frequency response of intershield windings," *IEEE Electrical Insulation Magazine*, vol. 32, *(5)*, pp. 32-40, 2016. . DOI: 10.1109/MEI.2016.7552374.

[43] M. Kaufhold, "Failure mechanism of the interturn insulation of low voltage electric machines fed by pulse controlled inverters," *Proceedings of 1995 Conference on Electrical Insulation and Dielectric Phenomena*, pp. 254-257, 1995. . DOI: 10.1109/CEIDP.1995.483711.

[44] Weijun Yin, "Failure mechanism of winding insulations in inverter-fed motors," *IEEE Electrical Insulation Magazine*, vol. 13, *(6)*, pp. 18-23, 1997. . DOI: 10.1109/57.637150.

[45] E. Lindell *et al*, "Influence of rise time on partial discharge extinction voltage at semi-square voltage waveforms," *IEEE Transactions on Dielectrics and Electrical Insulation*, vol. 17, *(1)*, pp. 141-148, 2010. . DOI: 10.1109/TDEI.2010.5412012.

[46] B. Florkowska *et al*, "Measurement and analysis of surface partial discharges at semi-square voltage waveforms," *IEEE Transactions on Dielectrics and Electrical Insulation*, vol. 18, *(4)*, pp. 990-996, 2011. . DOI: 10.1109/TDEI.2011.5976086.

[47] M. S. Moonesan, S. H. Jayaram and E. A. Cherney, "Time to failure of medium-voltage form-wound machine turn insulation stressed by unipolar square waves," *IEEE Transactions on Dielectrics and Electrical Insulation,* vol. 22, *(6),* pp. 3118-3125, 2015. . DOI: 10.1109/TDEI.2015.005201.

[48] M. Khanali, S. Jayaram and J. Cheng, "Effects of voltages with high-frequency contents on the transformer insulation properties," *2013 IEEE Electrical Insulation Conference (EIC),* pp. 235-238, 2013. . DOI: 10.1109/EIC.2013.6554240.

[49] M. Khanali and S. H. Jayaram, "Partial discharge activities in transformer insulation under steep front voltages," *2014 IEEE Conference on Electrical Insulation and Dielectric Phenomena (CEIDP),* pp. 204-207, 2014. . DOI: 10.1109/CEIDP.2014.6995881.

[50] M. Khanali and S. Jayaram, "Dielectric frequency response of transformer insulation system under high-dV/dt stresses," in - *2015 IEEE 11th International Conference on the Properties and Applications of Dielectric Materials (ICPADM),* 2015. . DOI: 10.1109/ICPADM.2015.7295295.

[51] M. Khanali and S. Jayaram, "A study on PD activities of oil-impregnated paper under pulse voltages using gas analysis," *IEEE Transactions on Dielectrics and Electrical Insulation,* vol. 24, *(4),* pp. 2503-2510, 2017. . DOI: 10.1109/TDEI.2017.006181.

[52] M. S. Moonesan, "A Study of Medium and High Voltage Form-Wound Coil Turn-to-Turn Insulation of Converter Fed Rotating Machines," University of Waterloo Thesis, Canada, 2016. Available: http://hdl.handle.net/10012/11069.

[53] T. L. Koltunowicz *et al*, "Investigation of the effects of fast transients on a transformer's paper insulation," *2010 IEEE International Symposium on Electrical Insulation,* pp. 1-5, 2010. . DOI: 10.1109/ELINSL.2010.5549724.

[54] T. L. Koltunowicz *et al*, "Exploring the feasibility of an aging model for paper insulation based on the repetition frequency of transients," *2010 IEEE International Symposium on Electrical Insulation,* pp. 1-5, 2010. . DOI: 10.1109/ELINSL.2010.5549773.

[55] T. Koltunowicz *et al*, "The effects of prolonged exposure of paper insulation to fast repeating transients," *2010 International Conference on High Voltage Engineering and Application,* pp. 180-183, 2010. . DOI: 10.1109/ICHVE.2010.5640836.

[56] T. L. Koltunowicz *et al*, "Repetitive transient aging, the influence of rise time," *2011 Electrical Insulation Conference (EIC).,* pp. 151-155, 2011. . DOI: 10.1109/EIC.2011.5996136.

[57] T. L. Koltunowicz *et al*, "Repetitive transient aging, the influence of repetition frequency," *2011 Electrical Insulation Conference (EIC).,* pp. 444-448, 2011. . DOI: 10.1109/EIC.2011.5996195.

[58] T. Koltunowicz *et al*, "The influence of square voltage waveforms on transformer insulation break down voltage," *2011 Annual Report Conference on Electrical Insulation and Dielectric Phenomena*, pp. 48-51, 2011. . DOI: 10.1109/CEIDP.2011.6232593.

[59] T. L. Koltunowicz *et al*, "A statistical aging model for paper oil insulation under repetitive transients," *2012 International Conference on High Voltage Engineering and Application*, pp. 128-132, 2012. . DOI: 10.1109/ICHVE.2012.6357013.

[60] T. Koltunowicz, G. Bajracharya and D. Djairam, "Defining a transformer's aging factors in the future," *CIRED 2009 - 20th International Conference and Exhibition on Electricity Distribution - Part 1*, pp. 1-4, 2009. . DOI: 10.1049/cp.2009.0948.

[61] A. J. Vandermaar *et al*, "The electrical breakdown characteristics of oil-paper insulation under steep front impulse voltages," *IEEE Transactions on Power Delivery*, vol. 9, *(4)*, pp. 1926-1935, 1994. . DOI: 10.1109/61.329525.

[62] R. C. Kiiza *et al*, "Change in partial discharge activity as related to degradation level in oil-impregnated paper insulation: effect of high voltage impulses," *IEEE Transactions on Dielectrics and Electrical Insulation*, vol. 21, *(3)*, pp. 1243-1250, 2014. . DOI: 10.1109/TDEI.2014.6832271.

[63] J. Wang, Q. Li and S. Liu, "Characteristics of partial discharge in oil-paper insulation system under high frequency voltage," in - *2017 IEEE 19th International Conference on Dielectric Liquids (ICDL)*, 2017. . DOI: 10.1109/ICDL.2017.8124603.

[64] Y. Li *et al*, "Insulation performance of aging transformer winding under transient impulse," *2017 IEEE 19th International Conference on Dielectric Liquids (ICDL)*, pp. 1-4, 2017. . DOI: 10.1109/ICDL.2017.8124731.

[65] W. Sima *et al*, "Impact of time parameters of lightning impulse on the breakdown characteristics of oil paper insulation," *High Voltage*, vol. 1, *(1)*, pp. 18-24, 2016. . DOI: 10.1049/hve.2016.0009.

[66] W. Sima *et al*, "Effects of waveform parameters on the breakdown characteristics of OIP subjected to impulse voltages and evaluation method for waveform equivalence," *IET Science, Measurement & Technology*, vol. 13, *(2)*, pp. 223-230, 2019. . DOI: 10.1049/iet-smt.2018.5362.

[67] T. Wang *et al*, "Turn-to-turn insulation breakdown characteristics under non-standard lightning impulse voltages," *2015 IEEE 11th International Conference on the Properties and Applications of Dielectric Materials (ICPADM)*, pp. 200-203, 2015. . DOI: 10.1109/ICPADM.2015.7295243.

[68] Z. Wang *et al*, "Breakdown characteristics of oil-paper insulation under lightning impulse waveforms with oscillations," *IEEE Transactions on Dielectrics and Electrical Insulation*, vol. 22, *(5)*, pp. 2620-2627, 2015. . DOI: 10.1109/TDEI.2015.005115.

[69] S. P. Balaji *et al*, "Effect of Repeated Impulses on Transformer Insulation," *IEEE Transactions on Dielectrics and Electrical Insulation,* vol. 18, *(6),* pp. 2069-2073, 2011. . DOI: 10.1109/TDEI.2011.6118645.

[70] S. P. Balaji, L. Lavanya and S. Usa, "Effect of repeated impulses on OIP," *2012 International Conference on High Voltage Engineering and Application,* pp. 558-561, 2012. . DOI: 10.1109/ICHVE.2012.6357044.

[71] T. L. Koltunowicz, "Accelerated Insulation Aging Due to Thermal and Electrical Stresses in Future Power Grids," Delft University of Technology, Netherlands, 2014.

[72] M. Anglhuber and M. Kruger, "Dielectric analysis of high-voltage power transformers ," *Transformers Magazine,* vol. 3, *(1),* 2016.

[73] M. Jaya, T. Leibfried and M. Koch, "Information within the dielectric response of power transformers for wide frequency ranges," *2010 IEEE International Symposium on Electrical Insulation,* pp. 1-5, 2010. . DOI: 10.1109/ELINSL.2010.5549839.

[74] Y. Zheng and Z. Wang, "Study on broadband loss characteristics of oil-immersed papers for fast transient modeling of power transformer," *IEEE Transactions on Dielectrics and Electrical Insulation,* vol. 20, *(2),* pp. 564-570, 2013. . DOI: 10.1109/TDEI.2013.6508760.

[75] R. B. Jadav, C. Ekanayake and T. K. Saha, "Understanding the impact of moisture and ageing of transformer insulation on frequency domain spectroscopy," *IEEE Transactions on Dielectrics and Electrical Insulation,* vol. 21, *(1),* pp. 369-379, 2014. . DOI: 10.1109/TDEI.2013.003984.

[76] R. Nikjoo *et al*, "Dielectric response of oil-impregnated paper by utilizing lightning and switching transients," *IEEE Transactions on Dielectrics and Electrical Insulation,* vol. 22, *(1),* pp. 335-344, 2015. . DOI: 10.1109/TDEI.2014.004664.

[77] M. Dong *et al*, "Explanation and analysis of oil-paper insulation based on frequency-domain dielectric spectroscopy," *IEEE Transactions on Dielectrics and Electrical Insulation,* vol. 22, *(5),* pp. 2684-2693, 2015. . DOI: 10.1109/TDEI.2015.005156.

[78] A. Pradhan *et al*, "Non-linear modeling of oil-paper insulation for condition assessment using non-sinusoidal excitation," *IEEE Transactions on Dielectrics and Electrical Insulation,* vol. 22, *(4),* pp. 2165-2175, 2015. . DOI: 10.1109/TDEI.2015.004504.

[79] I. Fofana, H. Hemmatjou and F. Meghnefi, "Effect of thermal transient on the polarization and depolarization current measurements," *IEEE Transactions on Dielectrics and Electrical Insulation,* vol. 18, *(2),* pp. 513-520, 2011. . DOI: 10.1109/TDEI.2011.5739457.

[80] R. B. Jadav, C. Ekanayake and T. K. Saha, "Dielectric response of transformer insulation - comparison of time domain and frequency domain measurements," *2010 Conference Proceedings IPEC*, pp. 199-204, 2010. . DOI: 10.1109/IPECON.2010.5697105.

[81] H. Ma, T. K. Saha and C. Ekanayake, "Interpretation of dielectric response measurements of transformer insulation under temperature variations and transient effects," *2012 IEEE Power and Energy Society General Meeting*, pp. 1-8, 2012. . DOI: 10.1109/PESGM.2012.6344903.

[82] S. Zeng *et al*, "Condition diagnosis of oil-paper insulation during the accelerated electrical aging test based on polarization and depolarization current," in - *2015 IEEE 11th International Conference on the Properties and Applications of Dielectric Materials (ICPADM)*, 2015. . DOI: 10.1109/ICPADM.2015.7295305.

[83] R. Nikjoo, N. Taylor and H. Edin, "Effect of high voltage impulses on partial discharge characteristics of oil-impregnated paper for online diagnostics," *2016 IEEE International Power Modulator and High Voltage Conference (IPMHVC)*, pp. 151-156, 2016. . DOI: 10.1109/IPMHVC.2016.8012807.

[84] Y. Yuan *et al*, "Lab investigation of PD development in transformer winding," *2010 IEEE International Symposium on Electrical Insulation*, pp. 1-4, 2010. . DOI: 10.1109/ELINSL.2010.5549777.

[85] W. Yuan *et al*, "Online PD Monitoring and Analysis for Step-up Transformers of Hydropower Plant," *2011 Third International Conference on Measuring Technology and Mechatronics Automation*, vol. 2, pp. 762-767, 2011. . DOI: 10.1109/ICMTMA.2011.474.

[86] M. Khanali *et al*, "Study on locating transformer internal faults using sweep frequency response analysis," *Electric Power Systems Research*, vol. 145, pp. 55-62, 2017. . DOI: https://doi.org/10.1016/j.epsr.2016.11.016.

[87] B. Gustavsen, "Wide band modeling of power transformers," *IEEE Transactions on Power Delivery*, vol. 19, *(1)*, pp. 414-422, 2004. . DOI: 10.1109/TPWRD.2003.820197.

[88] A. Holdyk *et al*, "Wideband Modeling of Power Transformers Using Commercial sFRA Equipment," *IEEE Transactions on Power Delivery*, vol. 29, *(3)*, pp. 1446-1453, 2014. . DOI: 10.1109/TPWRD.2014.2303174.

[89] A. H. Soloot, H. K. Høidalen and B. Gustavsen, "The effect of winding design on transformer frequency response with application on offshore wind farm energization," *2012 International Conference on Renewable Energy Research and Applications (ICRERA)*, pp. 1-5, 2012. . DOI: 10.1109/ICRERA.2012.6477279.

[90] M. F. M. Yousof, "Frequency Response Analysis for Transformer Winding Condition Monitoring." The University of Queensland, Australia, 2015.

[91] "IEEE Guide for the Application and Interpretation of Frequency Response Analysis for Oil-Immersed Transformers," *IEEE Std C57. 149-2012*, pp. 1-72, 2013. . DOI: 10.1109/IEEESTD.2013.6475950.

[92] *Mobil - Voltesso 35*. Available: https://www.mobil.ca/en- ca/lubricants/industrial/lubricants /products/products/voltesso-35.

[93] *Petro Canada Lubricants - Luminol TM TRi.* Available: https://lubricants.petro-canada.com/en-be/brand/luminol-tri.

[94] *MEGGER - IDAX 300 Insulation Diagnostic Analyser*. Available: https://embed.widencdn.net /pdf/plus/megger/exttnffbl6/IDAX300-350_UG_en.pdf.

[95] S. M. Gubanski *et al*, "Dielectric response methods for diagnostics of power transformers," CIGRE Technical Brochures, Tech. Rep. D1, 254, TF D1.01.09, 2004.

[96] IEC 60270, Ed., *High-Voltage Test Techniques – Partial Discharge Measurements.* IEC, 2015.

[97] *Neoptix - T2 Transformer Temperature Probe*. Available: https://neoptix.com/t2-transformer.asp.

[98] *InsuLogix® H Hyrdogen Monitor.* Available: https://www.weidmann-electrical.com/wp-content /uploads/InsuLogix-HM-1.pdf.

[99] J. A. S. B. Jayasinghe *et al*, "Winding movement in power transformers: a comparison of FRA measurement connection methods," *IEEE Transactions on Dielectrics and Electrical Insulation,* vol. 13, *(6)*, pp. 1342-1349, 2006. . DOI: 10.1109/TDEI.2006.258206.

[100] S. M. Gubanski, J. Blennow and B. Holmgren, "Dielectric response diagnoses for transformer windings," CIGRE Technical Brochures, Tech. Rep. D1, 414, WG D1.01 (TF 14), 2010.

[101] L. E. Lundgaard, D. Allan and I. A. Höhlein, "Ageing of cellulose in mineral-oil insulated transformers," CIGRE Technical Brochures, Tech. Rep. D1, 323, TF D1.01.10, 2007.

[102] I. M. Jarrar, E. A. Cherney and S. H. Jayaram, "Effect of Repetitive Impulse Waveform Characteristics on Partial Discharges in Type II Turn-to-Turn Insulation," *IEEE Transactions on Dielectrics and Electrical Insulation,* vol. 29, *(3)*, pp. 1183-1190, 2022. . DOI: 10.1109/TDEI.2022.3164855.

Appendix A
PSCAD Simulation

A.1 Transformer equivalent circuit

The transformer equivalent circuit is simulated in the PSCAD software to study the distribution of transients along the transformer winding as a function of the transient parameters. The equivalent circuit for the final tap, tap 11 of the transformer is shown in Figure A 1 (high voltage end – tap 11). The tap voltages from tap 11 to tap 1 are simulated and measured similar to the experiment carried out in Figure 3.4. Individual taps are divided into four sections, and the values for the elements of each section is given in Table A 1. The dimension of transformers T1, and T2 are used to calculate the values of the element of each section. The tap to tap capacitance, winding self-inductance, winding section capacitance, stray capacitance to tank are derived from the design parameters of transformers T1, and T2. A high value in the range of MΩ is chosen for insulation resistance.

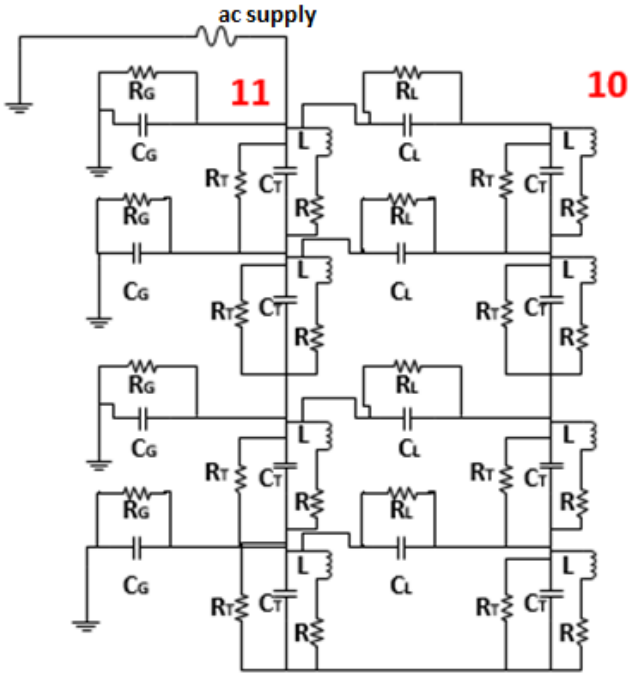

Figure A 1: Equivalent circuit of one of the taps (tap 11) for the transformer considered in the PSCAD simulation study.

Table A 1: Values for the elements in each section of the Transformer PSCAD equivalent circuit.

Element-Description	Value
L: Self-inductance of the winding	2.11 mH
R: Resistance of the winding	4.50 Ω
C_G: Stray capacitance to tank	0.06 nF
C_L: Tap to tap capacitance	64.3 nF
C_T: Section capacitance of the winding	0.79 pF
R_T, R_G: Dielectric resistance	3.00 MΩ

A.2 Distribution of transient voltage along the winding of the transformer

Figure A 2 shows the distribution of transient voltage along the taps of PSCAD simulated transformer equivalent circuit, for an input transient voltage of amplitude = 100 V, duty cycle = 10%, switching frequency = 1 kHz and rise time = 200 ns. The simulation response in Figure A 2 has larger oscillation and peak compared to the experimental response in Figure 4.17 because the simulation response cannot replicate the model transformer in terms of the entire frequency response characteristics.

The rate of rise (per unit) along the taps under various cases of transient voltage parameters for PSCAD simulation of transformer transient response is shown in Figure A 3. The rate of rise along the taps of the simulated transformer is highest for case 2, with an input transient voltage amplitude of 100 V, rise time of 200 ns, switching frequency of 1 kHz, and duty cycle of 50 %. Other than case 2, the rate of rise decreases with decrease in tap number for cases 1, 3 and 4. In the PSCAD simulation study, the amplitude of the transient voltage is not an important factor for the rate of rise along the transformer taps. Thus, the rate of rise in per unit for case 1 and case 3 of input transient voltage coincide with each other in Figure A 3. The lowest rate of rise is obtained for case 4 of the input transient voltage with rise time of 1000 ns. Tap-to-tap voltage difference (per unit) under various cases of transient voltage parameters for PSCAD simulation of transformer transient response is shown in Figure A 4. From Figure A 4, it is seen that the highest voltage difference along the taps is obtained for case 2 of the

transient input voltage with an amplitude of 100 V, rise time of 200 ns, switching frequency of 1 kHz and duty cycle of 50 %, which matches the voltage difference along the taps for the experimental transformer (Figure 4.19 and Figure 4.20). For cases 1, 3, and 4, the voltage difference along the taps, are similar. The rise time of 200 ns and the duty cycle of 50 % has the highest voltage energy spectrum, thus, case 2 has the highest voltage difference along the taps. The PSCAD simulation study is based on the design parameters of the transformer that includes only the high-frequency characteristics of the transformer modelled by using simple lumped elements. Thus, in Figure A 4, the transient voltage amplitude did not influence the voltage difference along the taps significantly. But the experimental results shown in Figure 4.19 to Figure 4.22 include all the coupling effects and the material properties of the transformer. Therefore, there are differences in the transient behavior of the transformer as a function of applied transient voltage amplitude. For the presented model transformer, the PSCAD simulation results and the experimental results match well in terms of overall trend, and thus the analysis of the distribution of transients along windings of other transformer models in a wind farm chain can be studied using PSCAD simulation software.

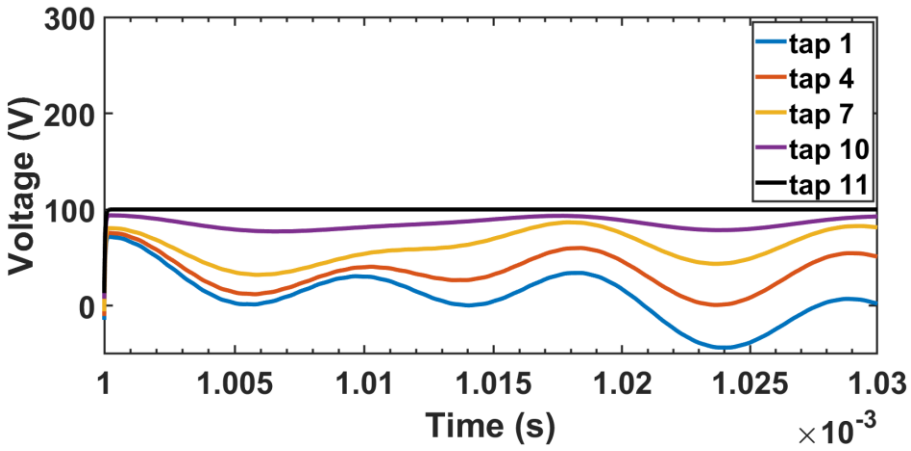

Figure A 2: Transformer transient response for an input voltage of amplitude = 100 V, duty cycle = 10%, switching frequency = 1 kHz, rise time = 200 ns for PSCAD simulation study.

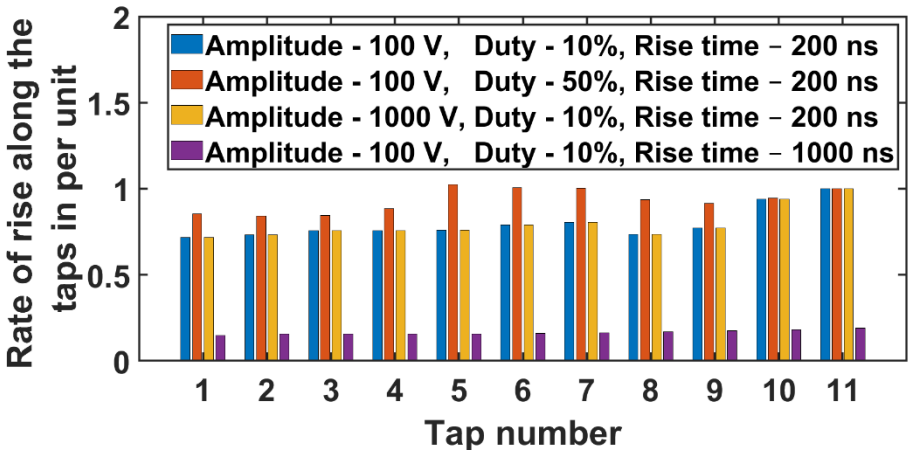

Figure A 3: Rate of rise along taps under various cases of transient voltage parameters for PSCAD simulation of transformer transient response.

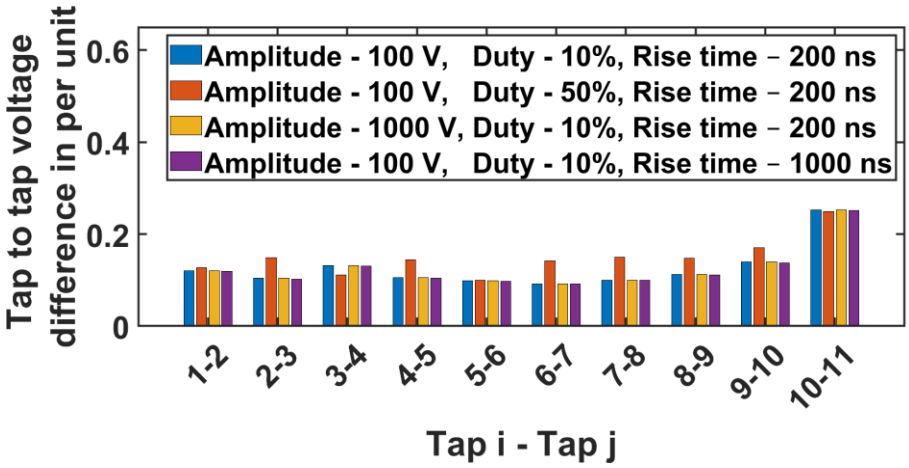

Figure A 4: Tap-to-tap voltage difference under various cases of transient voltage parameters for PSCAD simulation of transformer transient response.